Shape Control of Manipulators with Hyper Degrees of Freedom

by

Hiromi MOCHIYAMA

submitted to
Japan Advanced Institute of Science and Technology
in partial fulfillment of the requirements
for the degree of
Doctor of Philosophy

Supervisor : Professor Etsujiro Shimemura

School of Information Science
Japan Advanced Institute of Science and Technology

March 1998

Abstract

This thesis provides a theoretical framework to control a manipulator with hyper degrees of freedom. The term "Hyper Degrees Of Freedom" (HDOF for short) is an emblematic word to express strong necessity of much more kinematic degrees of freedom for a manipulator nowadays. An HDOF manipulator has ability to achieve various kind of tasks. In order to make full use of its ability, a shape control is proposed here, that is, not only the tip of a manipulator, but also its whole shape is controlled.

Before discussing the shape control, we rigorously define a shape correspondence between an HDOF manipulator and a spatial curve used for prescribing the desired shape. It is defined by using the solution of some nonlinear optimization problems termed the shape inverse problem. We give not only the existence theorem of its solution, but also a theorem on the existence region which allows us to convert control problems appeared later into more tractable ones.

Shape regulation control is considered first to bring an HDOF manipulator onto a given time invariant curve. The idea of estimating the desired curve parameter enables us to find the shape regulation law with curve parameter estimation law by Lyapunov design.

This crucial idea of curve parameter estimation is also effective for the shape tracking, where a time-varying curve is given to prescribe the desired shape. Two shape tracking control laws are derived by utilizing tracking control laws for conventional manipulator tracking.

Furthermore, it is shown that joint velocity signals are not essential to achieve the shape tracking, that is, the shape tracking using only joint angles is attained. Based on the idea of conceptual duality, we derive an observer that does not directly estimate the joint angle velocities, but estimate the velocity of the shape. After properly tuned, the modified shape tracking controller and shape velocity observer assure the local asymptotic stability of the closed-loop system.

We also give an example to show that new tasks which have never done before can be accomplished by shape control. The useful motion control for sophisticated obstacle avoidance is achieved by shape control idea. That is the motion along a curve useful

for going into a narrow space. Two controllers achieving this motion are shown as the counterparts of two shape tracking controllers derived before.

We also propose the way to find essentials of an HDOF manipulators by increase in DOF. Conditions for the kinematic structure are derived from a geometrically natural requirement that its direct kinematics tends to Frenet-Serret formula by increase in DOF.

The results in this thesis give a new vision for robotic manipulator control.

Acknowledgments

I would like, first of all, to express my sincere gratitude to my principal advisor Professor Etsujiro Shimemura of Japan Advanced Institute of Science and Technology for his constant encouragement, kind guidance and giving me an opportunity to study this subject.

I would like also to thank my advisor Professor Hisato Kobayashi of Hosei University for his helpful discussions and valuable suggestions.

I am deeply indebted to my advisor Associate Professor Masayuki Fujita of Japan Advanced Institute of Science and Technology for his helpful far-sighted comments and suggestions.

I would like to thank Professor Toshio Fukuda of Nagoya University, Professor Makoto Miyahara, Professor Teruo Matsuzawa and Associate Professor Taketoshi Yoshida of Japan Advanced Institute of Science and Technology for their reviewing my thesis and giving me valuable comments.

I also wish to express my thanks to Dr. Izumi Masubuchi and Dr. Christoph Ament of Japan Advanced Institute of Science and Technology for their suggestions and continuous encouragements.

I am grateful to Professor Kenkou Uchida of Waseda University, who was my advisor in my master course, gave me a lot of suggestions and kind encouragements.

I devote my sincere thanks and appreciation to my colleagues and friends.

Finally, I must also offer thanks to my parents for their support and constant encouragement via Email.

Notation

N	the set of natural numbers
$\Re$	the set of real numbers
$\Re_+$	the set of non-negative real numbers
$\Re^n$	the set of real vectors with n components
$\Re^{m\times n}$	the set of real $m \times n$ matrices
E^3	Euclidean space
$SO(n)$	the n-dimensional special orthogonal group
$so(n)$	the set of $n \times n$ real skew-symmetric matrices (the Lie algebra of $SO(n)$)
$\|a\|$	the absolute value of a scalar a
$\|\boldsymbol{a}\|$	the Euclidean norm of a vector $\boldsymbol{a}$
$\|\boldsymbol{A}\|$	the Euclidean norm of a matrix $\boldsymbol{A}$
$\boldsymbol{A}^T$	the transpose of a matrix $\boldsymbol{A}$
$\boldsymbol{A}^{-1}$	the inverse of a matrix $\boldsymbol{A}$
$\boldsymbol{A}^+$	the pseudo-inverse of a matrix $\boldsymbol{A}$
$\mathrm{diag}\{a_1, \cdots, a_n\}$	a diagonal matrix with diagonal elements a_1 to a_n
$\mathrm{blockdiag}\{\boldsymbol{A}_1, \cdots, \boldsymbol{A}_n\}$	a block diagonal matrix with diagonal blocks $\boldsymbol{A}_1$ to $\boldsymbol{A}_n$
$\lambda_M(\boldsymbol{P})$	the maximum eigenvalue of a symmetric matrix $\boldsymbol{P}$
$\lambda_m(\boldsymbol{P})$	the minimum eigenvalue of a symmetric matrix $\boldsymbol{P}$
$\boldsymbol{P} > 0$	a positive definite matrix $\boldsymbol{P}$
$\boldsymbol{P} \geq 0$	a positive semidefinite matrix $\boldsymbol{P}$
max	maximum
min	minimum
sup	supremum
inf	infimum
det	determinant
sgn	the signum function
$\wedge$	and
$\vee$	or
$\perp$	be perpendicular to
$\times$	outer product
$[\boldsymbol{a}\times]$	For a vector $\boldsymbol{a} = [a_x\ a_y\ a_z]^T \in \Re^3$, $[\boldsymbol{a}\times] := \begin{bmatrix} 0 & -a_z & a_y \\ a_z & 0 & -a_x \\ -a_y & a_x & 0 \end{bmatrix}$.
Π	products
$\boldsymbol{e}_x$	the x-directional unit vector in E^3, $[\ 1\ 0\ 0\ ]^T$
$\boldsymbol{e}_y$	the y-directional unit vector in E^3, $[\ 0\ 1\ 0\ ]^T$
$\boldsymbol{e}_z$	the z-directional unit vector in E^3, $[\ 0\ 0\ 1\ ]^T$
$\boldsymbol{I}_n$	the $n \times n$ elementary matrix

Contents

List of Figures

Chapter 1

Introduction

1.1 Motivation and Purpose

We require more flexible, more functional and more intelligent robotic manipulators due to recent social changes. For example, lack of helpers to aged people and structural change from mass production to wide-variety one according to customers' preferences are serious problems and expected to be solved by use of robots. Robot industry is expected to be a successor to automobile industry in twenty-first century coming soon. Unfortunately, the robots of today have too poor ability to come up to our expectations.

It is kinematic degrees of freedom that is essentially insufficient for conventional robotic manipulators to achieve various kinds of tasks. Most of conventional manipulators have only six degrees of freedom which is the minimum number to control its tip position and orientation in a three-dimensional space. Kinematic degrees of freedom is one of the most important indexes for dexterity. In other words, increase in kinematic degrees of freedom brings increase of ability to accomplish various kinds of tasks.

That is why we study a manipulator with much more degrees of freedom than ever. We named it a *Hyper Degrees Of Freedom manipulator* (HDOF manipulator, for short) to express that "the more degrees of freedom a manipulator has, the wider range of tasks can be achieved by it".

An HDOF manipulator has potential ability to achieve non-conventional tasks by itself, such as moving in highly constrained environment and grasping objects of various size and shapes which can never be attained before.

There are, however, a lot of obstacles to turn it into reality; due to difficulty to construct mechanical hardware and control problem because of high dimensionality.

The purpose of this thesis is to establish a theoretical framework for an HDOF manipulator, to clarify essentials of an HDOF manipulator based on the framework and finally

to realize it by putting all the obtained knowledge together.

Achievement of the purpose will bring an impact to a wide variety of fields where robotic manipulators are expected to be used necessarily.

1.2 Brief History

In 1997 at the IEEE International Conference on Robotics and Automation, the largest meeting on robotics in the world, there appeared the session on manipulators with "hyper" degrees of freedom. This fact shows a rise in hope for a new type of manipulator with many degrees of freedom.

There are a large number of studies on manipulators with hyper degrees of freedom [6, 7, 8, 10, 11, 13, 14, 18, 29]. Good reviews were done by Chirikjian in his Ph.D thesis [5], and by Hirose in his book [9] from a biological point of view. Here we will review the historical background of the studies focusing on two topics. One is the use of the whole manipulator to handle objects, and the other is the use of spatial curves for manipulator control.

It is sure that the tip of a manipulator is the typical part of handling objects in environments. However, it is natural for an HDOF manipulator to use its whole arm to make full use of its rich kinematic DOF. The concept of using the whole arm to handle objects in environments proposed first by Salisbury in 1987 [23]. This concept was termed the *Whole Arm Manipulation* (WAM for short). He suggested we could achieve many non-conventional tasks by the WAM, such as pushing, shoving, striking, cradling, cushioning and interlink grasping. To achieve this, he focused on controlling the forces of interaction between manipulators and the environment. There were some researchers of this WAM concept [21], but the theoretical aspects of the WAM mechanism have not been considered for a long time.

On the other hand, it is natural to regard the macroscopic form of an HDOF manipulator as a spatial curve. The curve utilization to manipulator control appeared in studies on Variable Geometry Truss Manipulators (VGTMs) in the late 80's [22, 16, 28]. In these studies, spatial curves were used for solving the inverse kinematics. First, a spatial curve satisfying given task conditions is derived, then, a VGTM was fitted the curve. Due to this outstanding strategy, high dimensional redundancy resolution problems were solved successfully. Chirikjian and Burdick further developed this concept to a more general and more geometric flavor [5]. They established a kinematic framework for HDOF manipulators, mainly for VGTMs. However, there were difficulties to establish a unified framework

including manipulator dynamics explicitly because of the complexity of dynamics of the parallel link mechanism.

It should be pointed out that the ideas of whole arm manipulation and the curve utilization for manipulator control have not been fused together completely. Salisbury suggested the use of trajectories of the whole arm in his paper in 1988 [24], but any concrete strategies have not been shown. Chirikjian mentioned the usefulness of the WAM [5], but he used the word "hyper redundant", which means that the tip of the manipulator is supposed to be used mainly for task accomplishment. This lack of harmony arises from neglect of the manipulator dynamics. To achieve the WAM, it is necessary to take manipulator dynamics into account, since in the WAM the manipulator needs to interact with the environment. Otherwise, it is very dangerous to move the manipulator in the environment. But, it is very difficult to apply control strategy to the complex dynamic model of an parallel-link HDOF manipulator.

Our basic policy of control of HDOF manipulators is to combine these two concepts in order to make new values. In consideration of the historical background above, we take the following choices:

1. *Serial-link mechanism* is adopted for an HDOF manipulator because it is the most fundamental style of mechanical structures. This choice allows us to take dynamics of an HDOF manipulator into account explicitly.

2. *Shape control* is proposed as a fundamental control scheme for an HDOF manipulator, that is, not only the tip of an HDOF manipulator, but also its whole shape is controlled. The shape control gives basic motions for the WAM.

To sum up, the *dynamics-based shape control* is the feature of this thesis.

A parallel-link mechanism has good properties from practical viewpoint; light weight and high rigidity. Thus, most researchers of HDOF manipulators mainly recommend a parallel-link mechanism such as VGTMs for an HDOF manipulator. As mentioned before, however, we need to consider its dynamics explicitly. It is better to start from a simpler mechanical structure at the first stage of the theoretical analysis in order to catch essences of an HDOF manipulator. Moreover, the aforementioned good properties of a parallel-link mechanism may not be essential, because these may change ten years later due to drastic technological progresses. Actually, some serial-link manipulators with considerable large number of DOF have been developed recently [26, 20].

1.3 Problems

Two dynamics-based shape control problems will be considered. One is a *shape regulation* which tries to bring the manipulator onto the desired shape. The other is a *shape tracking* to make the manipulator follow the moving desired shape. In both cases, we need some apparatus to prescribe the desired shape. In this thesis, parametric spatial curves are used for this purpose. Then, there appears the problem of shape correspondence between a manipulator and a spatial curve, that is, we have to define the correspondence between them in shape, before tackling the control problems.

Explicit consideration of manipulator dynamics means that a shape control problem is a kind of stabilization problems in the sense of Lyapunov [12]. In stabilization problems for conventional manipulators, it is possible to apply the Lyapunov design directly to look for control laws which achieve asymptotic stability at the desired point [4]. However, we will see that the desired point is implicitly given in shape control problems, then we need some tips to find control laws.

To show not only fundamental control laws, but also how to accomplish new tasks in shape control framework is also one of the substantial themes in this study. Specially in this thesis, an obstacle avoidance problem will be considered.

It is also important to look for essentials of an HDOF manipulator to realize it. The essentials could provide us highly suggestive information. There is a big problem to establish a methodology to find them.

1.4 Organization

This thesis is comprised of eight chapters which are related as shown in Figure 1.1.

In Chapter **2**, following this introductory chapter, two fundamental preliminaries are given. One is on spatial parametric curves in Euclidean space which is used for prescribing our control objective. The other is related to the kinematic and dynamic models of our controlled plant, an HDOF manipulator.

In Chapter **3**, we discuss a shape correspondence between an HDOF manipulator and a spatial curve, and also provide important results related to the shape correspondence.

Shape control problems are addressed in Chapter **4** to Chapter **6**. In Chapter **4**, a shape regulation, the most fundamental control problem, is discussed. It is shown that estimating the desired curve parameters is a crucial key to solve this problem. This idea allows us to achieve the control purpose of a shape regulation without solving the shape

inverse problem directly, which is time-consuming in this case.

In Chapter **5**, a shape tracking control is considered. We can see that the idea of estimating the desired curve parameters is effective for the shape tracking problem as well.

A shape tracking using only joint angle information is considered in Chapter **6**. We use an observer which has closed-loop dynamics dual to that of a shape tracking controller. This duality of the controller and the observer brings us a successful result to solve this problem by Lyapunov stability theory.

In Chapter **7**, an obstacle avoidance problem is considered in shape control framework. We convert the problem into a motion control problem which is solved by the idea of shape control.

In Chapter **8**, a novel way to look for essentials of an HDOF manipulator is proposed from the viewpoint of a shape control. This is a kind of a limit analysis via increase in DOF. A natural kinematic structure for HDOF manipulators is derived theoretically.

In Chapter **9**, we summarize main contributions of this thesis.

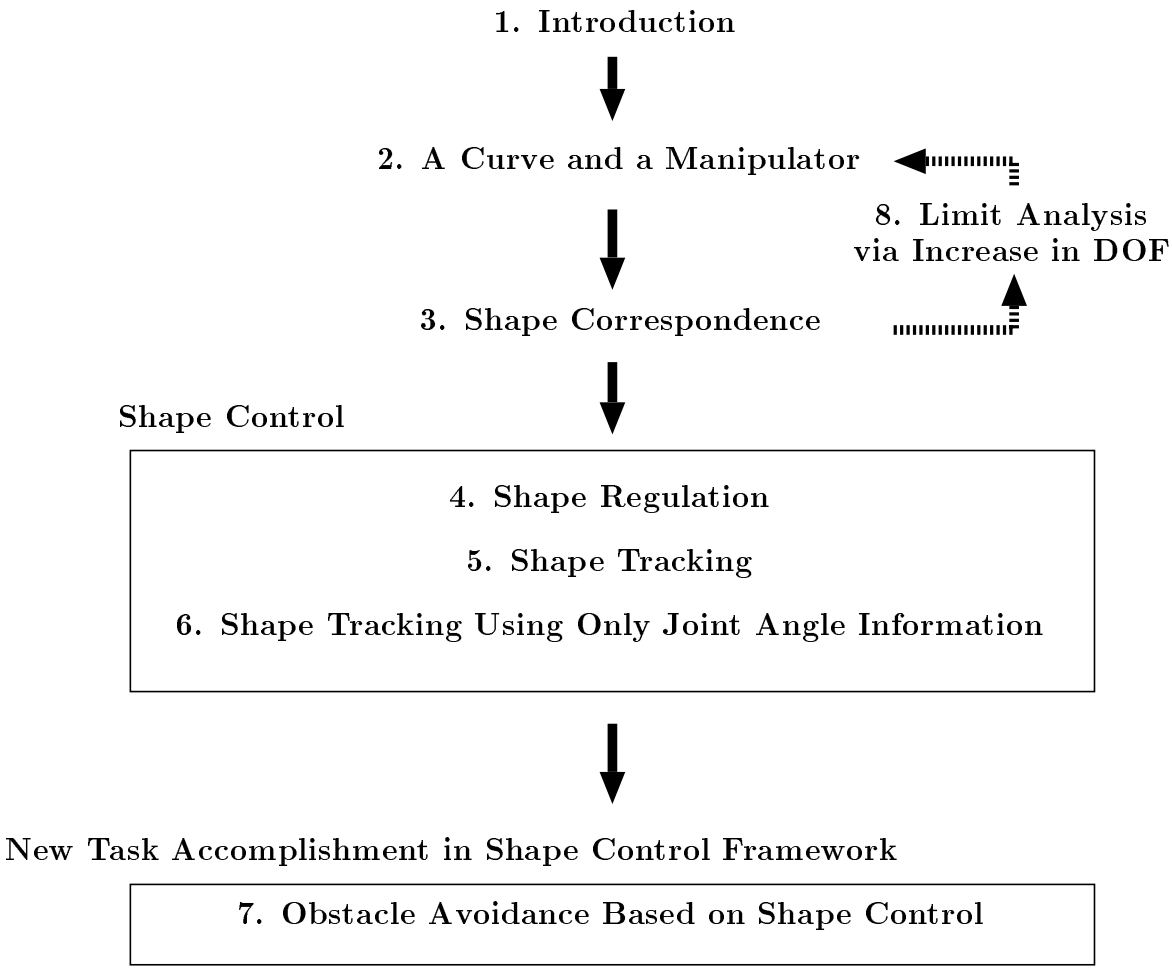

Figure 1.1: Organization of this thesis

Chapter 2

A Curve and a Manipulator

In this chapter, we give descriptions of two essentials in this study. One is a spatial curve which is used for prescribing our control objective, and the other is an HDOF manipulator which is the plant to be controlled here.

In Section **2.1**, we give descriptions of spatial parametric curves in both time invariant and time-varying cases. Also we show Frenet-Serret formula. Kinematic and dynamic models of an HDOF manipulator are shown in Section **2.2**.

2.1 Spatial Curves

The most natural and useful expression of spatial curves is the parametric representation. In this section, notations of parametric representation of both time invariant and time-varying curves are given and some weak assumptions on them are made for their smoothness. Frenet-Serret formula is also shown in this section. This formula is well known as a relation between a parametric curve and geometric parameters; a curvature and a torsion.

2.1.1 Parametric Representation

Both time invariant and time-varying curves are considered.

Time Invariant Curves

In the parametric representation of curves, a spatial curve in Euclidean space, E^3, is regarded as a mapping from $\Re$ to E^3. Let $\boldsymbol{c}$ be a mapping of $\Re$ into E^3, i.e.,

$$\boldsymbol{c} : \Re \rightarrow E^3 \ . \tag{2.1}$$

We can understand that, for a parameter $\sigma \in \Re$, a set $\{\boldsymbol{c}(\sigma) \in E^3 \,|\sigma \in \Re\}$ forms a spatial curve in E^3 (see Figure 2.1). The parameter σ is called a *curve parameter*.

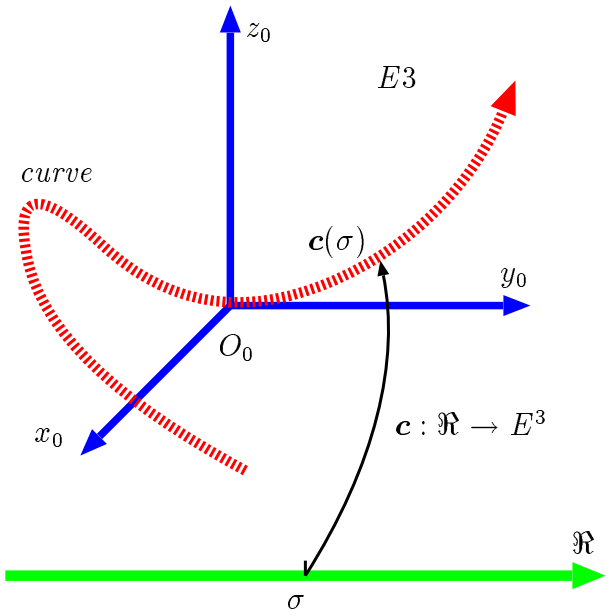

Figure 2.1: Time invariant parametric curve

Assume that the mapping $\boldsymbol{c}$ has the following properties:

Assumption 1 (Time Invariant Curves)

1. A mapping $\boldsymbol{c}$ is continuously differentiable in $\Re$.
2. There exists $\sigma_0 \in \Re$ such that $\boldsymbol{c}(\sigma_0) = \mathbf{o}$. Without loss of generality, we set $\sigma_0 = 0$. □

The first statement in the above assumption is related to smoothness of curves treated here. The reason for the requirement of continuous differentiability will become clear in the later chapter.

The second means that a curve passes through the origin of the world coodinate where the base of a manipulator is fixed. If $\sigma_0 \neq 0$, define $\boldsymbol{c}'(\sigma') := \boldsymbol{c}(\sigma - \sigma_0)$, then $\boldsymbol{c}'$ is the exactly same curve as $\boldsymbol{c}$ and has the origin at $\sigma' = 0$. That is why we can always set $\sigma_0 = 0$.

Time-varying Curves

A time-varying curve is represented by a mapping of the direct product, $\Re \times \Re_+$, into E^3. Let $\boldsymbol{c}$ be a mapping of $\Re \times \Re_+$ into E^3, that is,

$$\boldsymbol{c} : \Re \times \Re_+ \to E^3 \ . \tag{2.2}$$

A set $\{\boldsymbol{c}(\sigma,t) \in E^3 | \sigma \in \Re\}$ draws a curve at time $t \in \Re_+$ (see Figure 2.2).

Throughout this paper, a time-varying curve, $\boldsymbol{c}$, is supposed to have the following properties:

Assumption 2 (Time-varying Curves)

1. A mapping $\boldsymbol{c}$ is of class C^2 in $\Re \times \Re_+$.

2. For all $t \in \Re_+$, $\boldsymbol{c}(0,t) = \mathbf{o}$. □

As the previous assumption, the first one in the above statements is the smoothness of a curve, and also requires that it varies smoothly. The reason for smoothness of C^2 comes from the fact that a manipulator has 2nd-order dynamics since a time-varying curve is used as a desired movement of a manipulator.

The second means that a curve passes through the origin at $\sigma = 0$ *all the time.*

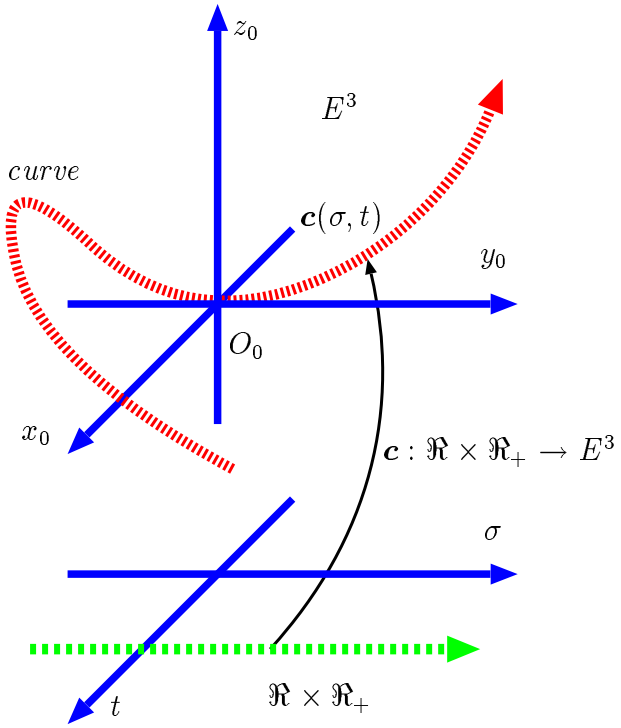

Figure 2.2: Time-varying parametric curve

2.1.2 Frenet-Serret Formula

Let $\boldsymbol{c}$ be a time invariant spatial curve and assume that any tangent vectors on the curve are normalized, that is,

$$\left\| \frac{d\boldsymbol{c}}{d\sigma}(\sigma) \right\| = 1 \ . \tag{2.3}$$

In this case, the curve parameter, σ, corresponds to arc length.

Frenet-Serret formula in E^3 is expressed by

$$\frac{d\boldsymbol{c}}{d\sigma}(\sigma) = \boldsymbol{\Phi}(\sigma)\boldsymbol{e}_x \ , \tag{2.4}$$

$$\frac{d\boldsymbol{\Phi}}{d\sigma}(\sigma) = \boldsymbol{\Phi}(\sigma)\left[\boldsymbol{\omega}(\sigma)\times\right] \ , \tag{2.5}$$

$$\boldsymbol{\omega}(\sigma) := \begin{bmatrix} \tau(\sigma) \\ 0 \\ \kappa(\sigma) \end{bmatrix} \ , \tag{2.6}$$

where $\boldsymbol{\Phi}(\sigma) \in SO(3)$ is the coordinate at $\boldsymbol{c}(\sigma)$ and called *Frenet frame* (see Figure 2.3). Parameters $\kappa(\sigma) \in \Re_+$ and $\tau(\sigma) \in \Re$ are *curvature* and *torsion* of the curve at σ respectively. For $\boldsymbol{a} = [a_x \ a_y \ a_z]^T \in \Re^3$, $[\boldsymbol{a}\times]$ denotes

$$[\boldsymbol{a}\times] := \begin{bmatrix} 0 & -a_z & a_y \\ a_z & 0 & -a_x \\ -a_y & a_x & 0 \end{bmatrix} \ , \tag{2.7}$$

that is, $[\boldsymbol{a}\times] \in so(3)$. It is important to note that, for $\boldsymbol{a}, \boldsymbol{b} \in \Re^3$,

$$[\boldsymbol{a}\times]\,\boldsymbol{b} = \boldsymbol{a} \times \boldsymbol{b} \tag{2.8}$$

where the symbol ' $\times$ ' denotes an outer product in E^3. A straight line is defined as the curve with $\kappa(\sigma) = 0$ and $\tau(\sigma) = 0$ for any σ.

2.2 Manipulator Models

In this section, kinematic and dynamic models of an HDOF manipulator are shown. Like a conventional manipulator, an HDOF manipulator is considered as an open serial kinemaic chain of rigid bodies connected by joints. An important difference of mechanical structure is use of two-degree-of-freedom (2DOF) joints (see Figure 2.4). It is essential for an HDOF manipulator to have 2DOF joints in order to form an arbitrary shape in Euclidean space.

A new kinematics for an HDOF manipulator is introduced here. This is more reasonable and more geometric than conventional kinematics based on Denavit-Hartenberg notation.

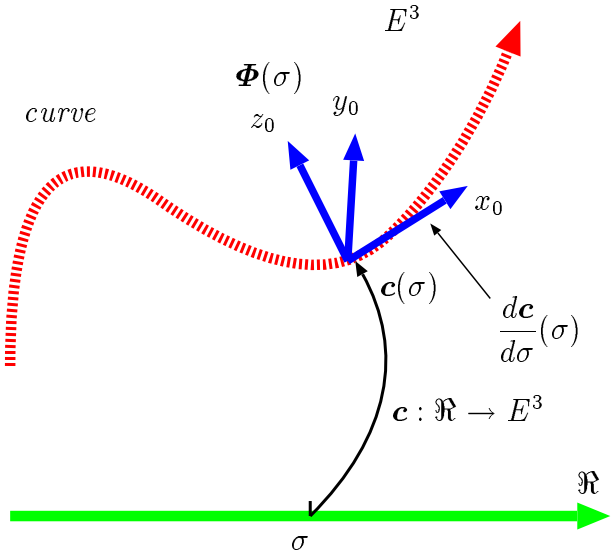

Figure 2.3: Frenet frame

A dynamic equation for an HDOF manipulator is given based on both Lagrange formulation and Newton-Euler formulation. Some important properties of Lagrangian dyanmics are reviewd, while Newton-Euler recursive formulas are shown for computation.

2.2.1 Kinematics for HDOF Manipulators

Coordinate Frame Setting

Consider $(n+1)$ rigid bodies and n two-degree-of-freedom joints in E^3. We attach coordinate frames to all rigid bodies and joints, and connect the rigid bodies with the joints in series in the following mannars:

1. For the i-th rigid body, let $\mathsf{p}_{\mathsf{t},i}$ and $\mathsf{p}_{\mathsf{h},i}$ be connecting points to the previous $(i-1)$-th rigid body and the next $(i+1)$-th rigid body respectively. Let l_i denote the line passing through $\mathsf{p}_{\mathsf{t},i}$ and $\mathsf{p}_{\mathsf{h},i}$. Define a positive constant, l_i, as the distance between these two points and call it the *link length*. See Figure 2.5.

2. Attach coordinate frame, $\boldsymbol{\Phi}_i \in SO(3)$, to the i-th rigid body at $\mathsf{p}_{\mathsf{h},i}$, so as to align its x axis with line l_i. In this setting, the coordinate is not uniquely decided. Let $\boldsymbol{\Phi}'_i$ be one of the coordinates. Then $\boldsymbol{\Phi}_i$ is represented by

$$\boldsymbol{\Phi}_i = \boldsymbol{\Phi}'_i \boldsymbol{R}(\boldsymbol{e}_x, \alpha_i) \ , \tag{2.9}$$

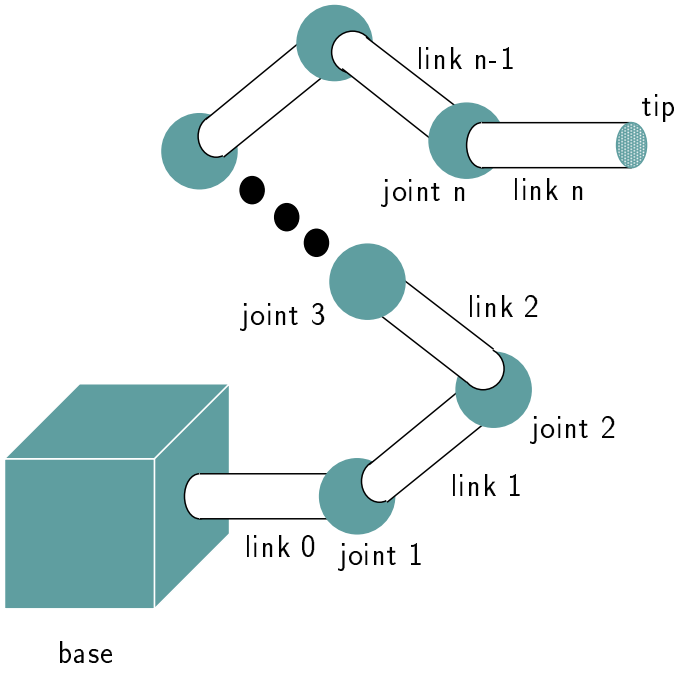

Figure 2.4: Manipulator with hyper degrees of freedom

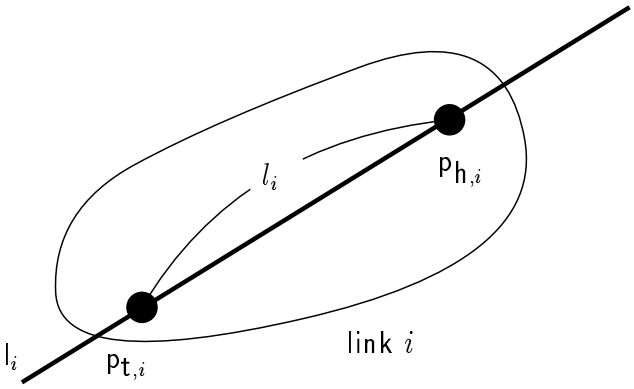

Figure 2.5: Link

where $\boldsymbol{e}_x := [\ 1\ 0\ 0\ ]^T$ is the x-directional unit vector, $\alpha_i \in (\ -\pi\ \pi\ ]$ is a real constant and $\boldsymbol{R}(\boldsymbol{a}, \theta) \in SO(3)$ denotes a rotational action about a unit axis $\boldsymbol{a} \in E^3$ by the amount $\theta \in (\ -\pi\ \pi\ ]$ in radians. See Figure 2.6.

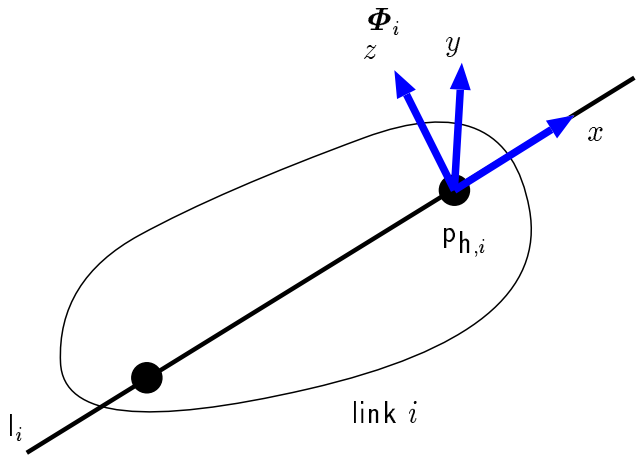

Figure 2.6: Attachment of a link frame

3. For the i-th joint, there are two rotational axes. We call rotational axes connected with the previous $(i-1)$-th joint and the next $(i+1)$-th joint the *Sub-axis* and the *Main-axis* respectively. Let $\mathsf{l}_{t,i}$ and $\mathsf{l}_{h,i}$ be lines align with the Sub-axis and the Main-axis respectively. Moreover, let p_i denote the intersection point of the two lines. See Figure 2.7.

4. Attach coordinates frames, $\boldsymbol{\Phi}_{s,i}$, $\boldsymbol{\Phi}_{m,i} \in SO(3)$, to the i-th joint at p_i, so as to align their z axes with $\mathsf{l}_{t,i}$ and $\mathsf{l}_{h,i}$ respectively. In this case, the coordinates are also not decided uniquely. In the same mannar as the previous step, let $\boldsymbol{\Phi}'_{s,i}$, $\boldsymbol{\Phi}'_{m,i}$ be those coordinates. Then $\boldsymbol{\Phi}_{s,i}$ and $\boldsymbol{\Phi}_{m,i}$ are represented by

$$\boldsymbol{\Phi}_{s,i} = \boldsymbol{\Phi}'_{s,i}\boldsymbol{R}(\boldsymbol{e}_z, \beta_i)\ , \tag{2.10}$$

$$\boldsymbol{\Phi}_{m,i} = \boldsymbol{\Phi}'_{m,i}\boldsymbol{R}(\boldsymbol{e}_z, \gamma_i)\ , \tag{2.11}$$

where $\boldsymbol{e}_z := [\ 0\ 0\ 1\ ]^T$ is the z-directional unit vector and $\beta_i, \gamma_i \in (\ -\pi\ \pi\ ]$ are real constants. Let $\theta_{s,i}$, $\theta_{m,i} \in (\ -\pi\ \pi\ ]$ be rotational angles about z axes of $\boldsymbol{\Phi}_{s,i}$ and $\boldsymbol{\Phi}_{m,i}$ from their x axes respectively. See Figure 2.8.

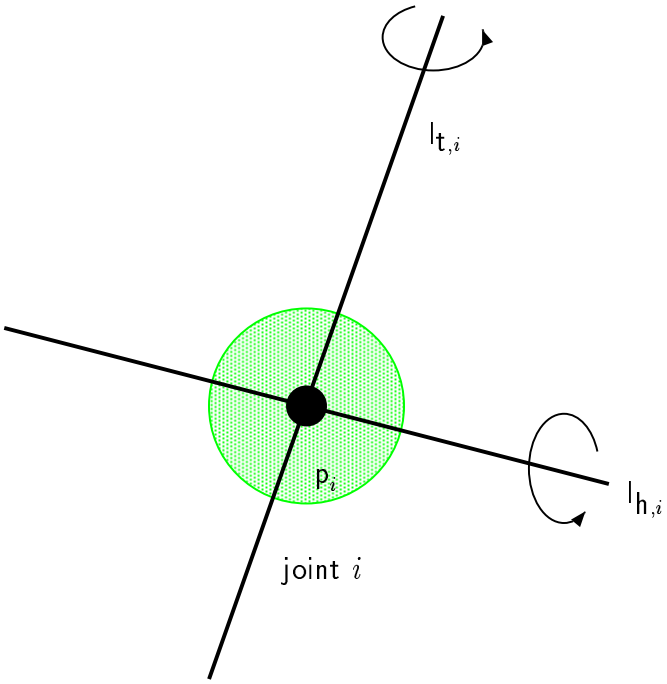

Figure 2.7: 2DOF joint

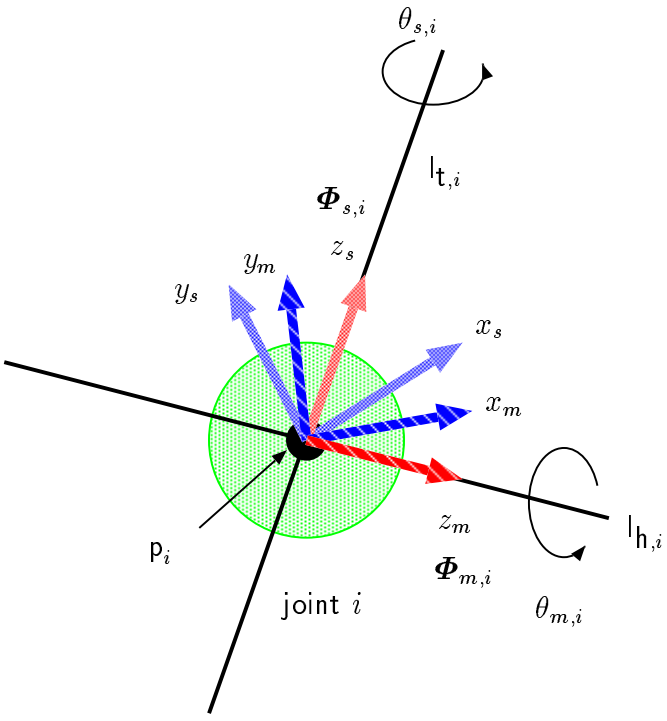

Figure 2.8: Attachment of joint frames

5. Define $\boldsymbol{Q}'_i \in SO(3)$ such that

$$\boldsymbol{\Phi}'_{m,i} = \boldsymbol{\Phi}_{s,i}\boldsymbol{R}(\boldsymbol{e}_z, \theta_{s,i})\boldsymbol{Q}'_i \ . \tag{2.12}$$

The constant matrix, $\boldsymbol{Q}'_i$, denotes the relationship between the two axes of the 2DOF joint.

6. Connect the $(i-1)$-th rigid body and the i-th rigid body by means of the i-th joint such that $\mathsf{p}_{\mathsf{h},i-1}$ in the $(i-1)$-th rigid body, $\mathsf{p}_{\mathsf{t},i}$ in the i-th rigid body and p_i in the i-th joint all coincide. Let $\boldsymbol{p}_{i-1} \in E^3$ be the position vector of the connecting point. Notice that $\boldsymbol{p}_i$ is not the position of the i-th joint, but the position of the $(i+1)$-th joint. Thus, we call $\boldsymbol{p}_i$ the *link position* (not joint position). See Figure 2.9.

7. Define $\boldsymbol{Q}'_{s,i}, \boldsymbol{Q}'_{m,i} \in SO(3)$ such that

$$\boldsymbol{\Phi}'_{s,i} = \boldsymbol{\Phi}'_{i-1}\boldsymbol{Q}'_{s,i} \ , \tag{2.13}$$

$$\boldsymbol{\Phi}'_i = \boldsymbol{\Phi}_{m,i}\boldsymbol{R}(\boldsymbol{e}_z, \theta_{m,i})\boldsymbol{Q}'_{m,i} \ . \tag{2.14}$$

These constant matrices describe the way of connection between the link and the joint.

By the above coordinate frame setting, the relation between the adjacent link coordinates is expressed by

$$\boldsymbol{\Phi}_i = \boldsymbol{\Phi}_{i-1}\boldsymbol{R}_{w,i} \ , \tag{2.15}$$

The matrix $\boldsymbol{R}_{w,i} \in SO(3)$ denotes 2DOF rotational action defined by

$$\boldsymbol{R}_{w,i} := \boldsymbol{Q}_{s,i}\boldsymbol{R}(\boldsymbol{e}_z, \theta_{s,i})\boldsymbol{Q}_i\boldsymbol{R}(\boldsymbol{e}_z, \theta_{m,i})\boldsymbol{Q}_{m,i} \ , \tag{2.16}$$

where $\boldsymbol{Q}_{s,i}$, $\boldsymbol{Q}_{m,i}$, $\boldsymbol{Q}_i \in SO(3)$ are

$$\boldsymbol{Q}_{s,i} := \boldsymbol{R}^T(\boldsymbol{e}_x, \alpha_{i-1})\boldsymbol{Q}'_{s,i}, \tag{2.17}$$

$$\boldsymbol{Q}_i := \boldsymbol{R}(\boldsymbol{e}_z, \beta_i)\boldsymbol{Q}'_i\boldsymbol{R}(\boldsymbol{e}_z, \gamma_i), \tag{2.18}$$

$$\boldsymbol{Q}_{m,i} := \boldsymbol{Q}'_{m,i}\boldsymbol{R}^T(\boldsymbol{e}_x, \alpha_i). \tag{2.19}$$

Notice that the constants α_i, β_i, γ_i depend only on the way of the coordinate frame setting, and are independent of the mechanical structure of joints. The mechanical structure is reflected by $\boldsymbol{Q}'_{s,i}$, $\boldsymbol{Q}'_{m,i}$ and $\boldsymbol{Q}'_i$.

The relation between the adjacent link positions is expressed by

$$\boldsymbol{p}_i = \boldsymbol{p}_{i-1} + l_i\boldsymbol{\Phi}_i\boldsymbol{e}_x \ . \tag{2.20}$$

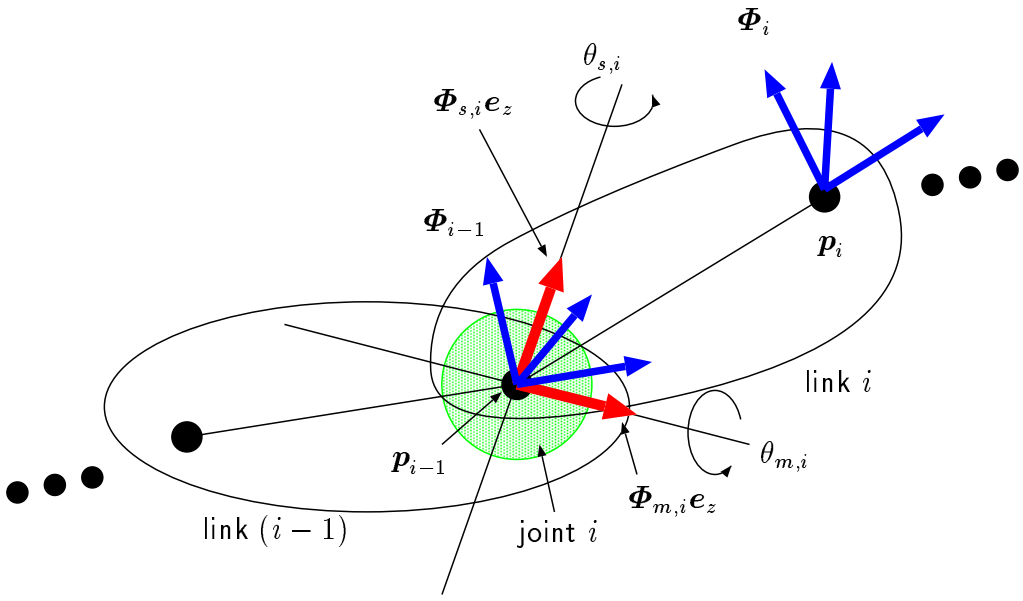

Figure 2.9: Serial connection of links and joints

Straight Line as a Reference

The constants α_i, β_i, γ_i express arbitrariness of the coordinate frame setting mentioned above. Here we make an adjustment for the coordinate frame setting to remove unnecessary arbitrariness.

Since a straight line is the most fundamental curve, we think it as a reference shape of a manipulator. In Frenet-Serret formula, a straight line is defined as a curve with a curvature and a torsion such that $\kappa(\sigma) = 0$ and $\tau(\sigma) = 0$ for all σ. This means that any coordinate frames on a straight line are identical, that is,

$$\forall \sigma_1, \sigma_2 \in \Re \quad \boldsymbol{\Phi}(\sigma_1) = \boldsymbol{\Phi}(\sigma_2) \ . \tag{2.21}$$

We require the same thing to the link frames of an HDOF manipulator, that is, that all link frames are identical when the HDOF manipulator shape a line, which is represented by

$$\forall i_1, i_2 \in \{1, \cdots, n\} \quad \boldsymbol{\Phi}_{i_1} = \boldsymbol{\Phi}_{i_2} \ . \tag{2.22}$$

We assume that $\theta_{s,i} = \theta_{m,i} = 0$ for all i when the HDOF manipulator shape a line. This means that the origin of joint angles corresponds to the reference of manipulator's shapes, a straight line. From the relation of the adjacent link frames (2.15), $\boldsymbol{\Phi}_i = \boldsymbol{\Phi}_{i-1}$ if $\boldsymbol{R}_{w,i} = \boldsymbol{I}_3$ for all i. Definition (2.16) and the fact $\boldsymbol{R}(\cdot, 0) = \boldsymbol{I}_3$ conclude that if

$$\forall i \in \{1, \cdots, n\} \quad \boldsymbol{Q}_{s,i}\boldsymbol{Q}_i\boldsymbol{Q}_{m,i} = \boldsymbol{I}_3 \ , \tag{2.23}$$

then all link frames of an HDOF manipulator are identical.

Suppose that the constants α_i, β_i, γ_i have been adjusted to satisfy condition (2.23) in the rest of the paper. Under this condition, $\boldsymbol{Q}_i$ is expressed as

$$\boldsymbol{Q}_i = \boldsymbol{Q}_{s,i}{}^T \boldsymbol{Q}_{m,i}{}^T \ . \tag{2.24}$$

Therefore, $\boldsymbol{R}_{w,i}$ is represented as

$$\boldsymbol{R}_{w,i} \ = \ \boldsymbol{R}(\boldsymbol{a}_{s,i}, \theta_{s,i}) \boldsymbol{R}(\boldsymbol{a}_{m,i}, \theta_{m,i}) \ , \tag{2.25}$$

where $\boldsymbol{a}_{s,i}, \boldsymbol{a}_{m,i} \in E^3$ are constant unit vectors defined by

$$\boldsymbol{a}_{s,i} \ := \ \boldsymbol{Q}_{s,i} \boldsymbol{e}_z \ , \tag{2.26}$$

$$\boldsymbol{a}_{m,i} \ := \ \boldsymbol{Q}_{m,i}{}^T \boldsymbol{e}_z \ . \tag{2.27}$$

Note that the constant vector $\boldsymbol{a}_{s,i}$ denotes the Sub-axis of the i-th joint from $\boldsymbol{\Phi}_{i-1}$, while $\boldsymbol{a}_{m,i}$ denotes the Main-axis of the i-th joint from $\boldsymbol{\Phi}_i$. The above expression of $\boldsymbol{R}_{w,i}$ means that $\boldsymbol{R}_{w,i}$ consists of the product of 1DOF rotational action with local rotational axes $\boldsymbol{a}_{s,i}$ and $\boldsymbol{a}_{m,i}$, and fixing these axes $\boldsymbol{a}_{s,i}$, $\boldsymbol{a}_{m,i}$ decides a kinematic strucutre of the manipulator completely.

Conventional Denavit-Hartenberg notation is more general than the notation here because it can also treat the type of manipulators with translational joints. However, Denavit-Hartenberg notation does not work well for our purpose because it is a notation only for describing the tip of a manipulator, but we are interested in all link positions. It is important to note that, in the coordinate frame setting proposed here, we attach the coordinate frames not only to joints but also to links, and we mainly use the link frames to describe the link position. Also we connect links and joints after attaching coordinate frames to them. This careful treatment of kinematics is very important if we try to see asymptotic properties by increase in DOF. This topic will be treated in Chapter **8**.

Differential Kinematics

Suppose joint angles are functions of time, that is, $\theta_{s,i}, \theta_{m,i} : \Re_+ \rightarrow (-\pi \ \pi]$ and $\theta_{s,i}(t)$, $\theta_{m,i}(t)$ denote the joint angles around the sub and main axes of the i-th joint at time t respectively. Then, the time derivative of the i-th link frame is expressed as

$$\dot{\boldsymbol{\Phi}}_i = [\boldsymbol{\omega}_i \times] \boldsymbol{\Phi}_i \ , \tag{2.28}$$

where $\boldsymbol{\omega}_i \in \Re^3$ denotes the angular velocity of the i-th link defined by

$$\boldsymbol{\omega}_i = \boldsymbol{\omega}_{i-1} + \boldsymbol{\Phi}_{i-1} \boldsymbol{a}_{s,i} \dot{\theta}_{s,i} + \boldsymbol{\Phi}_i \boldsymbol{a}_{m,i} \dot{\theta}_{m,i} \ . \tag{2.29}$$

Define the *joint angle pair*, $\boldsymbol{\theta}_i \in \Re^2$ ($i = 1, \cdots, n$), as

$$\boldsymbol{\theta}_i \;:=\; \begin{bmatrix} \theta_{s,i} \\ \theta_{m,i} \end{bmatrix}, \tag{2.30}$$

and also the *joint axis pair*, $\boldsymbol{A}_i \in \Re^{3\times 2}$ ($i = 1, \cdots, n$), as

$$\boldsymbol{A}_i \;:=\; \begin{bmatrix} \boldsymbol{R}_{w,i}{}^T \boldsymbol{a}_{s,i} & \boldsymbol{a}_{m,i} \end{bmatrix}. \tag{2.31}$$

Then, the angular velocity is expressed as

$$\boldsymbol{\omega}_i = \boldsymbol{\omega}_{i-1} + \boldsymbol{\Phi}_i \boldsymbol{A}_i \boldsymbol{\theta}_i. \tag{2.32}$$

We also have local expression of the above:

$${}^i\boldsymbol{\omega}_i = \boldsymbol{R}_{w,i}{}^{Ti-1}\boldsymbol{\omega}_{i-1} + \boldsymbol{A}_i \boldsymbol{\theta}_i. \tag{2.33}$$

2.2.2 Manipulator Dynamics

Ordinarily, we see two aspects of manipulator dynamics, that is, Lagrange formulation and Newton-Euler formulation.

Lagrange Formulation

Define $\boldsymbol{\theta} := \left[\boldsymbol{\theta}_1{}^T \;\cdots\; \boldsymbol{\theta}_n{}^T \right] \in \Re^{2n}$ and assume that we can generate torque $u_{s,i}, u_{m,i} \in \Re$ ($i = 1, \;\cdots, n$) at each revolutional axes of the i-th 2DOF joint. The dynamics of the manipulator with $2n$ degrees of freedom is expressed as

$$\boldsymbol{M}(\boldsymbol{\theta})\,\ddot{\boldsymbol{\theta}} + \boldsymbol{C}(\boldsymbol{\theta}, \dot{\boldsymbol{\theta}})\dot{\boldsymbol{\theta}} + \boldsymbol{g}(\boldsymbol{\theta}) = \boldsymbol{u}\ , \tag{2.34}$$

where $\boldsymbol{u} := [\; u_{s,1}\; u_{m,1}\; \cdots\; u_{s,n}\; u_{m,n}\;]^T \in \Re^{2n}$ is the control input torque vector, $\boldsymbol{M}(\boldsymbol{\theta}) \in \Re^{2n\times 2n}$ is the inertia matrix, $\boldsymbol{C}(\boldsymbol{\theta}, \dot{\boldsymbol{\theta}}) \in \Re^{2n\times 2n}$ is the matrix related to the Coriolis and centrifugal forces, and $\boldsymbol{g}(\boldsymbol{\theta}) \in \Re^{2n}$ is the gravitational torque vector. Throughout this paper, friction torques are neglected.

This dynamics has the following properties [4]:

Property 1 (Manipulator Dynamics)

1. There exist positive constants M_m and M_M such that

$$M_m \le \|\boldsymbol{M}(\boldsymbol{\theta})\| \le M_M, \tag{2.35}$$

for any $\boldsymbol{\theta}$.

2. There exists a positive constant C_M such that

$$\|\boldsymbol{C}(\boldsymbol{\theta}, \boldsymbol{x})\| \leq C_M \|\boldsymbol{x}\|, \tag{2.36}$$

for any $\boldsymbol{\theta}$ and $\boldsymbol{x} \in \Re^{2n}$.

3. For any $\boldsymbol{x}$, $\boldsymbol{y}$, $\boldsymbol{z} \in \Re^{2n}$ and $\alpha \in \Re$, $\boldsymbol{C}(\cdot, \cdot)$ satisfies

$$\boldsymbol{C}(\boldsymbol{\theta}, \boldsymbol{x})\boldsymbol{y} = \boldsymbol{C}(\boldsymbol{\theta}, \boldsymbol{y})\boldsymbol{x}, \tag{2.37}$$

$$\boldsymbol{C}(\boldsymbol{\theta}, \boldsymbol{z} + \alpha\boldsymbol{x})\boldsymbol{y} = \boldsymbol{C}(\boldsymbol{\theta}, \boldsymbol{z})\boldsymbol{y} + \alpha\boldsymbol{C}(\boldsymbol{\theta}, \boldsymbol{x})\boldsymbol{y}. \tag{2.38}$$

4. The matrix $\dot{\boldsymbol{M}}(\boldsymbol{\theta}, \dot{\boldsymbol{\theta}}) - 2\boldsymbol{C}(\boldsymbol{\theta}, \dot{\boldsymbol{\theta}})$ is skew symmetric for any $\boldsymbol{\theta}$ and $\dot{\boldsymbol{\theta}}$. □

Newton-Euler Formulation

Let m_i, $\boldsymbol{r}_i$, $\boldsymbol{I}_i$, be the mass, the center of mass, the inertia tensor of the i-th link with respect to the base frame respectively.

The position of the center of mass of the i-th link is expressed by

$$\boldsymbol{p}_{c,i} := \boldsymbol{p}_{i-1} + \boldsymbol{r}_i \ . \tag{2.39}$$

Newton-Euler equation is given by

$$\boldsymbol{f}_i = m_i \ddot{\boldsymbol{p}}_{c,i} + \boldsymbol{f}_{i+1} \ , \tag{2.40}$$

$$\boldsymbol{n}_i = \boldsymbol{I}_i \dot{\boldsymbol{\omega}}_i + \boldsymbol{\omega}_i \times (\boldsymbol{I}_i \boldsymbol{\omega}_i) + \boldsymbol{r}_i \times \left(m_i \ddot{\boldsymbol{p}}_{c,i}\right) + (l_i \boldsymbol{\Phi}_i \boldsymbol{e}_x) \times \boldsymbol{f}_{i+1} + \boldsymbol{n}_{i+1} \ . \tag{2.41}$$

where $\boldsymbol{f}_i, \boldsymbol{n}_i \in E^3$ denote the force and the moment exerted on the i-th link respectively. Let $\boldsymbol{u}_i := [u_{s,i} \ u_{m,i}]^T \in \Re^2$ be the driving torque of the i-th 2DOF joint. Then, $\boldsymbol{u}_i$ is

$$\boldsymbol{u}_i = {\boldsymbol{A}_i}^T {\boldsymbol{\Phi}_i}^T \boldsymbol{n}_i. \tag{2.42}$$

We call $\boldsymbol{u}_i$ the *joint torque pair*.

Let ${}^i\boldsymbol{r}_i$, ${}^i\boldsymbol{I}_i$, be the center of mass, the inertia tensor of the i-th link with respect to the i-th frame respectively. The position of the center of mass of the i-th link with respect to the i-th frame is expressed by

$${}^i\boldsymbol{p}_{c,i} := {\boldsymbol{R}_{w,i}}^{Ti} \boldsymbol{p}_{i-1} + {}^i\boldsymbol{r}_i \ . \tag{2.43}$$

Note that ${}^i\boldsymbol{r}_i$ is a constant vector. Hence, we obtain the local expression of Newton-Euler equations:

$$
\begin{aligned}
{}^i\boldsymbol{f}_i &= m_i {}^i\ddot{\boldsymbol{p}}_{c,i} + \boldsymbol{R}_{w,i+1}{}^{i+1}\boldsymbol{f}_{i+1} \ , && (2.44)\\
{}^i\boldsymbol{n}_i &= {}^i\boldsymbol{I}_i {}^i\dot{\boldsymbol{\omega}}_i + \boldsymbol{\omega}_i \times \left({}^i\boldsymbol{I}_i {}^i\boldsymbol{\omega}_i\right) + {}^i\boldsymbol{r}_i \times \left(m_i {}^i\ddot{\boldsymbol{p}}_{c,i}\right) \\
&\quad + l_i \boldsymbol{e}_x \times \left(\boldsymbol{R}_{w,i+1}{}^{i+1}\boldsymbol{f}_{i+1}\right) + \boldsymbol{R}_{w,i+1}{}^{i+1}\boldsymbol{n}_{i+1} \ , && (2.45)
\end{aligned}
$$

and another expression of joint torque pair:

$$
\boldsymbol{u}_i = \boldsymbol{A}_i{}^{T\,i}\boldsymbol{n}_i. \qquad (2.46)
$$

where ${}^i\boldsymbol{f}_i, {}^i\boldsymbol{n}_i \in E^3$ are the local expressions of the force and the moment respectively.

Summary

The representation of spatial curves, and kinematic and dynamics models of HDOF manipulators were shown. The proposed kinematics for HDOF manipulators was based on the geometric notation different from the conventional Denavit-Hartenberg notation. We will see in Chapter **8** this kinematics is strongly related to Frenet-Serret formula and enables a new analysis to find essentials of an HDOF manipulator.

Chapter 3

Shape Correspondence

We understand intuitively "shape" of a manipulator and "shape" of a spatial curve. But, there is no proper definition of these "shape" and the correspondence between them. In this chapter, we discuss the shape correspondence between an HDOF manipulator and a spatial curve, and also provide important theorems related to "shape".

In Section **3.1**, we rigorously define the shape correspondence between a manipulator and a spatial curve by using the solution of a nonlinear optimization problem termed the shape inverse problem. In Section **3.2**, we discuss the existence of the solution of the shape inverse problem. In Section **3.3**, we change our viewpoint from local Newton-Euler formulation to global Lagrangian formulation, and define the shape Jacobian and analyze its properties. A theorem on an existence region of the solution of the shape inverse problem is given in Section **3.4** under an assumption on the shape Jacobian. In the first four sections in this chapter, we only consider time invariant curves. In Section **3.5**, we extend the obtained results for time invariant curves to the case of time-varying curves.

3.1 Shape Inverse Problem

Suppose that there is an HDOF manipulator in E^3 whose kinematics is given in Section **2.2.1**. Also suppose that there is a "desired shape" in E^3 described by a spatial parametric curve $\boldsymbol{c} : \Re \rightarrow E^3$. What we would like to do here is to give a reasonable expression meaning that "shape" of an HDOF manipulator corresponds to "desired shape" prescribed by a spatial curve.

We start our discussion of shape correspondence from a natural requirement that if a "shape" of an HDOF manipulator corresponds to a "desired shape", then all the link positions of the HDOF manipulator are on the curve prescribing the "desired shape". The

apodosis above can be expressed as

$$\forall i \in \{1, \cdots, n\} \quad \boldsymbol{p}_i(\boldsymbol{\theta}) = \boldsymbol{c}({\sigma_i}^*), \tag{3.1}$$

where ${\sigma_i}^*$ ($i = 1, \cdots, n$) is a solution of the following equations:

$$\boldsymbol{c}({\sigma_0}^*) = \mathbf{o}, \tag{3.2}$$

$$\|\boldsymbol{c}({\sigma_i}^*) - \boldsymbol{c}({\sigma_{i-1}}^*)\| = l_i, \quad i = 1, \cdots, n, \tag{3.3}$$

and ${\sigma_0}^* = 0$, because $\boldsymbol{c}({\sigma_i}^*)$ is under the kinematic constraints of a manipulator. From (2.20), the kinematic constraints of a manipulator can be written as

$$\boldsymbol{p}_0 = \mathbf{o}, \tag{3.4}$$

$$\left\|\boldsymbol{p}_i(\boldsymbol{\theta}) - \boldsymbol{p}_{i-1}(\boldsymbol{\theta})\right\| = l_i, \quad i = 1, \cdots, n, \tag{3.5}$$

and we obtain (3.2), (3.3) by replacing $\boldsymbol{p}_i$ with $\boldsymbol{c}({\sigma_i}^*)$.

In other words, expression (3.1) requires that a given spatial curve becomes one of the interpolated curves of a sequence of link positions, $\{\boldsymbol{p}_1, \cdots, \boldsymbol{p}_n\}$. Expression (3.1) can be rewritten into a more geometric form. From (2.15), (2.20) and (3.3), we obtain

$$\boldsymbol{R}_{w,i}(\theta_{s,i}, \theta_{m,i})\boldsymbol{e}_x = {\boldsymbol{\Phi}_{i-1}}^T \frac{\boldsymbol{c}({\sigma_i}^*) - \boldsymbol{c}({\sigma_{i-1}}^*)}{\|\boldsymbol{c}({\sigma_i}^*) - \boldsymbol{c}({\sigma_{i-1}}^*)\|}. \tag{3.6}$$

In this expression, both sides of the equation are interpreted as points on the unit sphere which has the center at $\boldsymbol{c}({\sigma_{i-1}}^*)$ and the radius of $l_i = \|\boldsymbol{c}({\sigma_i}^*) - \boldsymbol{c}({\sigma_{i-1}}^*)\|$.

However, expression (3.1) does not imply shape correspondence between manipulator and spatial curve, because undesirable situations may occur even if (3.1) is satisfied. In other words, (3.1) is necessary for shape correspondence, but not sufficient.

For example, a manipulator may be *ill-ordered* on the curve as shown in Figure 3.1-(b) even if (3.1) is satisfied. Moreover, a manipulator may take a *shortcut* on the curve as shown in Figure 3.2 even if (3.3) is satisfied and the manipulator is not ill-ordered. Existence of these undesirable situations is related to the fact that equation (3.3) has generally multiple solutions. Multiplicity of solutions also occurs in equation (3.1) due to the indefiniteness of joint angles with a period of 2π. Thus, we need more careful treatments on its definition.

Ill-ordered situation can be described by

$$\exists i \quad {\sigma_{i-1}}^* > {\sigma_i}^*. \tag{3.7}$$

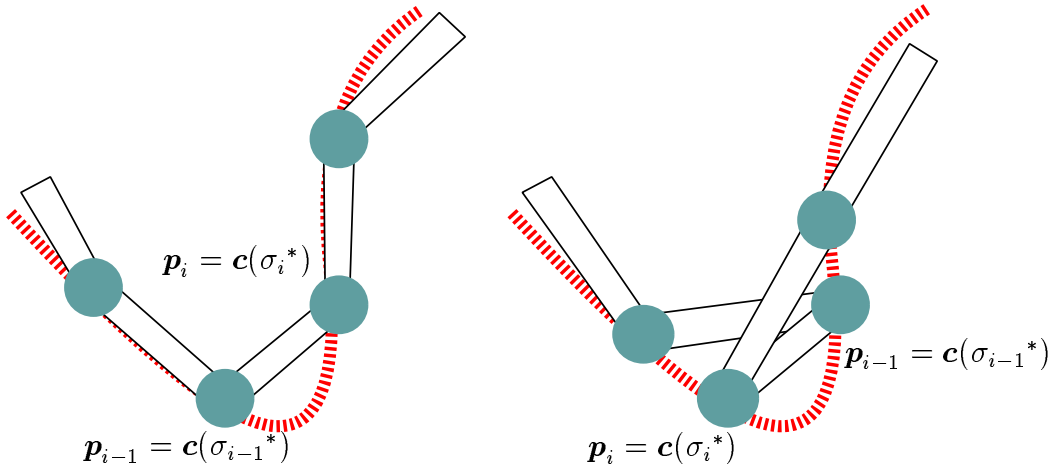

(a) well-ordered (b) ill-ordered

Figure 3.1: Well-ordered and ill-ordered situations

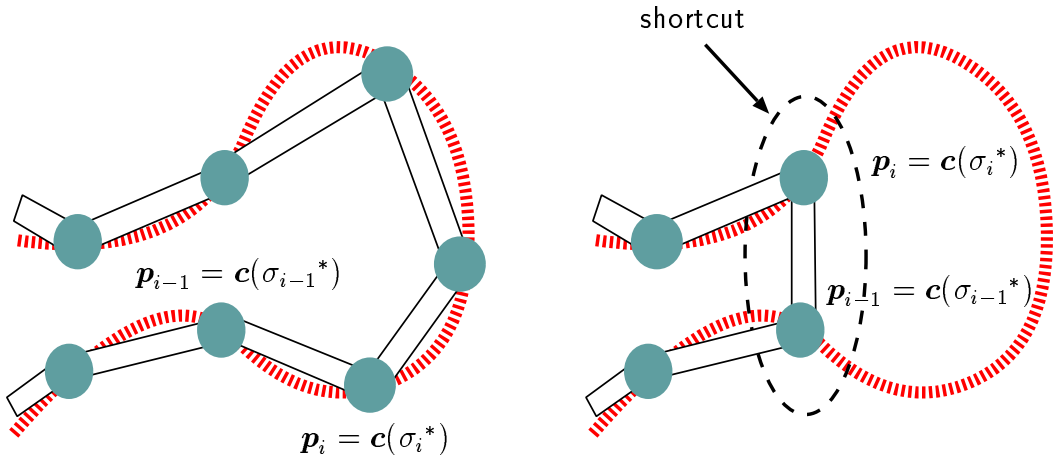

Figure 3.2: Shortcut situation

Thus, if we restrict the order of curve parameters as

$$0 = {\sigma_0}^* < {\sigma_1}^* < \cdots < {\sigma_n}^*, \tag{3.8}$$

or equivalently,

$$\forall i \in \{1, \cdots, n\} \quad 0 < {\sigma_i}^* - {\sigma_{i-1}}^*, \tag{3.9}$$

then the manipulator is *well-ordered* on the curve like Figure 3.1-(a).

In the case of shortcut situation, we can always find a less value of curve parameter, σ_i than ${\sigma_i}^*$ satisfying equation (3.3), i.e.,

$$\exists \sigma_i \in \Re \quad ({\sigma_{i-1}}^* < \sigma_i < {\sigma_i}^*) \wedge (\|\boldsymbol{c}(\sigma_i) - \boldsymbol{c}({\sigma_{i-1}}^*)\| = l_i)\,. \tag{3.10}$$

Therefore, if we find a solution minimizing the interval between the adjacent curve parameters:

$$|{\sigma_i}^* - {\sigma_{i-1}}^*|\,, \qquad i = 1,\ \cdots,\ n, \tag{3.11}$$

then shortcut situation never occurs.

The indefiniteness of the joint angles also can be avoided if we find a solution minimizing

$$\|\boldsymbol{\theta}_i\|\,, \qquad i = 1,\ \cdots,\ n. \tag{3.12}$$

where $\boldsymbol{\theta}_i := [\ \theta_{s,i}\ \theta_{m,i}]^{\,T} \in \Re^2$.

Here we state the *shape inverse problem* and define shape correspondence between manipulator and spatial curve rigorously by using the solution of the shape inverse problem as follows:

Problem 1 (Shape Inverse Problem)

Consider

1. an HDOF manipulator with the kinematics stated in Section **2.2.1**, and
2. a curve $\boldsymbol{c} : \Re \rightarrow E^3$ satisfying **Assumption 1**.

For $i = 1$ to n in turn, find the pair of joint angles, $\boldsymbol{\theta}_i^* := [\ {\theta_{s,i}}^*\ {\theta_{m,i}}^*\ ]^{\,T} \in \Re^2$, minimizing

$$\|\boldsymbol{\theta}_i\|\,, \tag{3.13}$$

subject to

$$\boldsymbol{R}_{w,i}(\theta_{s,i}, \theta_{m,i})\boldsymbol{e}_x = {\boldsymbol{\Phi}_{i-1}}^T \frac{\boldsymbol{c}({\sigma_i}^*) - \boldsymbol{c}({\sigma_{i-1}}^*)}{\|\boldsymbol{c}({\sigma_i}^*) - \boldsymbol{c}({\sigma_{i-1}}^*)\|}, \tag{3.14}$$

where ${\sigma_i}^*$ is the curve parameter minimizing

$$|{\sigma_i}^* - {\sigma_{i-1}}^*|, \tag{3.15}$$

subject to

$${\sigma_i}^* - {\sigma_{i-1}}^* > 0, \tag{3.16}$$

$$\|\boldsymbol{c}({\sigma_i}^*) - \boldsymbol{c}({\sigma_{i-1}}^*)\| = l_i. \tag{3.17}$$

We call $\boldsymbol{\theta}^* := [{\boldsymbol{\theta}_1}^{*T} \cdots {\boldsymbol{\theta}_n}^{*T}]^T \in \Re^{2n}$ the *desired joint angle* and $\boldsymbol{\sigma}^* := [{\sigma_1}^* \cdots {\sigma_n}^*]^T \in \Re^n$ the *desired curve parameter.* □

Definition 1 (Shape Correspondence)

Let $\boldsymbol{\theta}^*$ be the desired joint angle, that is, the solution of the shape inverse problem. An HDOF manipulator is said to be of shape correspondence with curve $\boldsymbol{c} : \Re \to E^3$ if the manipulator has the joint angle, $\boldsymbol{\theta}^*$. □

As stated above, the desired joint angle which defines the shape correspondence is obtained by solving two nonlinear optimization problems in turn. The problem solving the desired curve parameter has a geometric meaning to find the first intersection between the curve and the spherical surface which has the center at $\boldsymbol{c}({\sigma_{i-1}}^*)$ and the radius of l_i. The other problem solving the desired joint angle means finding joint angles of the i-th 2DOF joint such that the i-th link direction is aligned to the line connecting $\boldsymbol{c}({\sigma_{i-1}}^*)$ and $\boldsymbol{c}({\sigma_i}^*)$. It is one of remarkable features that the shape inverse problem is to be solved recursively with respect to link (or joint) number, i, and written with vectors in E^3 and matrices in $SO(3)$. This enables us to understand the geometric meaning of two sub-problems in Euclidean space. It is also important to notice that we can explicitly describe the undesirable ill-ordered and shortcut situations shown in Figure 3.1 and Figure 3.2 due to the parametric representation of curves, which leads us to the rigorous statement of the shape inverse problem.

3.2 Existence Theorem

The solution of the shape inverse problem does not necessarily exist. Thus, we need to give some conditions to assure the existence of the solution.

First, we make the following assumption on manipulator kinematics and spatial curves:

Assumption 3 (Manipulator Kinematics and Spatial Curves)

The following two conditions hold:

1. The curvature of a given spatial curve is bounded by the half of the reciprocal of the maximum link length, i.e.,

$$\sup_{\sigma\in\Re}\kappa(\sigma) \leq \frac{1}{2\max\limits_{i\in\{1,\cdots,n\}} l_i} \ , \tag{3.18}$$

where $\kappa : \Re \to \Re_+$ is the curvature function of the curve and l_i denotes the i-th link length.

2. Each Main-axis is perpendicular to the link direction, and each Sub-axis is perpendicular to the corresponding Main-axis, i.e.,

$$\forall i \in \{1, \cdots, n\} \quad (\boldsymbol{a}_{m,i} \perp \boldsymbol{e}_x) \wedge \left({\boldsymbol{R}_{w,i}}^T \boldsymbol{a}_{s,i} \perp \boldsymbol{a}_{m,i} \right) \ . \tag{3.19}$$

□

The following theorem is valid under **Assumption 3**:

Theorem 1 (Existence Theorem)

Under **Assumption 3**, there exists the solution of the shape inverse problem. □

Proof. The two conditions in **Assumption 3** assure the existence of ${\sigma_i}^*$ at (3.16), (3.17) and ${\boldsymbol{\theta}_i}^*$ at (3.14) respectively. Thus, we show the existence of ${\sigma_i}^*$ under (3.18) first, and the existence of ${\boldsymbol{\theta}_i}^*$ under condition (3.19).

The induction method with respect to i is used for the first proof. Assume that ${\sigma_{i-1}}^*$ exists. From Frenet-Serret formula, we can evaluate $\|\boldsymbol{c}(\sigma_i) - \boldsymbol{c}({\sigma_{i-1}}^*)\|$ as

$$\begin{aligned}
\|\boldsymbol{c}(\sigma_i) - \boldsymbol{c}({\sigma_{i-1}}^*)\| &= \left\| \int_{{\sigma_{i-1}}^*}^{\sigma_i} \frac{d\boldsymbol{c}}{d\sigma}(\sigma) d\sigma \right\| \\
&= \left\| \int_{{\sigma_{i-1}}^*}^{\sigma_i} \boldsymbol{\Phi}(\sigma) \boldsymbol{e}_x d\sigma \right\| \\
&= \left\| \int_{{\sigma_{i-1}}^*}^{\sigma_i} \left(\boldsymbol{\Phi}({\sigma_{i-1}}^*) + \int_{{\sigma_{i-1}}^*}^{\sigma} \frac{d}{ds}\boldsymbol{\Phi}(s) ds \right) \boldsymbol{e}_x d\sigma \right\| \\
&= \left\| \int_{{\sigma_{i-1}}^*}^{\sigma_i} \left(\boldsymbol{\Phi}({\sigma_{i-1}}^*) + \int_{{\sigma_{i-1}}^*}^{\sigma} \boldsymbol{\Phi}(s) \left[\boldsymbol{\omega}(s) \times \right] ds \right) \boldsymbol{e}_x d\sigma \right\| \\
&= \left\| \int_{{\sigma_{i-1}}^*}^{\sigma_i} \left(\boldsymbol{\Phi}({\sigma_{i-1}}^*) \boldsymbol{e}_x + \int_{{\sigma_{i-1}}^*}^{\sigma} \boldsymbol{\Phi}(s) \left[\boldsymbol{\omega}(s) \times \right] \boldsymbol{e}_x ds \right) d\sigma \right\| \\
&= \left\| \int_{{\sigma_{i-1}}^*}^{\sigma_i} \left(\boldsymbol{\Phi}({\sigma_{i-1}}^*) \boldsymbol{e}_x + \int_{{\sigma_{i-1}}^*}^{\sigma} \kappa(s) \boldsymbol{\Phi}(s) \boldsymbol{e}_y ds \right) d\sigma \right\| \\
&= \left\| \left(\int_{{\sigma_{i-1}}^*}^{\sigma_i} d\sigma \right) \boldsymbol{\Phi}({\sigma_{i-1}}^*) \boldsymbol{e}_x + \int_{{\sigma_{i-1}}^*}^{\sigma_i} \left(\int_{{\sigma_{i-1}}^*}^{\sigma} \kappa(s) \boldsymbol{\Phi}(s) \boldsymbol{e}_y ds \right) d\sigma \right\|
\end{aligned}$$

$$
\begin{aligned}
&= \left\| \ (\sigma_i - {\sigma_{i-1}}^*)\, \boldsymbol{\Phi}({\sigma_{i-1}}^*)\boldsymbol{e}_x \right. \\
&\quad \left. + \int_0^{\sigma_i - {\sigma_{i-1}}^*} \left(\int_{{\sigma_{i-1}}^*}^{\sigma + {\sigma_{i-1}}^*} \kappa(s)\boldsymbol{\Phi}(s)\boldsymbol{e}_y ds \right) d\sigma \ \right\| \\
&= \left\| \ (\sigma_i - {\sigma_{i-1}}^*)\, \boldsymbol{\Phi}({\sigma_{i-1}}^*)\boldsymbol{e}_x \right. \\
&\quad \left. + \int_0^{\sigma_i - {\sigma_{i-1}}^*} \left(\int_0^{\sigma} \kappa(s + {\sigma_{i-1}}^*)\boldsymbol{\Phi}(s + {\sigma_{i-1}}^*)\boldsymbol{e}_y ds \right) d\sigma \ \right\| . \qquad (3.20)
\end{aligned}
$$

For $\boldsymbol{a}, \boldsymbol{b} \in \Re^3$,

$$
\|\boldsymbol{a}\| \geq \|\boldsymbol{b}\| \quad \Rightarrow \quad \|\boldsymbol{a} + \boldsymbol{b}\| \geq \|\boldsymbol{a}\| - \|\boldsymbol{b}\| . \qquad (3.21)
$$

Then, we obtain

$$
\begin{aligned}
\|\boldsymbol{c}(\sigma_i) - \boldsymbol{c}({\sigma_{i-1}}^*)\| &\geq (\sigma_i - {\sigma_{i-1}}^*) \\
&\quad - \left\| \int_0^{\sigma_i - {\sigma_{i-1}}^*} \left(\int_0^{\sigma} \kappa(s + {\sigma_{i-1}}^*)\boldsymbol{\Phi}(s + {\sigma_{i-1}}^*)\boldsymbol{e}_y ds \right) d\sigma \right\| \qquad (3.22) \\
&\geq (\sigma_i - {\sigma_{i-1}}^*) \\
&\quad - \int_0^{\sigma_i - {\sigma_{i-1}}^*} \left(\int_0^{\sigma} \|\kappa(s + {\sigma_{i-1}}^*)\boldsymbol{\Phi}(s + {\sigma_{i-1}}^*)\boldsymbol{e}_y\| \, ds \right) d\sigma \\
&\geq (\sigma_i - {\sigma_{i-1}}^*) - \kappa_M \int_0^{\sigma_i - {\sigma_{i-1}}^*} \left(\int_0^{\sigma} ds \right) d\sigma \\
&\geq (\sigma_i - {\sigma_{i-1}}^*) - \kappa_M \int_0^{\sigma_i - {\sigma_{i-1}}^*} \sigma d\sigma \\
&= (\sigma_i - {\sigma_{i-1}}^*) - \frac{\kappa_M}{2} (\sigma_i - {\sigma_{i-1}}^*)^2 \\
&= -\frac{\kappa_M}{2} \left\{ (\sigma_i - {\sigma_{i-1}}^*) - \frac{1}{\kappa_M} \right\}^2 + \frac{1}{2\kappa_M}, \qquad (3.23)
\end{aligned}
$$

where $\kappa_M := \sup \kappa(\sigma)$. Thus, if condition (3.18) is satisfied, i.e.,

$$
\frac{1}{2\kappa_M} \geq l_M, \qquad (3.24)
$$

where $l_M := \max l_i$, then the inequality

$$
\|\boldsymbol{c}(\sigma_i) - \boldsymbol{c}({\sigma_{i-1}}^*)\| \geq l_M, \qquad (3.25)
$$

holds at

$$
\sigma_i = {\sigma_{i-1}}^* + \frac{1}{\kappa_M}. \qquad (3.26)
$$

Since $\boldsymbol{c}$ is continuous, invoking the intermediate value theorem leads to

$$
\exists {\sigma_i}^* \in \left({\sigma_{i-1}}^*, {\sigma_{i-1}}^* + \frac{1}{\kappa_M} \right] \quad \|\boldsymbol{c}({\sigma_i}^*) - \boldsymbol{c}({\sigma_{i-1}}^*)\| = l_i. \qquad (3.27)
$$

On the other hand, from the orthogonality between $\boldsymbol{e}_x$ and $\boldsymbol{a}_{m,i}$, $\boldsymbol{R}(\boldsymbol{a}_{m,i}, \theta_{m,i})\boldsymbol{e}_x$ draws a unit circle when $\theta_{m,i}$ moves from $-\pi$ to π. Thus, from the other orthogonality between $\boldsymbol{a}_{m,i}$ and $\boldsymbol{a}_{s,i}$, $\boldsymbol{R}_{w,i}\boldsymbol{e}_x = \boldsymbol{R}(\boldsymbol{a}_{s,i}, \theta_{s,i})\boldsymbol{R}(\boldsymbol{a}_{m,i}, \theta_{m,i})\boldsymbol{e}_x$ covers a unit sphere when $\theta_{m,i}, \theta_{s,i}$ move from $-\pi$ to π respectively, which means that we can always find $\theta_{s,i}$ and $\theta_{m,i}$ satisfying (3.14). (Q.E.D.)

The first conditon in **Assumption 3** shows the relation between given admissible curves and link length of a manipulator. Let L be the total length of the manipulator, i.e., $L := \sum_i l_i$, and suppose that L is constant. Then we obtain

$$l_M n \geq L, \tag{3.28}$$

where n is the number of DOF of the manipulator. Thus, condition (3.18) also means

$$\kappa_M \leq \frac{n}{2L}, \tag{3.29}$$

which states that the class of admissible curves enlarges as the number of DOF increases. The second condition in **Assumption 3** is related to the mechanical structure of a manipulator. We will discuss how it should be from another theoretical viewpoint in Chapter 8. Notice that the conditions in the theorem also have an effect to remove unnecessary winding curves, although these are quite conservative [†].

3.3 Shape Jacobian

Up to here, we have taken the local Newton-Euler viewpoint. Then, we zoom out to the global Lagrangian viewpoint.

Expression (3.1) can be converted to a more compact form as follows. Define $\boldsymbol{p}(\boldsymbol{\theta}) \in \Re^{3n}$ by arranging all the link positions in a row as

$$\boldsymbol{p}(\boldsymbol{\theta}) := \begin{bmatrix} \boldsymbol{p}_1(\boldsymbol{\theta}) \\ \vdots \\ \boldsymbol{p}_n(\boldsymbol{\theta}) \end{bmatrix}. \tag{3.30}$$

Define also $\boldsymbol{p}_d(\boldsymbol{\sigma}) \in \Re^{3n}$ for a given curve $\boldsymbol{c} : \Re \to E^3$ as

$$\boldsymbol{p}_d(\boldsymbol{\sigma}) := \begin{bmatrix} \boldsymbol{c}(\sigma_1) \\ \vdots \\ \boldsymbol{c}(\sigma_n) \end{bmatrix}, \tag{3.31}$$

[†]The conditions in the existence theorem are quite conservative since we use conservative inequality (3.21).

where $\sigma_i \in \Re$ $(i = 1, \cdots, n)$ is a variable (not the solution of equation (3.3)) and $\boldsymbol{\sigma} := [\sigma_1 \cdots \sigma_n]^T \in \Re^n$. Further define $\boldsymbol{e}(\boldsymbol{\theta}, \boldsymbol{\sigma}) \in \Re^{3n}$ as the difference between them, i.e.,

$$\boldsymbol{e}(\boldsymbol{\theta}, \boldsymbol{\sigma}) \;:=\; \boldsymbol{p}(\boldsymbol{\theta}) - \boldsymbol{p}_d(\boldsymbol{\sigma}). \tag{3.32}$$

Then we obtain a more compact expression of (3.1):

$$\boldsymbol{e}(\boldsymbol{\theta}, \boldsymbol{\sigma}^*) \;=\; \mathbf{o}, \tag{3.33}$$

where $\boldsymbol{\sigma}^*$ is the desired curve parameter. We call $\boldsymbol{p}(\boldsymbol{\theta})$ the *manipulator shape*, $\boldsymbol{p}_d(\boldsymbol{\sigma}^*)$ the *desired shape* and $\boldsymbol{e}(\boldsymbol{\theta}, \boldsymbol{\sigma}^*)$ the *desired shape error*.

Suppose that $\boldsymbol{\theta}$ and $\boldsymbol{\sigma}$ are time functions and differentiable with respect to time t in $\Re_+$. Then, the derivative of $\boldsymbol{e}$ becomes

$$\dot{\boldsymbol{e}}(\boldsymbol{q}, \dot{\boldsymbol{q}}) = \boldsymbol{J}(\boldsymbol{q})\dot{\boldsymbol{q}}, \tag{3.34}$$

where $\boldsymbol{q} := \left[\boldsymbol{\theta}^T \boldsymbol{\sigma}^T\right]^T \in \Re^{3n}$ and the matrix $\boldsymbol{J}(\boldsymbol{q}) \in \Re^{3n \times 3n}$ is defined as

$$\boldsymbol{J}(\boldsymbol{q}) := \left[\begin{array}{cc} \dfrac{\partial \boldsymbol{p}}{\partial \boldsymbol{\theta}}(\boldsymbol{\theta}) & -\dfrac{\partial \boldsymbol{p}_d}{\partial \boldsymbol{\sigma}}(\boldsymbol{\sigma}) \end{array} \right]. \tag{3.35}$$

We call $\boldsymbol{J}(\boldsymbol{q})$ the *Shape Jacobian*. The Shape Jacobian has the following properties:

Property 2 (Shape Jacobian)

1. The norm of the Shape Jacobian is bounded, i.e., there exists a positive constant J_M such that

   $$\forall \boldsymbol{q} \in \Re^{3n} \quad \|\boldsymbol{J}(\boldsymbol{q})\| \leq J_M. \tag{3.36}$$

   Moreover, if $\boldsymbol{J}(\boldsymbol{q})$ is non-singular, then there exists a positive constant J_m such that

   $$\forall \boldsymbol{q} \in \Re^{3n} \quad J_m \leq \|\boldsymbol{J}(\boldsymbol{q})\|. \tag{3.37}$$

2. The Shape Jacobian, $\boldsymbol{J}(\boldsymbol{q})$, is singular if and only if there exists a positive integer, $i \in \{1, \cdots, n\}$, such that at least one of the following two conditions holds:

   (a) Consider the three directions in E^3; the Sub-axis of the i-th joint, the Main-axis of the i-th joint, and the length direction of the i-th link. At least two among the directions align, i.e.,

   $$\det \left[\begin{array}{ccc} \boldsymbol{l}_i & \boldsymbol{R}^T(\boldsymbol{a}_{m,i}, \theta_{m,i})\boldsymbol{a}_{s,i} & \boldsymbol{a}_{m,i} \end{array} \right] = 0, \tag{3.38}$$

   where $\boldsymbol{l}_i := l_i \boldsymbol{e}_x$.

(b) The i-th link direction and the tangent at the point corresponding to the i-th link position cross at right angle, i.e.,

$$\left\{\boldsymbol{p}_i(\boldsymbol{\theta}) - \boldsymbol{p}_{i-1}(\boldsymbol{\theta})\right\}^T \frac{d\boldsymbol{c}}{d\sigma}(\sigma_i) = 0. \tag{3.39}$$

3. Define $\dot{\boldsymbol{J}}(\boldsymbol{q}, \dot{\boldsymbol{q}}) \in \Re^{3n\times 3n}$ as

$$\dot{\boldsymbol{J}}(\boldsymbol{q}, \dot{\boldsymbol{q}}) := \left[\frac{\partial \boldsymbol{J}}{\partial q_1}(\boldsymbol{q})\dot{\boldsymbol{q}} \ \cdots \ \frac{\partial \boldsymbol{J}}{\partial q_{3n}}(\boldsymbol{q})\dot{\boldsymbol{q}}\right]. \tag{3.40}$$

Then, there exists a positive constant J_H such that

$$\forall \boldsymbol{q} \in \Re^{3n} \quad \|\dot{\boldsymbol{J}}(\boldsymbol{q}, \dot{\boldsymbol{q}})\| \leq J_H \|\dot{\boldsymbol{q}}\|. \tag{3.41}$$

Moreover, for any $\boldsymbol{x}, \boldsymbol{y} \in \Re^{3n}$,

$$\dot{\boldsymbol{J}}(\boldsymbol{q}, \boldsymbol{x})\boldsymbol{y} = \dot{\boldsymbol{J}}(\boldsymbol{q}, \boldsymbol{y})\boldsymbol{x}. \tag{3.42}$$

□

Proof. The first and the third properties are immediately concluded from simple calculations and the boundedness of elements in $\boldsymbol{J}(\boldsymbol{q})$ and $\dot{\boldsymbol{J}}(\boldsymbol{q}, \dot{\boldsymbol{q}})$.

For the proof of the second property, let $\boldsymbol{I}_{i,j} \in \Re^{3n\times 3n}$ be the elementary matrix exchanging the i-th line for the j-th. This matrix has properties such that

$$\boldsymbol{I}_{i,j}{}^{-1} = \boldsymbol{I}_{i,j}{}^{T}, \tag{3.43}$$

$$\det \boldsymbol{I}_{i,j} = -1. \tag{3.44}$$

Using this elementary matrix, define $\boldsymbol{P} \in \Re^{3n\times 3n}$ as

$$\begin{aligned}\boldsymbol{P} &:= (\boldsymbol{I}_{2n,2n+1}\boldsymbol{I}_{2n-1,2n}\cdots\boldsymbol{I}_{3,4})\cdot(\boldsymbol{I}_{2n+1,2n+2}\boldsymbol{I}_{2n,2n+1}\cdots\boldsymbol{I}_{6,7}) \\ &\quad \cdots(\boldsymbol{I}_{2n+i-1,2n+i}\boldsymbol{I}_{2n+i-2,2n+i-1}\cdots\boldsymbol{I}_{3i,3i+1})\cdots(\boldsymbol{I}_{3n-2,3n-1}\boldsymbol{I}_{3n-3,3n-2}) \\ &= \prod_{i=1}^{n-1}\prod_{j=1}^{2(n-i)} \boldsymbol{I}_{2n+i-j,2n+i-j+1}.\end{aligned} \tag{3.45}$$

The number of the fundamental matrices appeared in the definition $\boldsymbol{P}$ is

$$\sum_{i=1}^{n-1} 2(n-i) = 2\left\{\sum_{i=1}^{n-1}(n-i)\right\}, \tag{3.46}$$

which is always even. Thus, $\boldsymbol{P}$ has properties:

$$\boldsymbol{P}^{-1} = \boldsymbol{P}^T, \tag{3.47}$$

$$\det \boldsymbol{P} = 1, \tag{3.48}$$

i.e., $\boldsymbol{P} \in SO(3n)$. Furthermore, using this $\boldsymbol{P}$, define $\bar{\boldsymbol{J}}(\boldsymbol{q}) \in \Re^{3n\times 3n}$ as

$$\bar{\boldsymbol{J}}(\boldsymbol{q}) := \boldsymbol{J}(\boldsymbol{q})\boldsymbol{P}. \tag{3.49}$$

Then, $\bar{\boldsymbol{J}}(\boldsymbol{q})$ can be represented as the following lower-triangular 3×3-block matrix:

$$\bar{\boldsymbol{J}} = \begin{bmatrix} \boldsymbol{J}_{11} & & & \\ \boldsymbol{J}_{21} & \boldsymbol{J}_{22} & & \\ \vdots & \vdots & \ddots & \\ \boldsymbol{J}_{n1} & \boldsymbol{J}_{n2} & \cdots & \boldsymbol{J}_{nn} \end{bmatrix}, \tag{3.50}$$

where $\boldsymbol{J}_{ij} \in \Re^{3\times 3}$ is defined as

$$\boldsymbol{J}_{ij} := \begin{cases} \begin{bmatrix} \dfrac{\partial \boldsymbol{p}_i}{\partial \theta_{s,j}}(\boldsymbol{\theta}) & \dfrac{\partial \boldsymbol{p}_i}{\partial \theta_{m,j}}(\boldsymbol{\theta}) & -\dfrac{d\boldsymbol{c}}{d\sigma}(\sigma_i) \end{bmatrix}, & i = j\ , \\ \begin{bmatrix} \dfrac{\partial \boldsymbol{p}_i}{\partial \theta_{s,j}}(\boldsymbol{\theta}) & \dfrac{\partial \boldsymbol{p}_i}{\partial \theta_{m,j}}(\boldsymbol{\theta}) & \mathbf{o} \end{bmatrix}, & i > j\ . \end{cases} \tag{3.51}$$

Thus, we obtain

$$\begin{aligned} \det \boldsymbol{J}(\boldsymbol{q}) &= \det \bar{\boldsymbol{J}}(\boldsymbol{q}) \\ &= \det \begin{bmatrix} \boldsymbol{J}_{11} & & & \\ \boldsymbol{J}_{21} & \boldsymbol{J}_{22} & & \\ \vdots & \vdots & \ddots & \\ \boldsymbol{J}_{n1} & \boldsymbol{J}_{n2} & \cdots & \boldsymbol{J}_{nn} \end{bmatrix} \\ &= \prod_{i=1}^{n} \det \boldsymbol{J}_{ii} \\ &= \prod_{i=1}^{n} \det \begin{bmatrix} \dfrac{\partial \boldsymbol{p}_i}{\partial \theta_{s,i}} & \dfrac{\partial \boldsymbol{p}_i}{\partial \theta_{m,i}} & -\dfrac{d\boldsymbol{c}}{d\sigma}(\sigma_i) \end{bmatrix} \\ &= (-1)^n \prod_{i=1}^{n} \left\{ \left(\frac{\partial \boldsymbol{p}_i}{\partial \theta_{s,i}} \times \frac{\partial \boldsymbol{p}_i}{\partial \theta_{m,i}} \right)^T \frac{d\boldsymbol{c}}{d\sigma}(\sigma_i) \right\}. \end{aligned}$$

The partial derivatives of $\boldsymbol{p}_i$ with respect to $\theta_{s,i}$ and $\theta_{m,i}$ are calculated as

$$\frac{\partial \boldsymbol{p}_i}{\partial \theta_{s,i}} = \boldsymbol{\Phi}_i \left[\boldsymbol{R}^T(\boldsymbol{a}_{m,i}, \theta_{m,i}) \boldsymbol{a}_{s,i} \times \right] \boldsymbol{l}_i, \tag{3.52}$$

$$\frac{\partial \boldsymbol{p}_i}{\partial \theta_{m,i}} = \boldsymbol{\Phi}_i \left[\boldsymbol{a}_{m,i} \times \right] \boldsymbol{l}_i. \tag{3.53}$$

Therefore, since

$$\begin{aligned} \frac{\partial \boldsymbol{p}_i}{\partial \theta_{s,i}} \times \frac{\partial \boldsymbol{p}_i}{\partial \theta_{m,i}} &= \left\{ \boldsymbol{\Phi}_i \left[\boldsymbol{R}^T(\boldsymbol{a}_{m,i}, \theta_{m,i}) \boldsymbol{a}_{s,i} \times \right] \boldsymbol{l}_i \right\} \times \left\{ \boldsymbol{\Phi}_i \left[\boldsymbol{a}_{m,i} \times \right] \boldsymbol{l}_i \right\} \\ &= \boldsymbol{\Phi}_i \left[\left\{ \left(\boldsymbol{R}^T(\boldsymbol{a}_{m,i}, \theta_{m,i}) \boldsymbol{a}_{s,i} \right) \times \boldsymbol{l}_i \right\} \times \left\{ \boldsymbol{a}_{m,i} \times \boldsymbol{l}_i \right\} \right] \end{aligned}$$

$$
\begin{aligned}
&= \boldsymbol{\Phi}_i \Big\{ \det \left[\begin{array}{cccc} \boldsymbol{R}^T(\boldsymbol{a}_{m,i}, \theta_{m,i}) \boldsymbol{a}_{s,i} & \boldsymbol{l}_i & \boldsymbol{l}_i \end{array} \right] \boldsymbol{a}_{m,i} \\
&\quad - \det \left[\begin{array}{cccc} \boldsymbol{R}^T(\boldsymbol{a}_{m,i}, \theta_{m,i}) \boldsymbol{a}_{s,i} & \boldsymbol{l}_i & \boldsymbol{a}_{m,i} \end{array} \right] \boldsymbol{l}_i \Big\} \\
&= \det \left[\begin{array}{cccc} \boldsymbol{l}_i & \boldsymbol{R}^T(\boldsymbol{a}_{m,i}, \theta_{m,i}) \boldsymbol{a}_{s,i} & \boldsymbol{a}_{m,i} \end{array} \right] \boldsymbol{\Phi}_i \boldsymbol{l}_i \\
&= \det \left[\begin{array}{cccc} \boldsymbol{l}_i & \boldsymbol{R}^T(\boldsymbol{a}_{m,i}, \theta_{m,i}) \boldsymbol{a}_{s,i} & \boldsymbol{a}_{m,i} \end{array} \right] (\boldsymbol{p}_i - \boldsymbol{p}_{i-1}), \qquad (3.54)
\end{aligned}
$$

then we obtain

$$
\det \boldsymbol{J}(\boldsymbol{q}) = (-1)^n \prod_{i=1}^{n} \left\{ \det \left[\begin{array}{cccc} \boldsymbol{l}_i & \boldsymbol{R}^T(\boldsymbol{a}_{m,i}, \theta_{m,i}) \boldsymbol{a}_{s,i} & \boldsymbol{a}_{m,i} \end{array} \right] (\boldsymbol{p}_i - \boldsymbol{p}_{i-1})^T \frac{d\boldsymbol{c}}{d\sigma}(\sigma_i) \right\}, \quad (3.55)
$$

which completes the proof. (Q.E.D.)

There are three remarkable points for the second property. First, the singularity condition of the Shape Jacobian can be described by completely separated n conditions for each link, joint and curve parameter. This is very helpful for the calculation. Second, each completely separated condition is further devided into two distinguished parts. One part, described by (3.38), is only related to the mechanical structure and joint angles, while the other, (3.39), depends on the tangent of the curve. Finally, the derived conditions (3.38) and (3.39) have geometric meaning in Euclidean space. That is, they can be explained by the geometric relation of vectors (e.g. inner product etc.) in Euclidean space (see Figure 3.3).

3.4 Existence Region Theorem

As mentioned before, the shape inverse problem is a kind of nonlinear optimization problems, which means that we can not expect to obtain any analytical solution. Thus, we have to use numerical methods in order to find some solutions. However, under a mild condition, $\boldsymbol{e} = \mathbf{o}$ implies the shape correspondence in a local region.

First we make the following assumption on the Shape Jacobian:

Assumption 4 (Shape Jacobian)

The Shape Jacobian is non-singular for the desired joint angle and curve parameter, $(\boldsymbol{\theta}^*, \boldsymbol{\sigma}^*)$, i.e.,

$$
\det \boldsymbol{J}(\boldsymbol{\theta}^*, \boldsymbol{\sigma}^*) \neq \mathbf{o}. \qquad (3.56)
$$

□

Now we state the following theorem on existence region of the shape inverse problem:

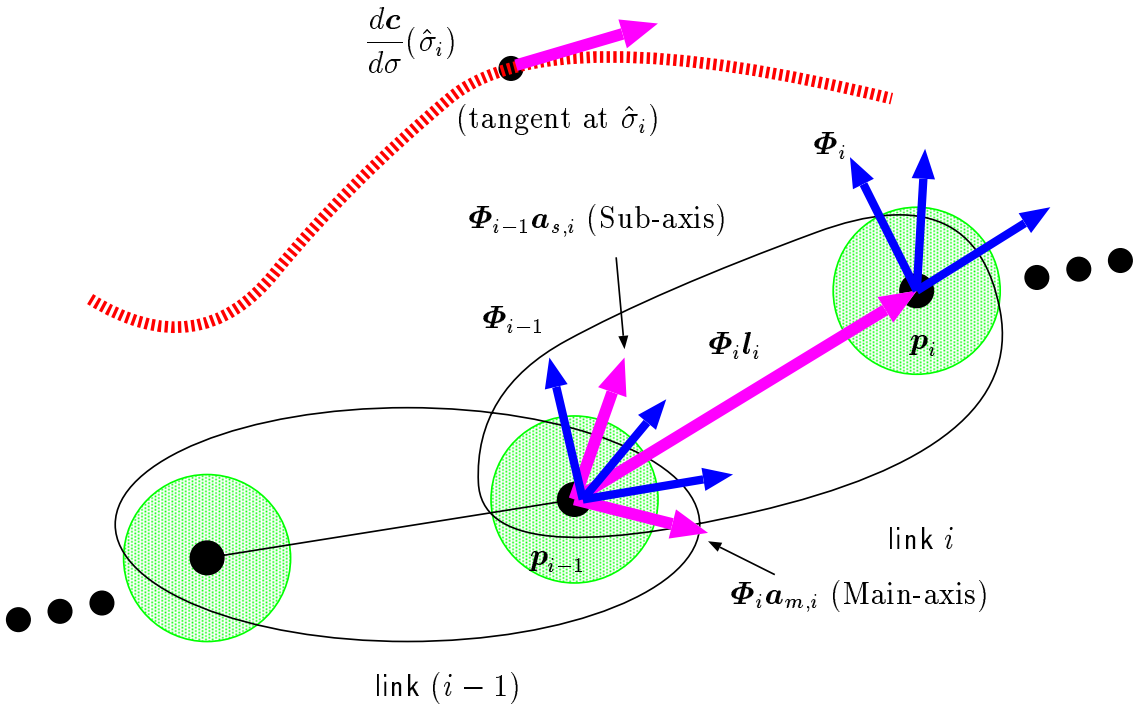

Figure 3.3: Geometrical meaning of singularities of the Shape Jacobian

Theorem 2 (Existence Region)

Define $\mathcal{D}_\delta \subset \Re^{3n}$ as

$$\mathcal{D}_\delta := \left\{ (\boldsymbol{\theta}, \boldsymbol{\sigma}) \in \Re^{3n} \,\middle|\, |\theta_{s,i}| < \pi,\ |\theta_{m,i}| < \pi,\ \delta < \sigma_i - \sigma_{i-1} < \frac{1}{\kappa_M} \right\}, \tag{3.57}$$

where $\delta \in [-l_M \ l_M]$. Then, under **Assumption 3** and **Assumption 4**, there exists a unique solution satisfying that

$$\boldsymbol{e}(\boldsymbol{\theta}, \boldsymbol{\sigma}) = \mathbf{o}, \tag{3.58}$$

$$(\boldsymbol{\theta}, \boldsymbol{\sigma}) \in \mathcal{D}_\delta, \tag{3.59}$$

for any δ. Moreover, the solution is exactly the pair of the desired joint angle and curve parameter, $(\boldsymbol{\theta}^*, \boldsymbol{\sigma}^*)$. □

Proof. We can evaluate $\|\boldsymbol{c}(\sigma_i) - \boldsymbol{c}({\sigma_{i-1}}^*)\|$ as

$$-\frac{\kappa_M}{2}\left\{\left(\sigma_i - \sigma_{i-1}^*\right) - \frac{1}{\kappa_M}\right\}^2 + \frac{1}{2\kappa_M} \le \|\boldsymbol{c}(\sigma_i) - \boldsymbol{c}({\sigma_{i-1}}^*)\| \le \sigma_i - {\sigma_{i-1}}^*, \tag{3.60}$$

from (3.20) and (3.23). Figure 3.4 shows the existence region of $\|\boldsymbol{c}(\sigma_i) - \boldsymbol{c}({\sigma_{i-1}}^*)\|$ by the shaded region. We choose $\Delta\sigma_i := \sigma_i - {\sigma_{i-1}}^*$ as the horizontal axis. The values ${\Delta\sigma_i}^*$ and ${\Delta\sigma_i}^{**}$ denote the intersections between the lower bound of $\|\boldsymbol{c}(\sigma_i) - \boldsymbol{c}({\sigma_{i-1}}^*)\|$ and

line $\|\boldsymbol{c}(\sigma_i) - \boldsymbol{c}({\sigma_{i-1}}^*)\| = l_M$. Thus, ${\Delta\sigma_i}^*$ corresponds to the optimal solution. From this figure, for any $\delta \in [-l_M \; l_M]$

$$\delta < {\sigma_i}^* - {\sigma_{i-1}}^* < \frac{1}{\kappa_M}, \tag{3.61}$$

under condition (3.18). Inequality (3.61) shows that there exists a unique solution of (3.17) in the interval $\left(\delta \; \frac{1}{\kappa_M}\right)$.

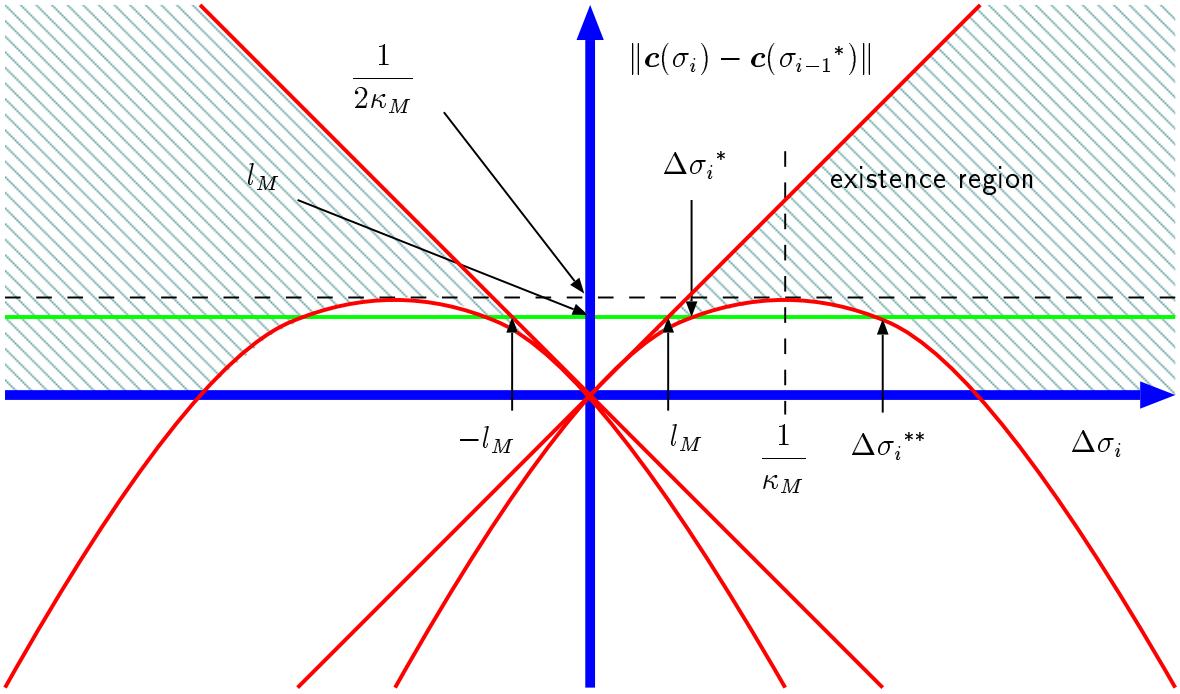

Figure 3.4: Solution of the shape inverse problem

Non-singularity of the Shape Jacobian, which states the isolation of the solution of $\boldsymbol{e} = \mathbf{o}$, and the orthogonality of joint axes assure that there exist unique solutions $\theta_{s,i}$ and $\theta_{m,i}$ in $(-\pi \; \pi)$. (Q.E.D.)

We will see that this theorem is successfully used for control purposes in later chapters.

3.5 Extension to the Case of Time-varying Curves

The obtained results for time invariant curves in this chapter can be extended to the case of time-varying curves.

Extended shape inverse problem for time-varying curves is stated as follows:

Problem 2 (Extended Shape Inverse Problem)

Consider

1. an HDOF manipulator with the kinematics stated in Section **2.2.1**, and

2. a curve $\boldsymbol{c} : \Re \times \Re_+ \rightarrow E^3$ satisfying **Assumption 2**.

For $i = 1$ to n in turn, find the pair of continuous joint angle functions, $\boldsymbol{\theta}_i{}^*(t) := [\ \theta_{s,i}{}^*(t)\ \theta_{m,i}{}^*(t)\ ]^T$, minimizing

$$\frac{1}{T}\int_0^T \|\boldsymbol{\theta}_i(t)\|\, dt, \tag{3.62}$$

for the time interval $[0\ T]$, subject to

$$\boldsymbol{R}_{w,i}(\theta_{s,i}(t), \theta_{m,i}(t))\boldsymbol{e}_x = \boldsymbol{\Phi}_{i-1}{}^T \frac{\boldsymbol{c}(\sigma_i{}^*(t), t) - \boldsymbol{c}(\sigma_{i-1}{}^*(t), t)}{\|\boldsymbol{c}(\sigma_i{}^*(t), t) - \boldsymbol{c}(\sigma_{i-1}{}^*(t), t)\|}, \tag{3.63}$$

where $\sigma_i{}^*(t)$ is the curve parameter function minimizing

$$\frac{1}{T}\int_0^T |\sigma_i{}^*(t) - \sigma_{i-1}{}^*(t)|\, dt, \tag{3.64}$$

subject to

$$\sigma_i{}^*(t) - \sigma_{i-1}{}^*(t) \ > \ 0, \tag{3.65}$$

$$\|\boldsymbol{c}(\sigma_i{}^*(t), t) - \boldsymbol{c}(\sigma_{i-1}{}^*(t), t)\| \ = \ l_i. \tag{3.66}$$

We call $\boldsymbol{\theta}^*(t) := [\boldsymbol{\theta}_1{}^{*T}(t)\ \cdots\ \boldsymbol{\theta}_n{}^{*T}(t)]^T$ the *desired joint angle function* and $\boldsymbol{\sigma}^*(t) := [\sigma_1{}^*(t) \cdots \sigma_n{}^*(t)]^T$ the *desired curve parameter function.* □

Definition 2 (Shape Correspondence at Time t)

Let $\boldsymbol{\theta}^*(t)$ be the desired joint angle, that is, the solution of the shape inverse problem. An HDOF manipulator is said to be of shape correspondence with curve $\boldsymbol{c} : \Re \times \Re_+ \rightarrow E^3$ at time t if the manipulator has the joint angle, $\boldsymbol{\theta}^*(t)$ at time t. □

First, we make the following assumption on manipulator kinematics and spatial curves:

Assumption 5 (Manipulator Kinematics and Time-varying Curves)

The following two conditions hold:

1. The curvature of a given spatial curve is bounded by the half of the reciprocal of the maximum link length, i.e.,

$$\sup_{\sigma \in \Re, t \in \Re_+} \kappa(\sigma, t) \leq \frac{1}{2 \max\limits_{i \in \{1, \cdots, n\}} l_i}\ , \tag{3.67}$$

   where $\kappa : \Re \times \Re_+ \rightarrow \Re_+$ is the curvature function of the curve and l_i denotes the i-th link length.

2. Each Main-axis is perpendicular to the link direction, and each Sub-axis is perpendicular to the corresponding Main-axis, i.e.,

$$\forall i \in \{1, \cdots, n\} \quad (\boldsymbol{a}_{m,i} \perp \boldsymbol{e}_x) \wedge \left({\boldsymbol{R}_{w,i}}^T \boldsymbol{a}_{s,i} \perp \boldsymbol{a}_{m,i} \right) \ . \tag{3.68}$$

□

Obviously from **Theorem 1**, this assumption assures that there exists the solution of the shape inverse problem for any t.

The following theorem is valid under **Assumption 5**:

Theorem 3 (Extended Existence Theorem)

Under **Assumption 5**, there exists the solution of the extended shape inverse problem. □

Proof. It is obvious from **Theorem 1** and continuous dependence of solution on parameters. (Q.E.D.)

In the case of a time-varying curve, define $\boldsymbol{p}_d(\boldsymbol{\sigma}, t) \in \Re^{3n}$ for a time-varying curve $\boldsymbol{c} : \Re \times \Re_+ \rightarrow E^3$ as

$$\boldsymbol{p}_d(\boldsymbol{\sigma}, t) := \begin{bmatrix} \boldsymbol{c}(\sigma_1, t) \\ \vdots \\ \boldsymbol{c}(\sigma_n, t) \end{bmatrix}. \tag{3.69}$$

In this case, $\boldsymbol{p}_d$ depends on time t. Also define $\boldsymbol{e}(\boldsymbol{q}, t) \in \Re^{3n}$ as

$$\boldsymbol{e}(\boldsymbol{q}, t) \ := \ \boldsymbol{p}(\boldsymbol{\theta}) - \boldsymbol{p}_d(\boldsymbol{\sigma}, t), \tag{3.70}$$

which also depends on time. Its derivative becomes

$$\dot{\boldsymbol{e}}(\boldsymbol{q}, \dot{\boldsymbol{q}}, t) = \boldsymbol{J}(\boldsymbol{q}, t)\dot{\boldsymbol{q}} - \frac{\partial \boldsymbol{p}_d}{\partial t}(\boldsymbol{\sigma}, t), \tag{3.71}$$

where $\boldsymbol{J}(\boldsymbol{q}, t) \in \Re^{3n \times 3n}$ is defined by

$$\boldsymbol{J}(\boldsymbol{q}, t) := \begin{bmatrix} \dfrac{\partial \boldsymbol{p}}{\partial \boldsymbol{\theta}}(\boldsymbol{\theta}) & -\dfrac{\partial \boldsymbol{p}_d}{\partial \boldsymbol{\sigma}}(\boldsymbol{\sigma}, t) \end{bmatrix}. \tag{3.72}$$

This Shape Jacobian for a time-varying curve also depends on time. The time derivative of the Shape Jacobian, $\dot{\boldsymbol{J}}(\boldsymbol{q}, \dot{\boldsymbol{q}}, t) \in \Re^{3n \times 3n}$ is expressed as

$$\dot{\boldsymbol{J}}(\boldsymbol{q}, \dot{\boldsymbol{q}}, t) \ = \ \dot{\boldsymbol{J}}_q(\boldsymbol{q}, \dot{\boldsymbol{q}}, t) + \dot{\boldsymbol{J}}_t(\boldsymbol{q}, t) \tag{3.73}$$

where $\dot{\boldsymbol{J}}_q(\boldsymbol{q}, \dot{\boldsymbol{q}}, t)$, $\dot{\boldsymbol{J}}_t(\boldsymbol{q}, t) \in \Re^{3n \times 3n}$ are defined as

$$\begin{aligned}
\dot{\boldsymbol{J}}_q(\boldsymbol{q}, \dot{\boldsymbol{q}}, t) &:= \frac{\partial \boldsymbol{J}}{\partial \boldsymbol{q}}(\boldsymbol{q}, t)\dot{\boldsymbol{q}} \\
&= \left[\frac{\partial \boldsymbol{J}}{\partial q_1}(\boldsymbol{q}, t)\dot{\boldsymbol{q}} \ \cdots \ \frac{\partial \boldsymbol{J}}{\partial q_{3n}}(\boldsymbol{q}, t)\dot{\boldsymbol{q}} \right], \qquad (3.74) \\
\dot{\boldsymbol{J}}_t(\boldsymbol{q}, t) &:= \frac{\partial \boldsymbol{J}}{\partial t}(\boldsymbol{q}, t) \\
&= \left[\ \mathbf{o} \ \ -\frac{\partial^2 \boldsymbol{p}_d}{\partial \boldsymbol{\sigma} \partial t}(\hat{\boldsymbol{\sigma}}, t) \ \right]. \qquad (3.75)
\end{aligned}$$

The property of the time-varying Shape Jacobian is almost same as the time invariant case:

Property 3 (Time-varying Shape Jacobian)

1. The norm of the Shape Jacobian is bounded, i.e., there exists a positive constant J_M such that

$$\forall t \in \Re_+, \ \forall \boldsymbol{q} \in \Re^{3n}, \ \|\boldsymbol{J}(\boldsymbol{q}, t)\| \leq J_M. \qquad (3.76)$$

   Moreover, if $\boldsymbol{J}(\boldsymbol{q}, t)$ is non-singular, then there exists a positive constant J_m such that

$$\forall t \in \Re_+, \ \forall \boldsymbol{q} \in \Re^{3n}, \ J_m \leq \|\boldsymbol{J}(\boldsymbol{q}, t)\|. \qquad (3.77)$$

2. The time-varying Shape Jacobian, $\boldsymbol{J}(\boldsymbol{q}, t)$, is singular at time t if and only if there exists a positive integer, $i \in \{1, \cdots, n\}$, such that at least one of the following two conditions holds:

   (a) Consider the three directions in E^3; the Sub-axis of the i-th joint, the Main-axis of the i-th joint, and the length direction of the i-th link. At least two among the directions align, i.e.,

$$\det \left[\ \boldsymbol{l}_i \ \ \boldsymbol{R}^T(\boldsymbol{a}_{m,i}, \theta_{m,i}(t))\boldsymbol{a}_{s,i} \ \ \boldsymbol{a}_{m,i} \ \right] = 0, \qquad (3.78)$$

   where $\boldsymbol{l}_i := l_i \boldsymbol{e}_x$.

   (b) The i-th link direction and the tangent at the point corresponding to the i-th link position cross at right angle, i.e.,

$$\left\{ \boldsymbol{p}_i(\boldsymbol{\theta}) - \boldsymbol{p}_{i-1}(\boldsymbol{\theta}) \right\}^T \frac{\partial \boldsymbol{c}}{\partial \sigma}(\sigma_i, t) = 0. \qquad (3.79)$$

3. There exists a positive constant J_H such that

$$\forall t \in \Re_+,\ \forall \boldsymbol{q} \in \Re^{3n},\ \|\dot{\boldsymbol{J}}_q(\boldsymbol{q}, \dot{\boldsymbol{q}}, t)\| \leq J_H \|\dot{\boldsymbol{q}}\|. \tag{3.80}$$

Moreover, for any $\boldsymbol{x}, \boldsymbol{y} \in \Re^{3n}$,

$$\dot{\boldsymbol{J}}_q(\boldsymbol{q}, \boldsymbol{x}, t)\boldsymbol{y} = \dot{\boldsymbol{J}}_q(\boldsymbol{q}, \boldsymbol{y}, t)\boldsymbol{x}. \tag{3.81}$$

for any t.

□

Proof. The proof is substantially same as the one of the time invariant case. (Q.E.D.)

We make the following assumption on the Shape Jacobian:

Assumption 6 (Time-varying Shape Jacobian)

The Shape Jacobian is non-singular for the desired joint angle function and curve parameter function, $(\boldsymbol{\theta}^*(t), \boldsymbol{\sigma}^*(t))$, for any t, i.e.,

$$\forall t \in \Re_+,\ \det \boldsymbol{J}(\boldsymbol{\theta}^*(t), \boldsymbol{\sigma}^*(t), t) \neq \mathbf{o}. \tag{3.82}$$

□

We state the following theorem on existence region of the extended shape inverse problem:

Theorem 4 (Extended Existence Region)

Under **Assumption 5** and **Assumption 6**, there exists a unique solution satisfying that

$$\boldsymbol{e}(\boldsymbol{\theta}(t), \boldsymbol{\sigma}(t)) = \mathbf{o}, \tag{3.83}$$

$$(\boldsymbol{\theta}(t), \boldsymbol{\sigma}(t)) \in \mathcal{D}_\delta, \tag{3.84}$$

for any $\delta \in [-l_M\ l_M]$, where $\mathcal{D}_\delta$ is defined by (3.57). Moreover, the solution is exactly the pair of the desired joint angle function and curve parameter function, $(\boldsymbol{\theta}^*(t), \boldsymbol{\sigma}^*(t))$.

□

Proof. It is concluded from **Theorem 2**. (Q.E.D.)

Note that all the results in this section reduce to the results in Section **3.1** to Section **3.4** when a curve is choosen to be time-invariant.

Summary

The shape correspondence between a spatial curve and an HDOF manipulator was defined by using the solution of a certain nonlinear optimization problem termed the shape inverse problem. The existence theorem of the solution of the shape inverse problem was provided under assumptions on a given curve and manipulator kinematics. The existence region theorem was also provided under assumption of non-singularity of the Shape Jacobian. This theorem will play an important role to convert control problems appeared later into more tractable ones.

Chapter 4

Shape Regulation

In this chapter, we discuss one of the most fundamental control problems, *shape regulation*. Control purpose of shape regulation is to bring an HDOF manipulator onto the desired shape prescribed by a time invariant parametric curve. Crucial key to solve this problem is to estimate the desired curve parameters. This idea allows us to achieve the control purpose of shape regulation without solving the shape inverse problem directly, which is time-consuming.

In Section **4.1**, we formulate the shape regulation problem and show the simple Proportional and Derivative (PD) feedback control in task space in order to compare with our control proposed later. In Section **4.2**, the idea of estimating the desired curve parameter is introduced. In Section **4.3**, a shape regulation control based on curve parameter estimation is proposed. It is proved that this control law assures local asymptotic convergence to the desired shape using LaSalle's theorem. The derived control law is homogeneously decomposed into recursive control laws with respect to link (or joint) numbers in Section **4.4**. A geometric interpretation of the recursive estimation law is also given. Simulation results with three-dimensional graphical animation are also provided in Section **4.5**.

4.1 Problem Statement

The control objective of shape regulation is to make the shape of an HDOF manipulator correspond to the desired shape prescribed by a given spatial parametric curve. From **Definition 1**, the *shape regulation problem* is stated as follows:

Problem 3 (Shape Regulation)

Consider

1. an HDOF manipulator with dynamics (2.34), and

2. a curve $\boldsymbol{c} : \Re \rightarrow E^3$ satisfying **Assumption 1**.

Moreover, suppose that **Assumption 3** holds. Then, find a control input, $\boldsymbol{u}$, in (2.34) achieving that

$$\boldsymbol{\theta}(t) \rightarrow \boldsymbol{\theta}^*, \tag{4.1}$$

$$\dot{\boldsymbol{\theta}}(t) \rightarrow \mathbf{o}, \tag{4.2}$$

as $t \rightarrow \infty$, where $\boldsymbol{\theta}^*$ is the desired joint angle, that is, the solution of the shape inverse problem. □

One of the simplest ideas to solve this problem is to use proportional and derivative (PD) feedback in joint space after solving the shape inverse problem directly. As we saw in Section **3.1**, however, the shape inverse problem includes two nonlinear optimization problems. Thus, it is very time-consuming to solve them in advance.

PD feedback in task space [27] can also be used for our purpose. Since the task variable is the shape error, $\boldsymbol{e}^* := \boldsymbol{e}(\boldsymbol{\theta}, \boldsymbol{\sigma}^*)$, in this case, we can consider the following PD feedback control law with respect to $\boldsymbol{e}^*$ and $\dot{\boldsymbol{\theta}}$:

$$\boldsymbol{u} = -\left\{\frac{\partial \boldsymbol{p}}{\partial \boldsymbol{\theta}}(\boldsymbol{\theta})\right\}^T \boldsymbol{K}_p \boldsymbol{e}^* - \boldsymbol{K}_v \dot{\boldsymbol{\theta}} + \boldsymbol{g}(\boldsymbol{\theta}), \tag{4.3}$$

where $\boldsymbol{K}_p, \in \Re^{3n \times 3n}$ and $\boldsymbol{K}_v \in \Re^{2n \times 2n}$ are symmetric positive definite matrices. Achievement of the shape regulation is proved by using the following scalar function $W(\boldsymbol{e}^*, \dot{\boldsymbol{\theta}})$:

$$W(\boldsymbol{e}^*, \dot{\boldsymbol{\theta}}) := \frac{1}{2}\dot{\boldsymbol{\theta}}^T \boldsymbol{M}(\boldsymbol{\theta})\, \dot{\boldsymbol{\theta}} + \frac{1}{2}\, \boldsymbol{e}^{*T} \boldsymbol{K}_p\, \boldsymbol{e}^*, \tag{4.4}$$

where $\boldsymbol{M}(\boldsymbol{\theta})$ is the inertia matrix shown in (2.34). Note that the desired curve parameter, $\boldsymbol{\sigma}^*$, appears in control law (4.3), that is, we still have to solve the shape inverse problem in order to get $\boldsymbol{\sigma}^*$ before we apply control input (4.3) to the manipulator. It is necessary to resort to some numerical method to solve the shape inverse problem in advance. This means that we need the time to solve the nonlinear optimization problem numerically in addition to the control time. In the following section, we will see that the idea of estimating the desired curve parameter, $\boldsymbol{\sigma}^*$, in the course of control gives us a more desirable result to achieve shape regulation without solving time-consuming shape inverse problem a priori to the control.

4.2 Estimation of the Desired Curve Parameters

Let $\hat{\boldsymbol{\sigma}} := [\, \hat{\sigma}_1 \cdots \hat{\sigma}_n]^T \in \Re^n$ be the estimate of $\boldsymbol{\sigma}^*$ and define the estimated shape error $\hat{\boldsymbol{e}} \in \Re^{3n}$ including $\hat{\boldsymbol{\sigma}}$ as

$$\begin{aligned} \hat{\boldsymbol{e}} &:= \boldsymbol{e}(\boldsymbol{\theta}, \hat{\boldsymbol{\sigma}}) \\ &= \boldsymbol{p}(\boldsymbol{\theta}) - \boldsymbol{p}_d(\hat{\boldsymbol{\sigma}}). \end{aligned} \tag{4.5}$$

Then, $\dot{\hat{\boldsymbol{e}}} \in \Re^{3n}$ becomes

$$\dot{\hat{\boldsymbol{e}}} = \boldsymbol{J}(\boldsymbol{\theta}, \hat{\boldsymbol{\sigma}}) \begin{bmatrix} \dot{\boldsymbol{\theta}} \\ \dot{\hat{\boldsymbol{\sigma}}} \end{bmatrix}. \tag{4.6}$$

Theorem 2 assures that if we achieve

$$\hat{\boldsymbol{e}}(\boldsymbol{\theta}, \hat{\boldsymbol{\sigma}}) \rightarrow \mathbf{o}, \tag{4.7}$$

$$\dot{\boldsymbol{\theta}} \rightarrow \mathbf{o}, \tag{4.8}$$

$$(\boldsymbol{\theta}, \hat{\boldsymbol{\sigma}}) \in \mathcal{D}_\delta, \tag{4.9}$$

then control objective of shape regulation (4.1), (4.2) is also achieved under the condition of non-singularity of the Shape Jacobian. Notice that in the objective above, $\boldsymbol{\sigma}^*$ does not appear any longer, which means we do not have to solve any nonlinear optimization problems in advance to the control.

4.3 Shape Regulation Based on Curve Parameter Estimation

Observing that the control objective of shape regulation is expressed by (4.7), (4.8) and (4.9), we consider the following positive scalar function, $V(\hat{\boldsymbol{e}}, \dot{\boldsymbol{\theta}})$:

$$V(\hat{\boldsymbol{e}}, \dot{\boldsymbol{\theta}}) := \frac{1}{2} \dot{\boldsymbol{\theta}}^T \boldsymbol{M}(\boldsymbol{\theta})\, \dot{\boldsymbol{\theta}} + \frac{1}{2}\, \hat{\boldsymbol{e}}^T \boldsymbol{K}_p\, \hat{\boldsymbol{e}}. \tag{4.10}$$

This function is positive definite with respect to $(\hat{\boldsymbol{e}}, \dot{\boldsymbol{\theta}})$ and becomes zero at our control objective point $(\hat{\boldsymbol{e}}, \dot{\boldsymbol{\theta}}) = (\mathbf{o}, \mathbf{o})$. If we compare this function with the scalar function for simple task space PD feedback control (4.3) stated in Section **4.1**, the only difference is that $\hat{\boldsymbol{e}}$ is used in the above function instead of $\boldsymbol{e}^*$ in function (4.4). Differentiating this V along the trajectory and taking **Property 1**-4 into account give the following:

$$\dot{V}(\hat{\boldsymbol{e}}, \dot{\boldsymbol{\theta}}) = \dot{\boldsymbol{\theta}}^T \boldsymbol{M}(\boldsymbol{\theta})\, \ddot{\boldsymbol{\theta}} + \frac{1}{2}\, \dot{\boldsymbol{\theta}}^T \dot{\boldsymbol{M}}(\boldsymbol{\theta})\, \dot{\boldsymbol{\theta}} + \hat{\boldsymbol{e}}^T \boldsymbol{K}_p \dot{\hat{\boldsymbol{e}}}$$

$$
\begin{aligned}
&= \dot{\boldsymbol{\theta}}^T \boldsymbol{u} - \dot{\boldsymbol{\theta}}^T \boldsymbol{C}(\boldsymbol{\theta}, \dot{\boldsymbol{\theta}})\dot{\boldsymbol{\theta}} - \dot{\boldsymbol{\theta}}^T \boldsymbol{g}(\boldsymbol{\theta}) \\
&\quad + \frac{1}{2}\dot{\boldsymbol{\theta}}^T \dot{\boldsymbol{M}}(\boldsymbol{\theta})\dot{\boldsymbol{\theta}} + \hat{\boldsymbol{e}}^T \boldsymbol{K}_p \boldsymbol{J}(\boldsymbol{\theta}, \hat{\boldsymbol{\sigma}}) \begin{bmatrix} \dot{\boldsymbol{\theta}} \\ \dot{\hat{\boldsymbol{\sigma}}} \end{bmatrix} \\
&= \dot{\boldsymbol{\theta}}^T \left[\boldsymbol{u} + \left\{ \frac{\partial \boldsymbol{p}}{\partial \boldsymbol{\theta}}(\boldsymbol{\theta}) \right\}^T \boldsymbol{K}_p \hat{\boldsymbol{e}} - \boldsymbol{g}(\boldsymbol{\theta}) \right] - \hat{\boldsymbol{e}}^T \boldsymbol{K}_p \frac{\partial \boldsymbol{p}_d}{\partial \boldsymbol{\sigma}}(\hat{\boldsymbol{\sigma}})\dot{\hat{\boldsymbol{\sigma}}}. \qquad (4.11)
\end{aligned}
$$

Consider a control law with a curve parameter estimation law as follows:

$$
\begin{aligned}
\boldsymbol{u} &= -\left\{ \frac{\partial \boldsymbol{p}}{\partial \boldsymbol{\theta}}(\boldsymbol{\theta}) \right\}^T \boldsymbol{K}_p \hat{\boldsymbol{e}} - \boldsymbol{K}_v \dot{\boldsymbol{\theta}} + \boldsymbol{g}(\boldsymbol{\theta}), \qquad (4.12) \\
\dot{\hat{\boldsymbol{\sigma}}} &= \boldsymbol{K}_\sigma \left\{ \frac{\partial \boldsymbol{p}_d}{\partial \boldsymbol{\sigma}}(\hat{\boldsymbol{\sigma}}) \right\}^T \boldsymbol{K}_p \hat{\boldsymbol{e}}, \qquad (4.13)
\end{aligned}
$$

where $\boldsymbol{K}_\sigma \in \Re^{n \times n}$ is a symmetric positive definite matrix. By substituting the above control law with curve parameter estimation into (4.11), $\dot{V}$ becomes

$$
\begin{aligned}
\dot{V}(\hat{\boldsymbol{e}}, \dot{\boldsymbol{\theta}}) &= -\dot{\boldsymbol{\theta}}^T \boldsymbol{K}_v \dot{\boldsymbol{\theta}} - \hat{\boldsymbol{e}}^T \boldsymbol{K}_p \frac{\partial \boldsymbol{p}_d}{\partial \boldsymbol{\sigma}}(\hat{\boldsymbol{\sigma}}) \boldsymbol{K}_\sigma \left\{ \frac{\partial \boldsymbol{p}_d}{\partial \boldsymbol{\sigma}}(\hat{\boldsymbol{\sigma}}) \right\}^T \boldsymbol{K}_p \hat{\boldsymbol{e}} \\
&\leq 0, \qquad (4.14)
\end{aligned}
$$

which shows negative semi-definiteness of $\dot{V}$ with respect to $(\hat{\boldsymbol{e}}, \dot{\boldsymbol{\theta}})$. Using LaSalle's theorem, we can conclude the convergence to the objective point. We summerize the result above in the following theorem and give the proof:

Theorem 5 (Shape Regulation based on Curve Parameter Estimation)

Consider a control law with a curve parameter estimation law as follows:

$$
\begin{aligned}
\boldsymbol{u} &= -\left\{ \frac{\partial \boldsymbol{p}}{\partial \boldsymbol{\theta}}(\boldsymbol{\theta}) \right\}^T \boldsymbol{K}_p \hat{\boldsymbol{e}} - \boldsymbol{K}_v \dot{\boldsymbol{\theta}} + \boldsymbol{g}(\boldsymbol{\theta}), \qquad (4.15) \\
\dot{\hat{\boldsymbol{\sigma}}} &= \boldsymbol{K}_\sigma \left\{ \frac{\partial \boldsymbol{p}_d}{\partial \boldsymbol{\sigma}}(\hat{\boldsymbol{\sigma}}) \right\}^T \boldsymbol{K}_p \hat{\boldsymbol{e}}, \qquad (4.16)
\end{aligned}
$$

where $\boldsymbol{K}_p, \in \Re^{3n \times 3n}$, $\boldsymbol{K}_v \in \Re^{2n \times 2n}$ and $\boldsymbol{K}_\sigma \in \Re^{n \times n}$ are all symmetric positive definite matrices. Then, under **Assumption 4**, the closed loop system with control law (4.15), (4.16) is locally asymptotically stable at the equilibrium point, $(\boldsymbol{\theta}, \dot{\boldsymbol{\theta}}) = (\boldsymbol{\theta}^*, \mathbf{o})$, which means the control objective of shape regulation is achieved locally. □

Proof. For a positive real constant, γ, consider the following set $\mathcal{N}_\gamma \subset \Re^{3n}$:

$$
\mathcal{N}_\gamma := \left\{ (\boldsymbol{\theta}, \hat{\boldsymbol{\sigma}}) \,\middle|\, \frac{1}{2}\hat{\boldsymbol{e}}^T(\boldsymbol{\theta}, \hat{\boldsymbol{\sigma}}) \boldsymbol{K}_p \hat{\boldsymbol{e}}(\boldsymbol{\theta}, \hat{\boldsymbol{\sigma}}) \leq \gamma \right\}. \qquad (4.17)
$$

The set $\mathcal{N}_\gamma$ is not bounded because the equation $\hat{\boldsymbol{e}}(\boldsymbol{\theta}, \hat{\boldsymbol{\sigma}}) = \mathbf{o}$ has multiple solutions. By taking γ sufficiently small, we can give the following properties to $\mathcal{N}_\gamma$:

1. $\forall(\boldsymbol{\theta}, \hat{\boldsymbol{\sigma}}) \in \mathcal{N}_\gamma$, $\det \boldsymbol{J}(\boldsymbol{\theta}, \hat{\boldsymbol{\sigma}}) \neq 0$.

2. $\mathcal{N}_\gamma$ is the union of countable disjoint sets, $\{\mathcal{N}_{\gamma,k}\}_{k=1}^{\infty}$, each of that is closed and bounded.

Let $\mathcal{N}_\gamma^* \subseteq \Re^{3n}$ be the element of $\{\mathcal{N}_{\gamma,i}\}_{i=1}^{\infty}$ that includes the desired point $(\boldsymbol{\theta}^*, \boldsymbol{\sigma}^*)$, that is, $(\boldsymbol{\theta}^*, \boldsymbol{\sigma}^*) \in \mathcal{N}_\gamma^*$. Define $\Omega \subset \Re^{5n}$ as follows:

$$\Omega := \left\{ (\boldsymbol{\theta}, \hat{\boldsymbol{\sigma}}, \dot{\boldsymbol{\theta}}) \,\middle|\, (\boldsymbol{\theta}, \hat{\boldsymbol{\sigma}}) \in \mathcal{N}_\gamma^*, V(\boldsymbol{\theta}, \hat{\boldsymbol{\sigma}}, \dot{\boldsymbol{\theta}}) \leq \gamma \right\}. \tag{4.18}$$

Since Ω is closed and bounded and $\dot{V} \leq 0$, Ω is positively invariant. Let E be the set satisfying $\dot{V} = 0$ in Ω, and $\mathcal{M}^*$ denotes the largest invariant set in E. Then, by LaSalle's theorem [12], any one state starting from the inside of Ω approaches $\mathcal{M}^*$. From (4.14), E is expressed as

$$E = \left\{ (\boldsymbol{\theta}, \hat{\boldsymbol{\sigma}}, \dot{\boldsymbol{\theta}}) \in \Omega \,\middle|\, \dot{\boldsymbol{\theta}} = \mathbf{o}, \left\{ \frac{\partial \boldsymbol{p}_d}{\partial \boldsymbol{\sigma}}(\hat{\boldsymbol{\sigma}}) \right\}^T \boldsymbol{K}_p \hat{\boldsymbol{e}}(\boldsymbol{\theta}, \hat{\boldsymbol{\sigma}}) = \mathbf{o} \right\}. \tag{4.19}$$

Therefore, the largest invariant set, $\mathcal{M}^*$, is

$$\mathcal{M}^* = \left\{ (\boldsymbol{\theta}, \hat{\boldsymbol{\sigma}}, \dot{\boldsymbol{\theta}}) \in \Omega \,\middle|\, \dot{\boldsymbol{\theta}} = \mathbf{o}, \hat{\boldsymbol{e}}(\boldsymbol{\theta}, \hat{\boldsymbol{\sigma}}) = \mathbf{o} \right\}. \tag{4.20}$$

Because, $\mathcal{M}^*$ consists of equilibrium states, which means $\mathcal{M}^*$ is an invariant set. Substituting $\dot{\boldsymbol{\theta}} = \mathbf{o}$ and $\hat{\boldsymbol{e}} \neq \mathbf{o}$ into the closed-loop system leads to the result $\dot{\boldsymbol{\theta}} \neq \mathbf{o}$, which means that any one state outside of $\mathcal{M}^*$ necessarily goes out from E. Thus $\mathcal{M}^*$ given by (4.20) represents the largest invariant set in E. From (4.20), we conclude that $\hat{\boldsymbol{e}} \to \mathbf{o}$ and $\dot{\boldsymbol{\theta}} \to \mathbf{o}$ in Ω, which means that $\boldsymbol{\theta} \to \boldsymbol{\theta}^*$ and $\dot{\boldsymbol{\theta}} \to \mathbf{o}$. Local asymptotic stability of the closed-loop system is proved. (Q.E.D.)

Compared with PD feedback control law in task space (4.3), control law (4.15) with curve parameter esitimator (4.16) uses the estimated shape error, $\hat{\boldsymbol{e}}$, instead of the real shape error, $\boldsymbol{e}^*$. Therefore, this new control law is not pure PD feedback control in task space. The great benefit of this control law is that, instead of solving the time-consuming shape inverse problem to obtain $\boldsymbol{\sigma}^*$ in advance. All that we have to do is very easy calculation of estimation law (4.16) in the course of control.

4.4 Recursive Expression

The recursive expression of a control law brings not only computational advantages but also geometric interpretation in Euclidean space. Here we decompose the control law

derived in the previous section into homogeneous n parts of the Newton-Euler flavor. To do this, we restrict the gain matrices to diagonal forms as follows:

$$\boldsymbol{K}_p = \text{blockdiag}\{\boldsymbol{K}_{p,1}, \cdots, \boldsymbol{K}_{p,n}\}, \tag{4.21}$$

$$\boldsymbol{K}_v = \text{blockdiag}\{\boldsymbol{K}_{v,1}, \cdots, \boldsymbol{K}_{v,n}\}, \tag{4.22}$$

$$\boldsymbol{K}_\sigma = \text{diag}\{k_{\sigma,1}, \cdots, k_{\sigma,n}\}, \tag{4.23}$$

where $\boldsymbol{K}_{p,i} \in \Re^{3\times 3}$, $\boldsymbol{K}_{v,i} \in \Re^{2\times 2}$ are symmetric positive definite matrices and $k_{\sigma,i}$ is a real positive constant. Note that $\dfrac{\partial \boldsymbol{p}}{\partial \boldsymbol{\theta}}$ has a block lower triangular form as

$$\frac{\partial \boldsymbol{p}}{\partial \boldsymbol{\theta}}(\boldsymbol{\theta}) = \begin{bmatrix} \dfrac{\partial \boldsymbol{p}_1}{\partial \boldsymbol{\theta}_1} & & & \\ \dfrac{\partial \boldsymbol{p}_2}{\partial \boldsymbol{\theta}_1} & \dfrac{\partial \boldsymbol{p}_2}{\partial \boldsymbol{\theta}_2} & & \\ \vdots & \vdots & \ddots & \\ \dfrac{\partial \boldsymbol{p}_n}{\partial \boldsymbol{\theta}_1} & \dfrac{\partial \boldsymbol{p}_n}{\partial \boldsymbol{\theta}_2} & \cdots & \dfrac{\partial \boldsymbol{p}_n}{\partial \boldsymbol{\theta}_n} \end{bmatrix}. \tag{4.24}$$

By using the following expressions

$$\frac{\partial \boldsymbol{p}_j}{\partial \boldsymbol{\theta}_{s,i}} = (\boldsymbol{\Phi}_{i-1}\boldsymbol{a}_{s,i}) \times \left(\boldsymbol{p}_j - \boldsymbol{p}_{i-1}\right), \tag{4.25}$$

$$\frac{\partial \boldsymbol{p}_j}{\partial \boldsymbol{\theta}_{m,i}} = (\boldsymbol{\Phi}_{i}\boldsymbol{a}_{m,i}) \times \left(\boldsymbol{p}_j - \boldsymbol{p}_{i-1}\right), \tag{4.26}$$

we obtain

$$\begin{aligned} \boldsymbol{u}_i &= -\sum_{j=i}^{n} \left(\frac{\partial \boldsymbol{p}_j}{\partial \boldsymbol{\theta}_i}^T \boldsymbol{K}_{p,j}\hat{\boldsymbol{e}}_j \right) - \boldsymbol{K}_{v,i}\dot{\boldsymbol{\theta}}_i \\ &= -\sum_{j=i}^{n} \left\{ \begin{bmatrix} \boldsymbol{R}_{w,i}{}^T\boldsymbol{a}_{s,i} & \boldsymbol{a}_{m,i} \end{bmatrix} \boldsymbol{\Phi}_i{}^T \left[\left(\boldsymbol{p}_j - \boldsymbol{p}_{i-1}\right) \times \right] \boldsymbol{K}_{p,j}\hat{\boldsymbol{e}}_j \right\} - \boldsymbol{K}_{v,i}\dot{\boldsymbol{\theta}}_i \\ &= -\boldsymbol{A}_i{}^T\boldsymbol{\Phi}_i{}^T \sum_{j=i}^{n} \left\{ \left(\boldsymbol{p}_j - \boldsymbol{p}_{i-1}\right) \times \boldsymbol{K}_{p,j}\hat{\boldsymbol{e}}_j \right\} \\ &= -\boldsymbol{A}_i{}^T\boldsymbol{\Phi}_i{}^T \left\{ \sum_{j=i}^{n} \left(\boldsymbol{p}_j \times \boldsymbol{K}_{p,j}\hat{\boldsymbol{e}}_j\right) - \boldsymbol{p}_{i-1} \times \sum_{j=i}^{n} \left(\boldsymbol{K}_{p,j}\hat{\boldsymbol{e}}_j\right) \right\} - \boldsymbol{K}_{v,i}\dot{\boldsymbol{\theta}}_i \end{aligned} \tag{4.27}$$

where $\hat{\boldsymbol{e}}_i := \boldsymbol{p}_i - \boldsymbol{c}(\hat{\sigma}_i)$. If we define $\boldsymbol{\alpha}_i, \boldsymbol{\beta}_i \in \Re^3$ $(i = 1, \cdots, n)$ as

$$\boldsymbol{\alpha}_i = \boldsymbol{\alpha}_{i+1} + \boldsymbol{K}_{p,i}\boldsymbol{e}_i, \tag{4.28}$$

$$\boldsymbol{\beta}_i = \boldsymbol{\beta}_{i+1} + \boldsymbol{p}_i \times \boldsymbol{K}_{p,i}\boldsymbol{e}_i, \tag{4.29}$$

with initial values, $\boldsymbol{\alpha}_{n+1} = \boldsymbol{\beta}_{n+1} = \mathbf{o}$, then we have the following recursive expression of $\boldsymbol{u}_i$:

$$\boldsymbol{u}_i \;=\; -\boldsymbol{A}_i{}^T\boldsymbol{\Phi}_i{}^T\left(\boldsymbol{\beta}_i - \boldsymbol{p}_{i-1}\times\boldsymbol{\alpha}_i\right) - \boldsymbol{K}_{v,i}\dot{\boldsymbol{\theta}}_i. \tag{4.30}$$

Simple calculations lead to the following recursive estimation law:

$$\dot{\hat{\sigma}}_i = k_{\sigma,i}\left\{\frac{d\boldsymbol{c}}{d\sigma_i}(\hat{\sigma}_i)\right\}^T \boldsymbol{K}_{p,i}\hat{\boldsymbol{e}}_i. \tag{4.31}$$

Here we give the reason why very simple estimation law (4.16) works well by considering geometric interpretation in Euclidean space where a manipulator actually moves.

Since estimation law (4.16) is effective locally near the desired state, we consider the case that a HDOF manipulator is on a given curve specifying the desired shape. That is, a link position $\boldsymbol{p}_i$ coinsides with the desired link position on the curve $\boldsymbol{c}(\sigma_i{}^*)$, where $\sigma_i{}^*$ is the real desired curve parameter. To see the meaning of the estimator more clearly, we set $\boldsymbol{K}_{p,i} = \boldsymbol{I}_3$ and $k_{\sigma,i} = 1$ for all i. Then, estimation law (4.31) becomes

$$\dot{\hat{\sigma}}_i = \left\{\frac{d\boldsymbol{c}}{d\sigma_i}(\hat{\sigma}_i)\right\}^T \left\{\boldsymbol{p}_i - \boldsymbol{c}(\hat{\sigma}_i)\right\}. \tag{4.32}$$

This decomposed estimation law states that the inner product between the tangent $\dfrac{\partial \boldsymbol{c}}{\partial \sigma_i}$ and the position error $\{\boldsymbol{p}_i - \boldsymbol{c}(\sigma_i)\}$ should be the time derivative of the estimate of curve parameter. This is explained by using Figure 4.1 as follows.

The left one in Figure 4.1 shows that if the estimated curve parameter $\hat{\sigma}_i$ is larger than the true one, estimator (4.32) makes $\dot{\hat{\sigma}}_i$ be negative, then $\hat{\sigma}_i$ decreases to the true value $\sigma_i{}^*$. On the other hand, in the right in Figure 4.1, the estimate $\hat{\sigma}_i$ is smaller than the true value $\sigma_i{}^*$ so that estimator (4.32) give the answer that $\dot{\hat{\sigma}}_i$ should be positive, then $\hat{\sigma}_i$ tends to the true value $\sigma_i{}^*$ as increasing. Therefore, we can see that the estimated value $\hat{\sigma}_i$ converges to the true value σ_i if we employ estimation law (4.32).

The reason why we can obtain such a simple and understandable estimation law comes from the choice of physically meaningful scalar function V. This function consists of kinetic energy and artificial potential energy and becomes zero at the objective point.

4.5 Simulation

In this section, we show the simulation results applying shape regulation control law (4.15) with curve parameter estimation law (4.16) to a manipulator system with 20 DOF.

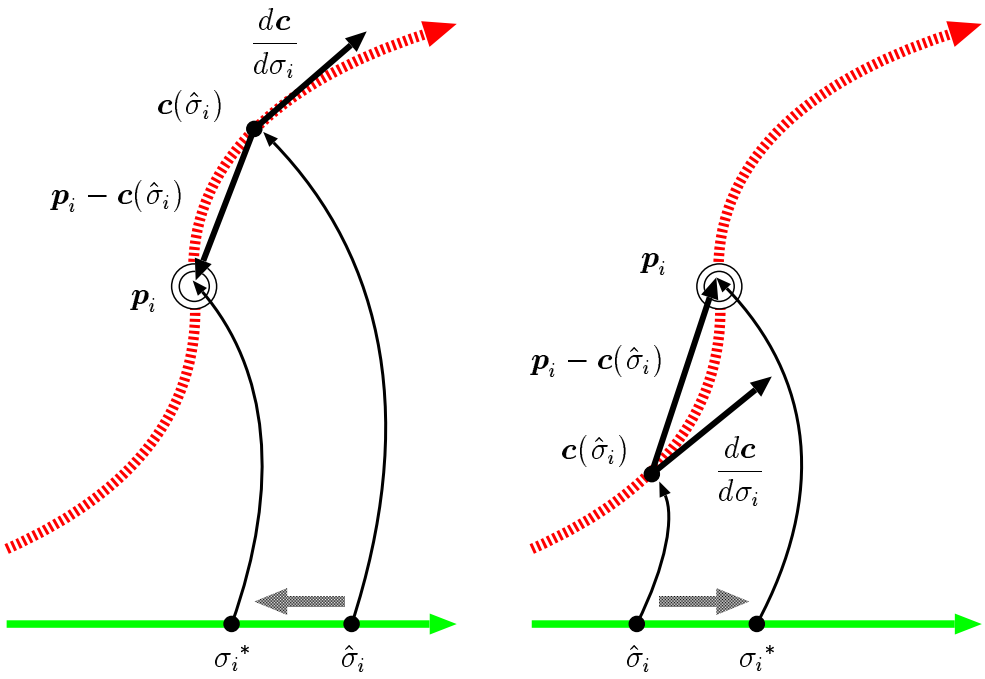

Figure 4.1: Geometric interpretation of the estimation law

For simplicity, we assume that the manipulator in this simulation has completely identical links and 2DOF joints. We also suppose that the link has a cylindrical shape and uniform distribution of mass density. The physical values related to the link are shown in Table 4.1.

Table 4.1: Link physical parameters

the radius of a bottom surface: r_b	0.05 [m]
the link length: l	0.10 [m]
the link mass: m	1.00 [kg]

The 2DOF joint used in this simulation has the mechanical structure with $\boldsymbol{a}_{s,i} = \boldsymbol{e}_y$ and $\boldsymbol{a}_{m,i} = \boldsymbol{e}_z$ for all i. In this case, the rotational matrix of the i-th 2DOF joint, $\boldsymbol{R}_{w,i}$, becomes

$$\begin{aligned} \boldsymbol{R}_{w,i} &= \boldsymbol{R}(\boldsymbol{e}_y, \theta_{s,i})\boldsymbol{R}(\boldsymbol{e}_z, \theta_{m,i}) \\ &= \begin{bmatrix} \cos\theta_{s,i}\cos\theta_{m,i} & -\cos\theta_{s,i}\sin\theta_{m,i} & \sin\theta_{s,i} \\ \sin\theta_{m,i} & \cos\theta_{m,i} & 0 \\ -\sin\theta_{s,i}\cos\theta_{m,i} & \sin\theta_{s,i}\sin\theta_{m,i} & \cos\theta_{s,i} \end{bmatrix}. \end{aligned} \tag{4.33}$$

The design parameters are set to $\boldsymbol{K}_p = k_p\boldsymbol{I}$, $\boldsymbol{K}_v = k_v\boldsymbol{I} + k_d\frac{\partial \boldsymbol{p}}{\partial \boldsymbol{\theta}}^T\frac{\partial \boldsymbol{p}}{\partial \boldsymbol{\theta}}$ and $\boldsymbol{K}_\sigma = k_\sigma\boldsymbol{I}$

where $k_p = 40.0$, $k_d = 5.00$, $k_v = 1.00$ and $k_\sigma = 40.0$.

The following helix is given as a desired shape in this simulation:

$$\boldsymbol{c}(\sigma) = \begin{bmatrix} \bar{\alpha}\sigma \\ R\cos(\bar{u}(\sigma)) + C_y \\ R\sin(\bar{u}(\sigma)) + C_z \end{bmatrix}, \tag{4.34}$$

where

$$\begin{aligned} \bar{\alpha} &:= \bar{A}, \\ \bar{u}(\sigma) &:= \frac{\sqrt{1-\bar{\alpha}^2}}{R}\sigma + \phi, \\ C_y &:= -R\cos\phi, \\ C_z &:= -R\sin\phi, \end{aligned} \tag{4.35}$$

and $\bar{A}$, R and ϕ are all constants. In this simulation, we set $\bar{A} = 0.50$, $R = 0.10$ and $\phi = -0.50\pi$. The initial joint angles and joint angular velocities are all set to zero, i.e., $\boldsymbol{\theta} = \dot{\boldsymbol{\theta}} = \mathbf{o}$. The initial estimates of the desired curve parameters are set to $\sigma_i = li = 0.10i$ where $i = 1, \cdots, n$.

Figure 4.2 shows the manipulator's movement from the initial time 0.0 [s] to 1.25 [s] every 0.25 second, from two viewpoints. We can see that the 'shape' of the manipulator changes from a straight line to the helix smoothly. From Figure 4.3, the error approaches zero gradually, but very slowly after 1.00 [s]. We also observe slow convergence of the curve parameter estimation from Figure 4.5. We only assure the asymptotic stability here.

Summary

Shape regulation control was successfully accomplished due to the idea of estimating the desired curve parameter. The shape regulation law with curve parameter estimation law was derived by Lyapunov design. Recursive expression of the shape regulation law was also given for both geometric interpretation of the estimation law and computational convenient. The simulation results applying the shape regulation law were provided with three-dimensional graphical figures.

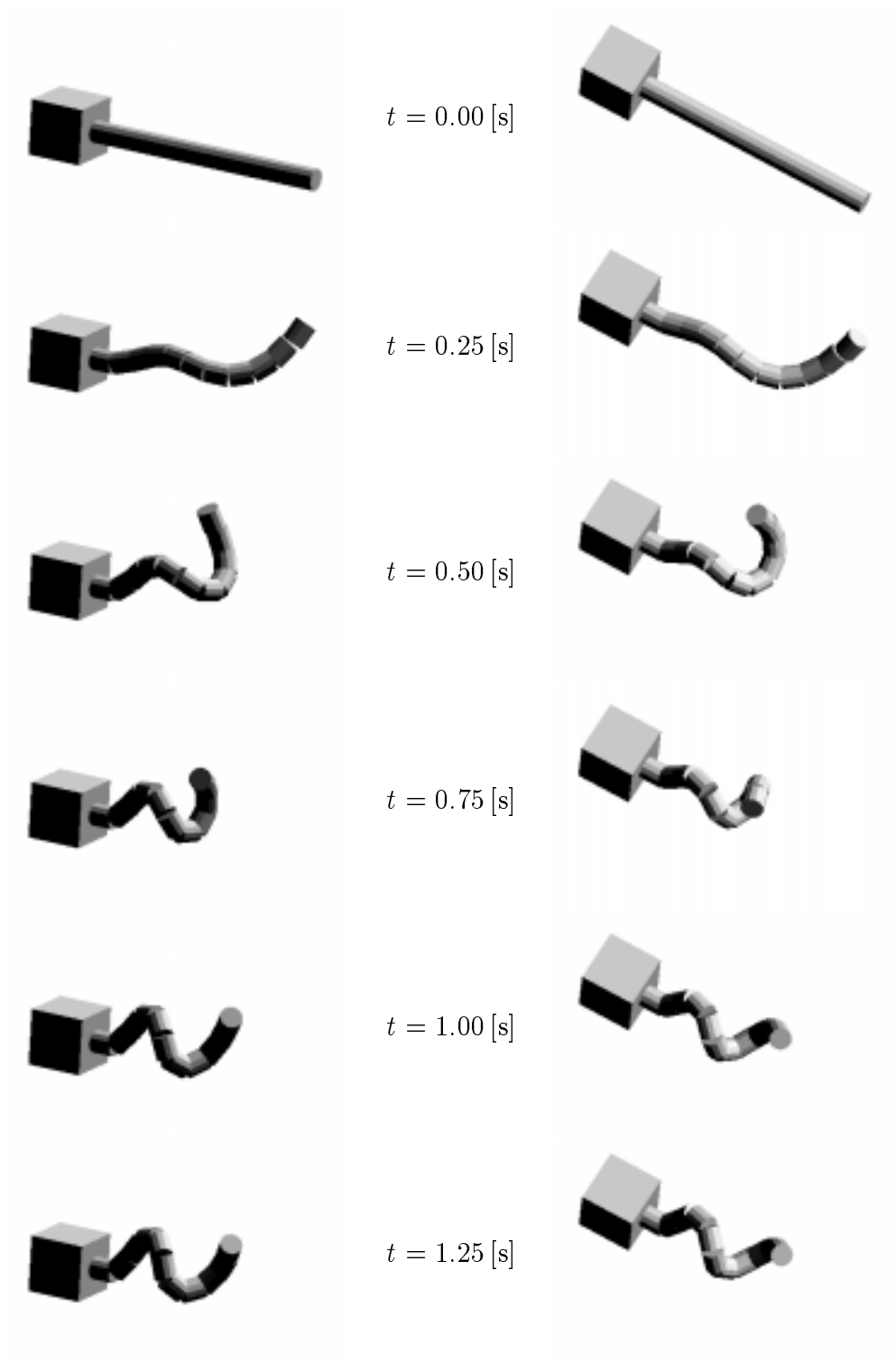

Figure 4.2: Manipulator movement (shape regulation)

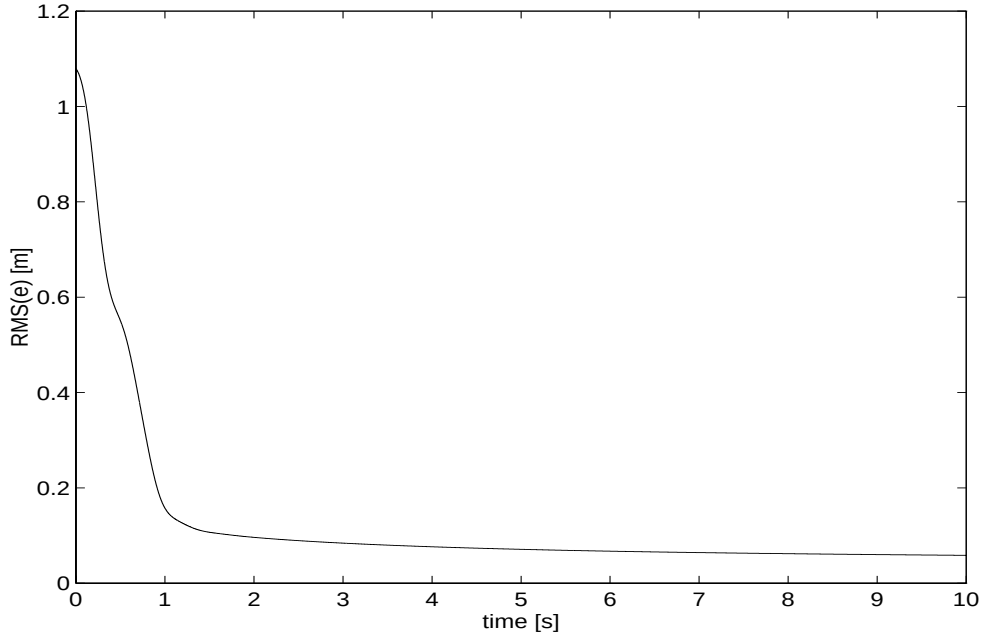

Figure 4.3: Estimated shape error (shape regulation)

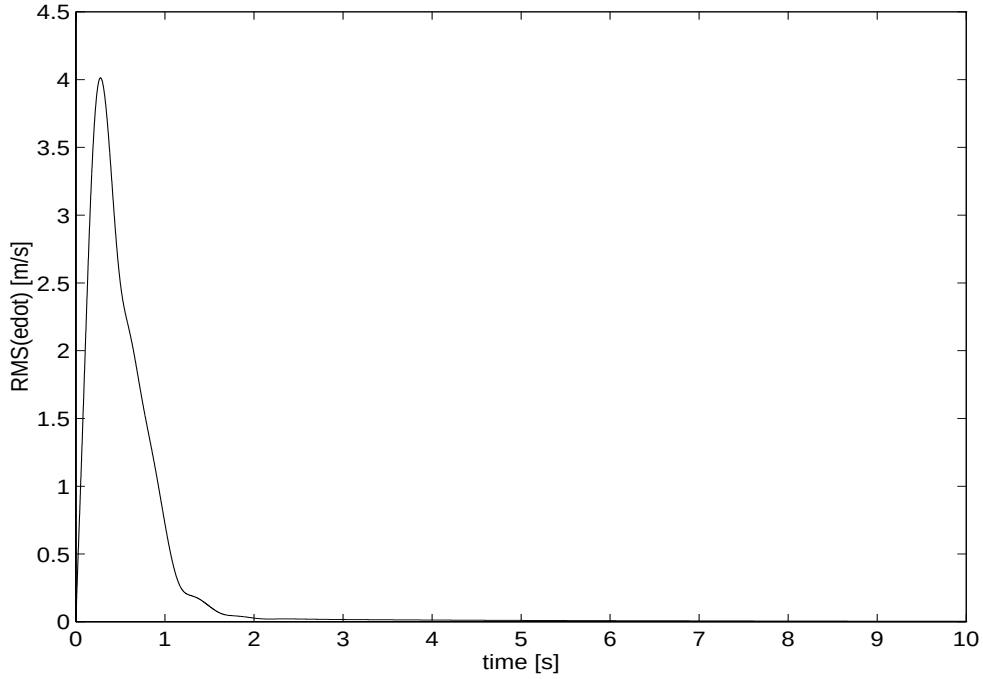

Figure 4.4: Estimated shape error velocity (shape regulation)

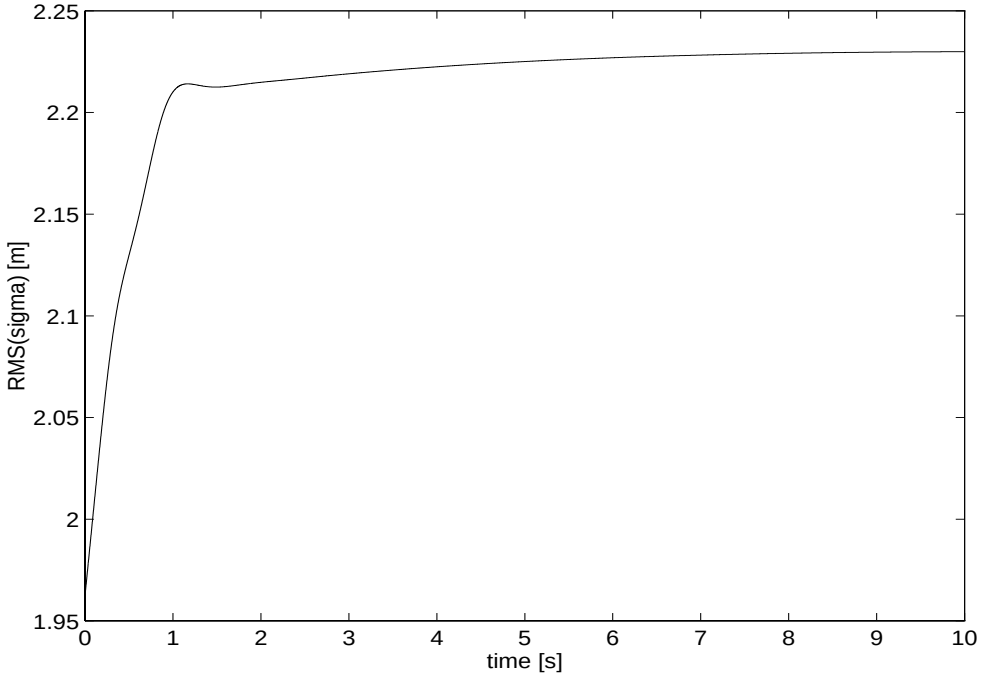

Figure 4.5: Estimated curve parameter (shape regulation)

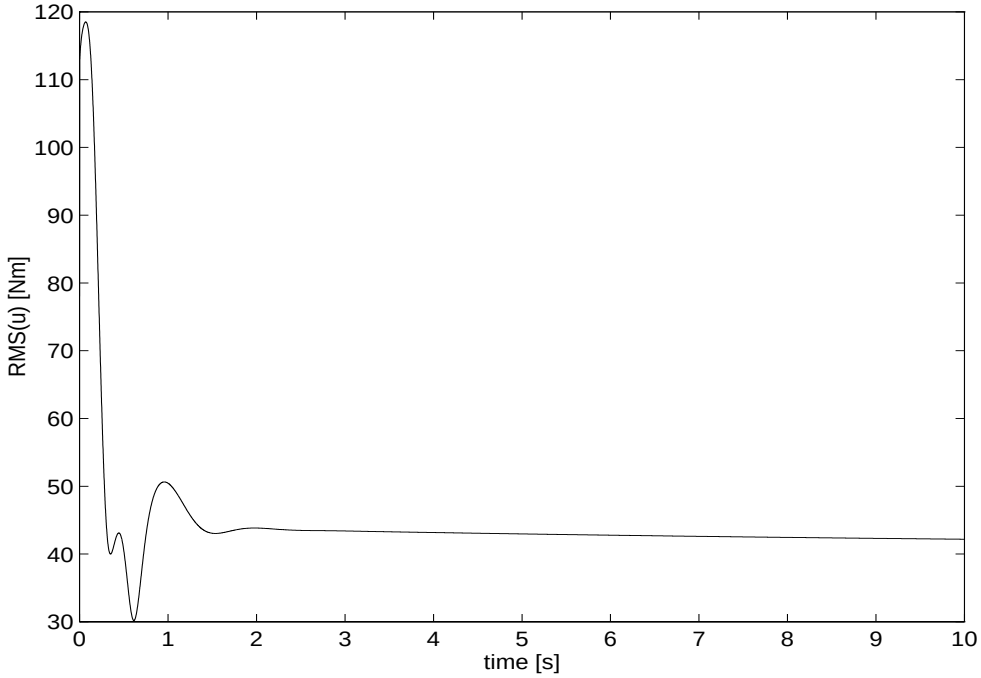

Figure 4.6: Input torgue (shape regulation)

Chapter 5

Shape Tracking

If we try to achieve dynamical motion by an HDOF manipulator, we need a control to move it along the desired shape changing continuously in time, that is, *shape tracking*. In this chapter, we consider a shape tracking problem where a time-varying curve is given to specify the desired shape. The idea of estimating the desired curve parameters is effective for the shape tracking problem as well. Introducing an estimator with 2nd-order dynamics and coupling it with manipulator dynamics allow us to utilize some familiar design methods for manipulator tracking to solve the shape tracking problem.

After a shape tracking control problem is stated in Section **5.1**, a curve parameter estimator with 2nd-order dynamics is introduced and coupled with manipulator dynamics in Section **5.2**. We will see that the coupled dynamics has the same properties as the original manipulator dynamics. In Section **5.3**, two illustrative examples are shown to explain how to find the shape tracking control law by using the tracking control law for a conventional manipulator. One is derived by the ID(inverse dynamics)-based method and the other by the Lyapunov-based method. We also show the recursive law and the simulation results in Section **5.4** and Section **5.5** respectively.

5.1 Problem Statement

The objective of shape tracking control is to make manipulator's shape follow a given time-varying curve. *Shape tracking problem* is stated as follows:

Problem 4 (Shape Tracking)

Consider

1. an HDOF manipulator with dynamics (2.34), and
2. a time-varying curve $\boldsymbol{c} : \Re \times \Re_+ \to E^3$ satisfying **Assumption 2**.

Moreover, suppose that **Assumption 5** holds. Then, find a control input, $\boldsymbol{u}$, in (2.34) achieving that

$$\boldsymbol{\theta}(t) \rightarrow \boldsymbol{\theta}^*(t), \tag{5.1}$$

$$\dot{\boldsymbol{\theta}}(t) \rightarrow \dot{\boldsymbol{\theta}}^*(t), \tag{5.2}$$

as $t \rightarrow \infty$, where $\boldsymbol{\theta}^*(t)$ is the desired joint angle function, that is, the solution of the extended shape inverse problem. □

In the same manner as the previous chapter, let $\hat{\boldsymbol{\sigma}} := [\ \hat{\sigma}_1 \cdots \hat{\sigma}_n]^T \in \Re^n$ be the estimate of $\boldsymbol{\sigma}^*$ and define the estimated shape error for a time-varying curve $\hat{\boldsymbol{e}} \in \Re^{3n}$ including $\hat{\boldsymbol{\sigma}}$ as

$$\begin{aligned} \hat{\boldsymbol{e}} &:= \boldsymbol{e}(\boldsymbol{\theta}, \hat{\boldsymbol{\sigma}}(t)) \\ &= \boldsymbol{p}(\boldsymbol{\theta}) - \boldsymbol{p}_d(\hat{\boldsymbol{\sigma}}(t)). \end{aligned} \tag{5.3}$$

In this case, $\dot{\hat{\boldsymbol{e}}} \in \Re^{3n}$ becomes

$$\dot{\hat{\boldsymbol{e}}} := \boldsymbol{J}(\boldsymbol{\theta}, \hat{\boldsymbol{\sigma}}(t)) \begin{bmatrix} \dot{\boldsymbol{\theta}} \\ \dot{\hat{\boldsymbol{\sigma}}} \end{bmatrix} - \frac{\partial \boldsymbol{p}_d}{\partial t}(\hat{\boldsymbol{\sigma}}(t)). \tag{5.4}$$

From **Theorem 4**, it is enough to aim at

$$\hat{\boldsymbol{e}}(\boldsymbol{\theta}, \hat{\boldsymbol{\sigma}}) \rightarrow \mathbf{o}, \tag{5.5}$$

$$\dot{\hat{\boldsymbol{e}}}(\boldsymbol{\theta}, \hat{\boldsymbol{\sigma}}, \dot{\boldsymbol{\theta}}, \dot{\hat{\boldsymbol{\sigma}}}) \rightarrow \mathbf{o}, \tag{5.6}$$

$$(\boldsymbol{\theta}, \hat{\boldsymbol{\sigma}}) \in \mathcal{D}_\delta, \tag{5.7}$$

instead of objectives (5.1) and (5.2) under the condition of non-singularity of Shape Jacobian for any t.

5.2 Estimation with 2nd-order Dynamics

For the shape tracking problem, we give an effective strategy to find the control law. Consider the following estimator with 2nd-order dynamics:

$$\boldsymbol{M}_\sigma \ddot{\hat{\boldsymbol{\sigma}}} = \boldsymbol{u}_\sigma, \tag{5.8}$$

where $\boldsymbol{M}_\sigma \in \Re^{n \times n}$ is symmetric positive definite and $\boldsymbol{u}_\sigma \in \Re^n$ is an input vector to the estimator. The reason of this choice will become clear after we explore the coupled dynamics of the manipulator and this estimator.

The coupled dynamics of manipulator (2.34) and estimator (5.8) can be expressed as

$$\bar{\boldsymbol{M}}(\boldsymbol{q})\,\ddot{\boldsymbol{q}} + \bar{\boldsymbol{C}}(\boldsymbol{q},\dot{\boldsymbol{q}})\dot{\boldsymbol{q}} + \bar{\boldsymbol{g}}(\boldsymbol{q}) = \bar{\boldsymbol{u}}, \tag{5.9}$$

where $\bar{\boldsymbol{M}} \in \Re^{3n\times 3n}$, $\bar{\boldsymbol{C}} \in \Re^{3n\times 3n}$, $\bar{\boldsymbol{g}} \in \Re^{3n}$ and $\bar{\boldsymbol{u}} \in \Re^{3n}$ are

$$\bar{\boldsymbol{M}}(\boldsymbol{q}) := \begin{bmatrix} \boldsymbol{M}(\boldsymbol{\theta}) & \\ & \boldsymbol{M}_\sigma \end{bmatrix}, \tag{5.10}$$

$$\bar{\boldsymbol{C}}(\boldsymbol{q},\dot{\boldsymbol{q}}) := \begin{bmatrix} \boldsymbol{C}(\boldsymbol{\theta},\dot{\boldsymbol{\theta}}) & \\ & \mathbf{o} \end{bmatrix}, \tag{5.11}$$

$$\bar{\boldsymbol{g}}(\boldsymbol{q}) := \begin{bmatrix} \boldsymbol{g}(\boldsymbol{\theta}) \\ \mathbf{o} \end{bmatrix}, \tag{5.12}$$

$$\bar{\boldsymbol{u}} := \begin{bmatrix} \boldsymbol{u} \\ \boldsymbol{u}_\sigma \end{bmatrix}. \tag{5.13}$$

Also define constants $\bar{M}_m, \bar{M}_M, \bar{C}_M$ as

$$\bar{M}_m := \min\{M_m, \lambda_m(\boldsymbol{M}_\sigma)\}, \tag{5.14}$$

$$\bar{M}_M := \max\{M_M, \lambda_M(\boldsymbol{M}_\sigma)\}, \tag{5.15}$$

$$\bar{C}_M := C_M, \tag{5.16}$$

where $\lambda_m(\cdot)$ and $\lambda_M(\cdot)$ denote the minimum and maximum eigenvalues respectively. The values M_m, M_M and C_M appeared in **Property 1** in Section **2.2**. Note that coupled dynamics (5.9) has exactly the same form as manipulator dynamics (2.34), and in addition, **Property 1** is preserved for $\bar{\boldsymbol{M}}(\boldsymbol{q})$ and $\bar{\boldsymbol{C}}(\boldsymbol{q},\dot{\boldsymbol{q}})$. That is, the norm of $\bar{\boldsymbol{M}}(\boldsymbol{q})$ has the lower and the upper bounds, $\bar{M}_m, \bar{M}_M$, and the norm of $\bar{\boldsymbol{C}}(\boldsymbol{q},\dot{\boldsymbol{q}})$ is also bounded from above by $\bar{C}_M\|\dot{\boldsymbol{q}}\|$. As a result, we can apply the familiar design methods for tracking (see the book [4], for example) to coupled system (5.9), that is the reason for our choice of estimator with 2nd-order dynamics (5.8).

The role of the estimator can also be explained as follows. In considering an estimator with 2nd-order dynamics, joint space is extended to one where the state variable is the pair, $(\boldsymbol{\theta},\hat{\boldsymbol{\sigma}})$, and its derivative. Consequently, the extended joint space is explicitly related to the task space of shape tracking, see (5.3) and (5.4). This fact allows us to discuss the stability in the task space.

5.3 Shape Tracking Based on Curve Parameter Estimation

In this section, we give two concrete examples to show how to derive the shape tracking control law. One is based on inverse dynamics, while the other is Lyapunov-based controller.

Inverse-dynamics-based Shape Tracking

For coupled system (5.9), we can consider the following ID-based control law in the similar way as [4]:

$$\bar{\boldsymbol{u}} = \bar{\boldsymbol{M}}(\boldsymbol{q})\bar{\boldsymbol{u}}_0 + \bar{\boldsymbol{C}}(\boldsymbol{q},\dot{\boldsymbol{q}})\dot{\boldsymbol{q}} + \bar{\boldsymbol{g}}(\boldsymbol{q}), \tag{5.17}$$

$$\bar{\boldsymbol{u}}_0 = \boldsymbol{J}^{-1}(\boldsymbol{q},t)\left\{\ddot{\boldsymbol{x}}_d - \dot{\boldsymbol{J}}(\boldsymbol{q},\dot{\boldsymbol{q}},t)\dot{\boldsymbol{q}} - \boldsymbol{K}_p\hat{\boldsymbol{e}} - \boldsymbol{K}_d\dot{\hat{\boldsymbol{e}}}\right\}, \tag{5.18}$$

where $\boldsymbol{K}_p$, $\boldsymbol{K}_d \in \Re^{3n\times 3n}$ are symmetric positive definite matrices, and $\ddot{\boldsymbol{x}}_d \in \Re^{3n}$ is defined as the derivative of $\dot{\boldsymbol{x}}_d$ that is interpreted as the estimated desired shape velocity with $\dot{\hat{\boldsymbol{\sigma}}} = \mathbf{o}$, i.e.,

$$\dot{\boldsymbol{x}}_d := \frac{\partial \boldsymbol{p}_d}{\partial t}(\hat{\boldsymbol{\sigma}},t) \tag{5.19}$$

$$= \dot{\boldsymbol{p}}_d(\hat{\boldsymbol{\sigma}},\mathbf{o},t). \tag{5.20}$$

By substituting control law (5.17) and (5.18) into coupled system (5.9), we obtain the following error system:

$$\ddot{\hat{\boldsymbol{e}}} + \boldsymbol{K}_d\dot{\hat{\boldsymbol{e}}} + \boldsymbol{K}_p\hat{\boldsymbol{e}} = \mathbf{o}, \tag{5.21}$$

which shows that $\hat{\boldsymbol{e}}$ and $\dot{\hat{\boldsymbol{e}}}$ converge to zero exponentially when $\boldsymbol{K}_p$ and $\boldsymbol{K}_d$ are symmetric positive definite.

We summarize this result in the following theorem in the form of exposing the estimator:

Theorem 6 (ID-based Shape Tracking)

Consider a control law with a curve parameter estimation law as follows :

$$\boldsymbol{u} = \boldsymbol{M}(\boldsymbol{\theta})\ddot{\boldsymbol{\theta}}_d + \boldsymbol{C}(\boldsymbol{\theta},\dot{\boldsymbol{\theta}})\dot{\boldsymbol{\theta}} + \boldsymbol{g}(\boldsymbol{\theta}), \tag{5.22}$$

$$\ddot{\hat{\boldsymbol{\sigma}}} = \ddot{\boldsymbol{\sigma}}_d, \tag{5.23}$$

where $\ddot{\boldsymbol{\theta}}_d \in \Re^{2n}$ and $\ddot{\boldsymbol{\sigma}}_d \in \Re^n$ are

$$\begin{bmatrix} \ddot{\boldsymbol{\theta}}_d \\ \ddot{\boldsymbol{\sigma}}_d \end{bmatrix} = \boldsymbol{J}^{-1}(\boldsymbol{q},t)\left\{\ddot{\boldsymbol{x}}_d - \dot{\boldsymbol{J}}(\boldsymbol{q},\dot{\boldsymbol{q}},t)\dot{\boldsymbol{q}} - \boldsymbol{K}_p\hat{\boldsymbol{e}} - \boldsymbol{K}_d\dot{\hat{\boldsymbol{e}}}\right\}, \tag{5.24}$$

and $\dot{\boldsymbol{x}}_d \in \Re^{3n}$ is defined by

$$\dot{\boldsymbol{x}}_d \;:=\; \frac{\partial \boldsymbol{p}_d}{\partial t}(\hat{\boldsymbol{\sigma}}, t) \tag{5.25}$$

and $\boldsymbol{K}_p, \boldsymbol{K}_d \in \Re^{3n\times 3n}$ are symmetric positive definite matrices. Then, under **Assumption 6**, the closed loop system with the control law is locally asymptotically stable at the equilibrium point, $(\boldsymbol{\theta}, \dot{\boldsymbol{\theta}}) = (\boldsymbol{\theta}^*, \dot{\boldsymbol{\theta}}^*)$, which means the control objective of shape tracking is achieved locally. □

Proof. Consider a map $T : \Re^{6n} \to \Re^{6n}$ defined by

$$\boldsymbol{z} \;=\; T(\boldsymbol{x}), \tag{5.26}$$

where $\boldsymbol{x}, \boldsymbol{z} \in \Re^{6n}$ are

$$\boldsymbol{x} \;:=\; \begin{bmatrix} \boldsymbol{q} - \boldsymbol{q}^* \\ \dot{\boldsymbol{q}} - \dot{\boldsymbol{q}}^* \end{bmatrix}, \tag{5.27}$$

$$\boldsymbol{z} \;:=\; \begin{bmatrix} \hat{\boldsymbol{e}} \\ \dot{\hat{\boldsymbol{e}}} \end{bmatrix}. \tag{5.28}$$

A map, T, is a diffeomorphism, because

$$\begin{aligned} \det \left.\frac{\partial T}{\partial \boldsymbol{x}}\right|_{\boldsymbol{x}=\mathbf{o}} &= \det \begin{bmatrix} \boldsymbol{J}(\boldsymbol{q}^*, t) & \mathbf{o} \\ * & \boldsymbol{J}(\boldsymbol{q}^*, t) \end{bmatrix} \\ &= \{\det \boldsymbol{J}(\boldsymbol{q}^*, t)\}^2 \\ &\neq 0, \end{aligned} \tag{5.29}$$

under **Assumption 6**. From (5.21),

$$\boldsymbol{z} \to \mathbf{o}. \tag{5.30}$$

Therefore, there exists a neighborhood of $\boldsymbol{x} = \mathbf{o}$ such that $\boldsymbol{x} \to \mathbf{o}$ if $\boldsymbol{x}$ starts from a point in the neighborhood. Then local asymptotic stability is proved. (Q.E.D.)

Note that $\ddot{\boldsymbol{\theta}}_d$ and $\ddot{\hat{\boldsymbol{\sigma}}}_d$ are strongly coupled by expression (5.24), while expression (5.22) simply means the inverse dynamics. In this controller, the desired joint angle accelleration, $\ddot{\boldsymbol{\theta}}_d$, is generated based on the dynamic curve paramter estimator.

Lyapunov-based Shape Tracking

We apply the idea of Lyapunov-based control [4], that is originated by Slotine and Li [25], to shape tracking control. That is, we try to bring a state of the system not directly to the objective point, but its sliding surface.

First, consider the following sliding surface where any states converge to the objective point:

$$\dot{\hat{\boldsymbol{e}}} + \boldsymbol{\Lambda}\hat{\boldsymbol{e}} = \mathbf{o}, \tag{5.31}$$

where $\boldsymbol{\Lambda} \in \Re^{3n\times 3n}$ is a symmetric positive definite matrix. Second, consider the following surface:

$$\boldsymbol{J}^{-1}(\boldsymbol{q},t)\left(\dot{\hat{\boldsymbol{e}}} + \boldsymbol{\Lambda}\hat{\boldsymbol{e}}\right) = \mathbf{o}, \tag{5.32}$$

that is also a sliding surface of the objective point if the Shape Jacobian is non-singular. This sliding surface is interpreted as the sliding surface in the extended joint space. We define a sliding variable, $\boldsymbol{s}_c \in \Re^{3n}$, as the left-hand side of the surface above, i.e.,

$$\boldsymbol{s}_c \;:=\; \boldsymbol{J}^{-1}(\boldsymbol{q},t)\left(\dot{\hat{\boldsymbol{e}}} + \boldsymbol{\Lambda}\hat{\boldsymbol{e}}\right). \tag{5.33}$$

Furthermore, we define a virtual reference velocity, $\dot{\boldsymbol{q}}_r \in \Re^{3n}$, composed of $\dot{\boldsymbol{\theta}}_r \in \Re^{2n}$ and $\dot{\hat{\boldsymbol{\sigma}}}_r \in \Re^{n}$, such that $\boldsymbol{s}_c := \dot{\boldsymbol{q}} - \dot{\boldsymbol{q}}_r$, i.e.,

$$\begin{aligned}
\dot{\boldsymbol{q}}_r &= \begin{bmatrix} \dot{\boldsymbol{\theta}}_r \\ \dot{\hat{\boldsymbol{\sigma}}}_r \end{bmatrix} && (5.34)\\
&:= \dot{\boldsymbol{q}} - \boldsymbol{s}_c \\
&= \dot{\boldsymbol{q}} - \boldsymbol{J}^{-1}(\boldsymbol{q},t)\left(\dot{\hat{\boldsymbol{e}}} + \boldsymbol{\Lambda}\hat{\boldsymbol{e}}\right) \\
&= \boldsymbol{J}^{-1}(\boldsymbol{q},t)\left\{\boldsymbol{J}(\boldsymbol{q},t)\dot{\boldsymbol{q}} - \dot{\hat{\boldsymbol{e}}} + \boldsymbol{\Lambda}\hat{\boldsymbol{e}}\right\} \\
&= \boldsymbol{J}^{-1}(\boldsymbol{q},t)\left\{\boldsymbol{J}(\boldsymbol{q},t)\dot{\boldsymbol{q}} - \boldsymbol{J}(\boldsymbol{q},t)\dot{\boldsymbol{q}} + \frac{\partial \boldsymbol{p}_d}{\partial t}(\hat{\boldsymbol{\sigma}},t) + \boldsymbol{\Lambda}\hat{\boldsymbol{e}}\right\} \\
&= \boldsymbol{J}^{-1}(\boldsymbol{q},t)\left\{\frac{\partial \boldsymbol{p}_d}{\partial t}(\hat{\boldsymbol{\sigma}},t) - \boldsymbol{\Lambda}\hat{\boldsymbol{e}}\right\}. && (5.35)
\end{aligned}$$

Here we consider the following Lyapunov-based control law for the coupled system [1]:

$$\bar{\boldsymbol{u}} \;=\; \bar{\boldsymbol{M}}(\boldsymbol{q})\ddot{\boldsymbol{q}}_r + \bar{\boldsymbol{C}}(\boldsymbol{q},\dot{\boldsymbol{q}})\dot{\boldsymbol{q}}_r + \bar{\boldsymbol{g}}(\boldsymbol{q}) - \boldsymbol{J}^T(\boldsymbol{q},t)\boldsymbol{K}_p\hat{\boldsymbol{e}} - \boldsymbol{K}_v\boldsymbol{s}_c, \tag{5.36}$$

where $\boldsymbol{K}_p \in \Re^{3n\times 3n}$, and $\boldsymbol{K}_v \in \Re^{2n\times 2n}$ are symmetric positive definite matrices. By substituting control law (5.36) into coupled system (5.9) and using definition (5.33), we obtain the following closed-loop dynamics:

$$\bar{\boldsymbol{M}}(\boldsymbol{q})\,\dot{\boldsymbol{s}}_c + \bar{\boldsymbol{C}}(\boldsymbol{q},\dot{\boldsymbol{q}})\boldsymbol{s}_c + \boldsymbol{K}_v\boldsymbol{s}_c + \boldsymbol{J}^T(\boldsymbol{q},t)\boldsymbol{K}_p\hat{\boldsymbol{e}} = \mathbf{o}. \tag{5.37}$$

Let $V_c : \Re^{3n} \to \Re_+$ be the following positive definite function with respect to $(\boldsymbol{s}_c, \hat{\boldsymbol{e}})$:

$$V_c(\boldsymbol{s}_c,\hat{\boldsymbol{e}}) := \frac{1}{2}\boldsymbol{s}_c{}^T\bar{\boldsymbol{M}}(\boldsymbol{q})\,\boldsymbol{s}_c + \frac{1}{2}\hat{\boldsymbol{e}}^T\boldsymbol{K}_p\hat{\boldsymbol{e}}. \tag{5.38}$$

Differentiating (5.38) along the trajectory and considering **Property 1**-4 yield

$$\begin{aligned}\dot{V}(\boldsymbol{s}_c, \hat{\boldsymbol{e}}) &= \boldsymbol{s}_c{}^T \bar{\boldsymbol{M}}(\boldsymbol{q})\, \dot{\boldsymbol{s}}_c + \frac{1}{2}\boldsymbol{s}_c{}^T \dot{\bar{\boldsymbol{M}}}(\boldsymbol{q})\, \boldsymbol{s}_c + \hat{\boldsymbol{e}}^T \boldsymbol{K}_p \dot{\hat{\boldsymbol{e}}} \\ &= -\boldsymbol{s}_c{}^T \boldsymbol{K}_v\, \boldsymbol{s}_c + \frac{1}{2}\boldsymbol{s}_c{}^T \left\{ \dot{\bar{\boldsymbol{M}}}(\boldsymbol{q}) - 2\bar{\boldsymbol{C}}(\boldsymbol{q}, \dot{\boldsymbol{q}}) \right\} \boldsymbol{s}_c - \boldsymbol{s}_c{}^T \boldsymbol{J}^T(\boldsymbol{q}, t) \boldsymbol{K}_p \hat{\boldsymbol{e}} + \hat{\boldsymbol{e}}^T \boldsymbol{K}_p \dot{\hat{\boldsymbol{e}}} \\ &= -\boldsymbol{s}_c{}^T \boldsymbol{K}_v \boldsymbol{s}_c - \hat{\boldsymbol{e}}^T \boldsymbol{\Lambda}^T \boldsymbol{K}_p \hat{\boldsymbol{e}}, \end{aligned} \tag{5.39}$$

which shows $\dot{V}$ is negative definite with respect to $(\boldsymbol{s}_c, \hat{\boldsymbol{e}})$ if $\boldsymbol{\Lambda}^T \boldsymbol{K}_p = \boldsymbol{K}_p{}^T \boldsymbol{\Lambda} > 0$. Thus, by Lyapunov theorem, we conclude that $\hat{\boldsymbol{e}}$ and $\boldsymbol{s}_c$ converge to zero asymptotically, that is equivalent to asymptotic convergence of $\hat{\boldsymbol{e}}$ and $\dot{\hat{\boldsymbol{e}}}$ to zero, by the definition of $\boldsymbol{s}_c$.

We show a theorem summarizing the above result:

Theorem 7 (Lyapunov-based Shape Tracking)

Consider a control law with a curve parameter estimation law as follows:

$$\boldsymbol{u} = \boldsymbol{M}(\boldsymbol{\theta})\ddot{\boldsymbol{\theta}}_r + \boldsymbol{C}(\boldsymbol{\theta}, \dot{\boldsymbol{\theta}})\dot{\boldsymbol{\theta}}_r + \boldsymbol{g}(\boldsymbol{\theta}) + \boldsymbol{\tau}_\theta, \tag{5.40}$$

$$\ddot{\hat{\boldsymbol{\sigma}}} = \ddot{\hat{\boldsymbol{\sigma}}}_r + \boldsymbol{K}_\sigma \boldsymbol{\tau}_\sigma, \tag{5.41}$$

where $\boldsymbol{\tau}_\theta \in \Re^{2n}$ and $\boldsymbol{\tau}_\sigma \in \Re^n$ are

$$\begin{bmatrix} \boldsymbol{\tau}_\theta \\ \boldsymbol{\tau}_\sigma \end{bmatrix} = -\boldsymbol{J}^T(\boldsymbol{q}, t)\boldsymbol{K}_p \hat{\boldsymbol{e}} - \boldsymbol{K}_v (\dot{\boldsymbol{q}} - \dot{\boldsymbol{q}}_r), \tag{5.42}$$

and $\dot{\boldsymbol{q}}_r \in \Re^{3n}$, $\dot{\boldsymbol{\theta}}_r \in \Re^{2n}$, $\dot{\hat{\boldsymbol{\sigma}}}_r \in \Re^n$, are defined by

$$\dot{\boldsymbol{q}}_r = \begin{bmatrix} \dot{\boldsymbol{\theta}}_r \\ \dot{\hat{\boldsymbol{\sigma}}}_r \end{bmatrix} := \boldsymbol{J}^{-1}(\boldsymbol{q}, t) \left\{ \frac{\partial \boldsymbol{p}_d}{\partial t}(\hat{\boldsymbol{\sigma}}, t) - \boldsymbol{\Lambda}\hat{\boldsymbol{e}} \right\}, \tag{5.43}$$

and $\boldsymbol{K}_p, \boldsymbol{\Lambda} \in \Re^{3n \times 3n}$ are symmetric positive definite matrices with the relation $\boldsymbol{\Lambda}^T \boldsymbol{K}_p = \boldsymbol{K}_p{}^T \boldsymbol{\Lambda} > 0$, $\boldsymbol{K}_v \in \Re^{2n \times 2n}$ and $\boldsymbol{K}_\sigma := \boldsymbol{M}_\sigma{}^{-1} \in \Re^{n \times n}$ are also symmetric positive definite matrices. Then, under **Assumption 6**, the closed loop system with the control law is locally asymptotically stable at the equilibrium point, $(\boldsymbol{\theta}, \dot{\boldsymbol{\theta}}) = (\boldsymbol{\theta}^*, \dot{\boldsymbol{\theta}}^*)$, which means the control objective of shape tracking is achieved locally. □

Proof. This proof can be achieved in the similar mannar as the proof of the previous theorem. (Q.E.D.)

Since $\boldsymbol{M}_\sigma$ is not a matrix of a manipulator system (not a given value), but one of estimator (5.8) (a design value), its positive definite inverse $\boldsymbol{K}_\sigma$ is also a design value. Matrix $\boldsymbol{K}_\sigma$ is regarded as a gain of the estimator. Note that this kind of estimator gain does not appear in the ID-based control law.

The control input $\boldsymbol{u}$ and the estimator are strongly coupled by not only (5.42) but also (5.35), although the first expression seems to be an ordinary Lyapunov-based control law.

5.4 Recursive Expression

We show the recursive expression for the shape tracking control law derived in the previous section.

ID-based Shape Tracking

Since (5.22) is calculated recursively by the Newton-Euler method for the calculation of manipulator dyanmics, we only show a recursive expression of (5.24).

Assume that gain matrices have the following diagonal forms:

$$\boldsymbol{K}_p = \mathrm{blockdiag}\{\boldsymbol{K}_{p,1}, \cdots, \boldsymbol{K}_{p,n}\}, \tag{5.44}$$

$$\boldsymbol{K}_d = \mathrm{blockdiag}\{\boldsymbol{K}_{d,1}, \cdots, \boldsymbol{K}_{d,n}\}, \tag{5.45}$$

where $\boldsymbol{K}_{p,i}, \boldsymbol{K}_{d,i} \in \Re^{3\times 3}$ are symmetric positive definite matrices.

Multiplying the both sides of (5.24) by $\boldsymbol{J}(\boldsymbol{q},t)$ leads to

$$\boldsymbol{J}(\boldsymbol{q},t)\begin{bmatrix} \ddot{\boldsymbol{\theta}}_d \\ \ddot{\boldsymbol{\sigma}}_d \end{bmatrix} = \ddot{\boldsymbol{x}}_d - \dot{\boldsymbol{J}}(\boldsymbol{q},\dot{\boldsymbol{q}},t)\dot{\boldsymbol{q}} - \boldsymbol{K}_p\hat{\boldsymbol{e}} - \boldsymbol{K}_d\dot{\hat{\boldsymbol{e}}}. \tag{5.46}$$

Divide $\ddot{\boldsymbol{\theta}}_d$ and $\ddot{\boldsymbol{\sigma}}_d$ into n parts, and let $\ddot{\boldsymbol{\theta}}_{d,i} \in \Re^2$ and $\ddot{\sigma}_{d,i} \in \Re$ be their i-th elements respectively. Furthermore, define $\ddot{\tilde{\boldsymbol{q}}}_{d,i} := \left[\ddot{\boldsymbol{\theta}}_{d,i}^T \ \ddot{\sigma}_{d,i}\right]^T \in \Re^3$. Then, $\ddot{\tilde{\boldsymbol{q}}}_{d,i}$ can be written as follows due to the lower-triangular structure of the Shape Jacobian (see (3.50)):

$$\begin{aligned} \ddot{\tilde{\boldsymbol{q}}}_{d,i} &= \begin{bmatrix} \ddot{\boldsymbol{\theta}}_{d,i} \\ \ddot{\sigma}_{d,i} \end{bmatrix} \\ &= \bar{\boldsymbol{J}}_{ii}^{-1}\left\{\ddot{\boldsymbol{c}}(\hat{\sigma}_i, 0, 0, t) - \sum_{k=1}^{i-1}\bar{\boldsymbol{J}}_{ik}\ddot{\tilde{\boldsymbol{q}}}_{d,k} - \sum_{k=1}^{i}\dot{\bar{\boldsymbol{J}}}_{ik}\dot{\tilde{\boldsymbol{q}}}_k - \boldsymbol{K}_{p,i}\hat{\boldsymbol{e}}_i - \boldsymbol{K}_{d,i}\dot{\hat{\boldsymbol{e}}}_i\right\}. \end{aligned} \tag{5.47}$$

From (3.51), the definition of $\bar{\boldsymbol{J}}_{ik}$, the second term in the bracket in the above expression is written as

$$-\sum_{k=1}^{i-1}\bar{\boldsymbol{J}}_{ik}\ddot{\tilde{\boldsymbol{q}}}_{d,k} = \sum_{k=1}^{i-1}\left\{\left(\boldsymbol{p}_i - \boldsymbol{p}_{k-1}\right) \times \Delta\dot{\boldsymbol{\omega}}_{2,k}(\boldsymbol{\theta}, \ddot{\boldsymbol{\theta}}_d)\right\}, \tag{5.48}$$

where $\Delta\dot{\boldsymbol{\omega}}_{2,k}(\boldsymbol{\theta}, \ddot{\boldsymbol{\theta}}) \in \Re^3$ is defined as

$$\Delta\dot{\boldsymbol{\omega}}_{2,k}(\boldsymbol{\theta}, \ddot{\boldsymbol{\theta}}) := \boldsymbol{\Phi}_{i-1}\boldsymbol{a}_{s,i}\ddot{\theta}_{s,i} + \boldsymbol{\Phi}_i\boldsymbol{a}_{m,i}\ddot{\theta}_{m,i}. \tag{5.49}$$

The third term in the bracket becomes

$$
\begin{aligned}
-\sum_{k=1}^{i} \dot{\boldsymbol{J}}_{ik}\dot{\boldsymbol{q}}_k &= \sum_{k=1}^{i} \left\{ \left(\boldsymbol{p}_i - \boldsymbol{p}_{k-1}\right) \times \Delta\dot{\boldsymbol{\omega}}_{1,k} + \left(\dot{\boldsymbol{p}}_i - \dot{\boldsymbol{p}}_{k-1}\right) \times \Delta\boldsymbol{\omega}_k \right\} \\
&\quad + \frac{\partial^2 \boldsymbol{c}}{\partial\sigma^2}(\hat{\sigma}_i, t)\dot{\hat{\sigma}}_i^2 + \frac{\partial^2 \boldsymbol{c}}{\partial\sigma\partial t}(\hat{\sigma}_i, t)\dot{\hat{\sigma}}_i, \qquad (5.50)
\end{aligned}
$$

where $\Delta\dot{\boldsymbol{\omega}}_{1,k}\,,\ \Delta\boldsymbol{\omega}_k \in \Re^3$ are defined as

$$
\begin{aligned}
\Delta\dot{\boldsymbol{\omega}}_{1,k}(\boldsymbol{\theta}, \dot{\boldsymbol{\theta}}) &:= [\boldsymbol{\omega}_{i-1}\times]\,\boldsymbol{\Phi}_{i-1}\boldsymbol{a}_{s,i}\dot{\theta}_{s,i} + [\boldsymbol{\omega}_i\times]\,\boldsymbol{\Phi}_i\boldsymbol{a}_{m,i}\dot{\theta}_{m,i}, \qquad (5.51) \\
\Delta\boldsymbol{\omega}_k(\boldsymbol{\theta}, \dot{\boldsymbol{\theta}}) &:= \boldsymbol{\Phi}_{i-1}\boldsymbol{a}_{s,i}\dot{\theta}_{s,i} + \boldsymbol{\Phi}_i\boldsymbol{a}_{m,i}\dot{\theta}_{m,i}. \qquad (5.52)
\end{aligned}
$$

Notice that the following relationships:

$$
\begin{aligned}
\boldsymbol{\omega}_k - \boldsymbol{\omega}_{k-1} &= \Delta\boldsymbol{\omega}_k, \\
\dot{\boldsymbol{\omega}}_k - \dot{\boldsymbol{\omega}}_{k-1} &= \Delta\dot{\boldsymbol{\omega}}_{1,k} + \Delta\dot{\boldsymbol{\omega}}_{2,k}.
\end{aligned}
$$

This implies that

$$
\ddot{\boldsymbol{c}}(\hat{\sigma}_i, 0, 0, t) + \frac{\partial^2 \boldsymbol{c}}{\partial\sigma^2}(\hat{\sigma}_i, t)\dot{\hat{\sigma}}_i^2 + \frac{\partial^2 \boldsymbol{c}}{\partial\sigma\partial t}(\hat{\sigma}_i, t)\dot{\hat{\sigma}}_i = \ddot{\boldsymbol{c}}(\hat{\sigma}_i, \dot{\hat{\sigma}}_i, 0, t), \qquad (5.53)
$$

and

$$
\begin{aligned}
&\sum_{k=1}^{i-1} \left\{ \left(\boldsymbol{p}_i - \boldsymbol{p}_{k-1}\right) \times \Delta\dot{\boldsymbol{\omega}}_{2,k}(\boldsymbol{\theta}, \ddot{\boldsymbol{\theta}}_d) \right\} + \sum_{k=1}^{i} \left\{ \left(\boldsymbol{p}_i - \boldsymbol{p}_{k-1}\right) \times \Delta\dot{\boldsymbol{\omega}}_{1,k} + \left(\dot{\boldsymbol{p}}_i - \dot{\boldsymbol{p}}_{k-1}\right) \times \Delta\boldsymbol{\omega}_k \right\} \\
&= \sum_{k=1}^{i} \left\{ \left(\boldsymbol{p}_i - \boldsymbol{p}_{k-1}\right) \times \Delta\dot{\boldsymbol{\omega}}_k(\boldsymbol{\theta}, \dot{\boldsymbol{\theta}}, \ddot{\boldsymbol{\theta}}_d)\Big|_{\ddot{\boldsymbol{\theta}}_{d,i}=\mathbf{o}} + \left(\dot{\boldsymbol{p}}_i - \dot{\boldsymbol{p}}_{k-1}\right) \times \Delta\boldsymbol{\omega}_k \right\} \\
&= \sum_{k=1}^{i} \frac{d}{dt} \left\{ \left(\boldsymbol{p}_i - \boldsymbol{p}_{k-1}\right) \times \Delta\boldsymbol{\omega}_k \right\}\Big|_{\ddot{\boldsymbol{\theta}}=\ddot{\boldsymbol{\theta}}_d, \ddot{\boldsymbol{\theta}}_{d,i}=\mathbf{o}} \\
&= \frac{d}{dt} \sum_{k=1}^{i} \left\{ \left(\boldsymbol{p}_i - \boldsymbol{p}_{k-1}\right) \times \Delta\boldsymbol{\omega}_k \right\}\Big|_{\ddot{\boldsymbol{\theta}}=\ddot{\boldsymbol{\theta}}_d, \ddot{\boldsymbol{\theta}}_{d,i}=\mathbf{o}} \\
&= -\ddot{\boldsymbol{p}}_i(\boldsymbol{\theta}, \dot{\boldsymbol{\theta}}, \ddot{\boldsymbol{\theta}}_d)\Big|_{\ddot{\boldsymbol{\theta}}_{d,i}=\mathbf{o}}\,. \qquad (5.54)
\end{aligned}
$$

Then, we have the following recursive expression of $\ddot{\boldsymbol{q}}_d$:

$$
\begin{aligned}
\ddot{\boldsymbol{q}}_d &= \begin{bmatrix} \ddot{\boldsymbol{\theta}}_{d,i} \\ \ddot{\sigma}_{d,i} \end{bmatrix} \\
&= \bar{\boldsymbol{J}}_{ii}^{-1} \left(\ddot{\boldsymbol{c}}(\hat{\sigma}_i, \dot{\hat{\sigma}}_i, 0, t) - \ddot{\boldsymbol{p}}_i(\boldsymbol{\theta}, \dot{\boldsymbol{\theta}}, \ddot{\boldsymbol{\theta}}_d)\Big|_{\ddot{\boldsymbol{\theta}}_{d,i}=\mathbf{o}} - \boldsymbol{K}_{p,i}\hat{\boldsymbol{e}}_i - \boldsymbol{K}_{d,i}\dot{\hat{\boldsymbol{e}}}_i \right) \\
&= -\bar{\boldsymbol{J}}_{ii}^{-1} \left(\ddot{\hat{\boldsymbol{e}}}_i(\boldsymbol{q}, \dot{\boldsymbol{q}}, \ddot{\boldsymbol{q}}_d)\Big|_{\ddot{\boldsymbol{q}}_{d,i}=\mathbf{o}} + \boldsymbol{K}_{d,i}\dot{\hat{\boldsymbol{e}}}_i + \boldsymbol{K}_{p,i}\hat{\boldsymbol{e}}_i \right). \qquad (5.55)
\end{aligned}
$$

It is worth noting that $\bar{\boldsymbol{J}}_{ii}^{-1}$ is calculated by

$$\bar{\boldsymbol{J}}_{ii}^{-1} = \frac{1}{\Delta_J} \begin{bmatrix} \boldsymbol{j}_1^T \\ \boldsymbol{j}_2^T \\ \boldsymbol{j}_3^T \end{bmatrix}, \tag{5.56}$$

where $\Delta_J \in \Re$, $\boldsymbol{j}_1, \boldsymbol{j}_2, \boldsymbol{j}_3 \in \Re^3$ are

$$\Delta_J = -\det \begin{bmatrix} \boldsymbol{p}_i - \boldsymbol{p}_{i-1} & \boldsymbol{\Phi}_{i-1}\boldsymbol{a}_{s,i} & \boldsymbol{\Phi}_i\boldsymbol{a}_{m,i} \end{bmatrix} \boldsymbol{t}_i^T \left(\boldsymbol{p}_i - \boldsymbol{p}_{i-1}\right), \tag{5.57}$$

$$\boldsymbol{j}_1 = \left\{\boldsymbol{t}_i^T \left(\boldsymbol{p}_i - \boldsymbol{p}_{i-1}\right)\right\} \boldsymbol{\Phi}_i\boldsymbol{a}_{m,i} - \left\{\boldsymbol{t}_i^T \boldsymbol{\Phi}_i\boldsymbol{a}_{m,i}\right\} \left(\boldsymbol{p}_i - \boldsymbol{p}_{i-1}\right), \tag{5.58}$$

$$\boldsymbol{j}_2 = \left\{\boldsymbol{t}_i^T \boldsymbol{\Phi}_{i-1}\boldsymbol{a}_{s,i}\right\} \left(\boldsymbol{p}_i - \boldsymbol{p}_{i-1}\right) - \left\{\boldsymbol{t}_i^T \left(\boldsymbol{p}_i - \boldsymbol{p}_{i-1}\right)\right\} \boldsymbol{\Phi}_{i-1}\boldsymbol{a}_{s,i}, \tag{5.59}$$

$$\boldsymbol{j}_3 = \det \begin{bmatrix} \boldsymbol{p}_i - \boldsymbol{p}_{i-1} & \boldsymbol{\Phi}_{i-1}\boldsymbol{a}_{s,i} & \boldsymbol{\Phi}_i\boldsymbol{a}_{m,i} \end{bmatrix} \left(\boldsymbol{p}_i - \boldsymbol{p}_{i-1}\right). \tag{5.60}$$

In the expressions above, we abbreviate $\dfrac{\partial \boldsymbol{c}}{\partial \sigma}(\hat{\sigma}_i, t)$ as $\boldsymbol{t}_i$. This expression of $\bar{\boldsymbol{J}}_{ii}^{-1}$ shows that $\bar{\boldsymbol{J}}_{ii}^{-1}$ is composed of four significant vectors in E^3, the link vector ($\boldsymbol{p}_i - \boldsymbol{p}_{i-1}$), the Sub-axis ($\boldsymbol{\Phi}_{i-1}\boldsymbol{a}_{s,i}$), the Main-axis ($\boldsymbol{\Phi}_i\boldsymbol{a}_{m,i}$), and the tangent vector ($\boldsymbol{t}_i$).

Lyapunov-based Shape Tracking

The first three terms in the right-hand side of (5.40) are calculated by the same way as the ordinary Lyapunov-based method. Since (5.42) also has the same structure as the shape regulation law shown in the previous chapter, we only consider the recursive expressions of $\dot{\boldsymbol{q}}_r$ and $\ddot{\boldsymbol{q}}_r$ here.

First, choose $\boldsymbol{\Lambda}$ as

$$\boldsymbol{\Lambda} = \text{blockdiag}\left\{\boldsymbol{\Lambda}_1, \cdots, \boldsymbol{\Lambda}_n\right\}, \tag{5.61}$$

where $\boldsymbol{\Lambda}_i \in \Re^{3\times 3}$ is symmetric positive definite matrix.

Define $\dot{\tilde{\boldsymbol{q}}}_{r,i}$ in the same mannar as the definition of $\ddot{\tilde{\boldsymbol{q}}}_{d,i}$. Then, we obtain

$$\begin{aligned} \dot{\tilde{\boldsymbol{q}}}_{r,i} &= \begin{bmatrix} \dot{\boldsymbol{\theta}}_{r,i} \\ \dot{\sigma}_{r,i} \end{bmatrix} \\ &= \bar{\boldsymbol{J}}_{ii}^{-1} \left\{\dot{\boldsymbol{c}}(\hat{\sigma}_i, 0, t) - \sum_{k=1}^{i-1} \bar{\boldsymbol{J}}_{ik}\dot{\tilde{\boldsymbol{q}}}_{r,k} - \boldsymbol{\Lambda}_i\hat{\boldsymbol{e}}_i\right\}. \end{aligned} \tag{5.62}$$

Since the second term in the bracket in the expression above is expressed as

$$-\sum_{k=1}^{i-1} \bar{\boldsymbol{J}}_{ik}\dot{\tilde{\boldsymbol{q}}}_{r,k} = -\dot{\boldsymbol{p}}_{i-1}(\boldsymbol{\theta}, \dot{\boldsymbol{\theta}}_r), \tag{5.63}$$

then (5.62) can be rewritten as

$$\begin{aligned}\dot{\bar{\boldsymbol{q}}}_{r,i} &= \begin{bmatrix} \dot{\boldsymbol{\theta}}_{r,i} \\ \dot{\sigma}_{r,i} \end{bmatrix} \\ &= \bar{\boldsymbol{J}}_{ii}^{-1} \left\{ \dot{\boldsymbol{c}}(\hat{\sigma}_i, 0, t) - \dot{\boldsymbol{p}}_i(\boldsymbol{\theta}, \dot{\boldsymbol{\theta}}_r)\Big|_{\dot{\boldsymbol{\theta}}_{r,i}=\mathbf{o}} - \boldsymbol{\Lambda}_i \hat{\boldsymbol{e}}_i \right\} \\ &= -\bar{\boldsymbol{J}}_{ii}^{-1} \left\{ \dot{\hat{\boldsymbol{e}}}_i(\boldsymbol{q}, \dot{\boldsymbol{q}}_r)\Big|_{\dot{\boldsymbol{q}}_{r,i}=\mathbf{o}} + \boldsymbol{\Lambda}_i \hat{\boldsymbol{e}}_i \right\}. \end{aligned} \tag{5.64}$$

On the other hand, $\ddot{\bar{\boldsymbol{q}}}_{r,i}$ can be written as

$$\begin{aligned}\ddot{\bar{\boldsymbol{q}}}_{r,i} &= \begin{bmatrix} \ddot{\boldsymbol{\theta}}_{r,i} \\ \ddot{\sigma}_{r,i} \end{bmatrix} \\ &= \bar{\boldsymbol{J}}_{ii}^{-1} \left\{ \ddot{\boldsymbol{c}}(\hat{\sigma}_i, \dot{\hat{\sigma}}_i, 0, t) - \sum_{k=1}^{i-1} \bar{\boldsymbol{J}}_{ik} \ddot{\bar{\boldsymbol{q}}}_{r,k} - \sum_{k=1}^{i} \dot{\bar{\boldsymbol{J}}}_{ik} \dot{\bar{\boldsymbol{q}}}_{r,k} - \boldsymbol{\Lambda}_i \dot{\hat{\boldsymbol{e}}}_i \right\}. \end{aligned} \tag{5.65}$$

The second and third terms in the bracket above are expressed as

$$-\sum_{k=1}^{i-1} \bar{\boldsymbol{J}}_{ik} \ddot{\bar{\boldsymbol{q}}}_{r,k} = \sum_{k=1}^{i-1} \left\{ \left(\boldsymbol{p}_i - \boldsymbol{p}_{k-1} \right) \times \Delta\dot{\boldsymbol{\omega}}_{2,k}(\boldsymbol{\theta}, \ddot{\boldsymbol{\theta}}_r) \right\} \tag{5.66}$$

and

$$\begin{aligned}-\sum_{k=1}^{i} \dot{\bar{\boldsymbol{J}}}_{ik} \dot{\bar{\boldsymbol{q}}}_{r,k} &= \sum_{k=1}^{i} \left\{ \left(\boldsymbol{p}_i - \boldsymbol{p}_{k-1} \right) \times \Delta\dot{\boldsymbol{\omega}}_{1,k}(\boldsymbol{\theta}, \dot{\boldsymbol{\theta}}, \dot{\boldsymbol{\theta}}_r) + \left(\dot{\boldsymbol{p}}_i - \dot{\boldsymbol{p}}_{k-1} \right) \times \Delta\boldsymbol{\omega}_k(\boldsymbol{\theta}, \dot{\boldsymbol{\theta}}_r) \right\} \\ &\quad + \frac{\partial^2 \boldsymbol{c}}{\partial \sigma^2}(\hat{\sigma}_i, t) \dot{\hat{\sigma}}_i \dot{\hat{\sigma}}_{r,i} + \frac{\partial^2 \boldsymbol{c}}{\partial \sigma \partial t}(\hat{\sigma}_i, t) \dot{\hat{\sigma}}_{r,i}. \end{aligned} \tag{5.67}$$

By using the following relationships

$$\ddot{\boldsymbol{c}}(\hat{\sigma}_i, 0, 0, t) + \frac{\partial^2 \boldsymbol{c}}{\partial \sigma^2}(\hat{\sigma}_i, t) \dot{\hat{\sigma}}_i \dot{\hat{\sigma}}_{r,i} + \frac{\partial^2 \boldsymbol{c}}{\partial \sigma \partial t}(\hat{\sigma}_i, t) \dot{\hat{\sigma}}_{r,i} = \ddot{\boldsymbol{c}}(\hat{\sigma}_i, \dot{\hat{\sigma}}_i, \dot{\hat{\sigma}}_{r,i}, 0, t), \tag{5.68}$$

and

$$\begin{aligned}&\sum_{k=1}^{i-1} \left\{ \left(\boldsymbol{p}_i - \boldsymbol{p}_{k-1} \right) \times \Delta\dot{\boldsymbol{\omega}}_{2,k}(\boldsymbol{\theta}, \ddot{\boldsymbol{\theta}}_r) \right\} \\ &\quad + \sum_{k=1}^{i} \left\{ \left(\boldsymbol{p}_i - \boldsymbol{p}_{k-1} \right) \times \Delta\dot{\boldsymbol{\omega}}_{1,k}(\boldsymbol{\theta}, \dot{\boldsymbol{\theta}}, \dot{\boldsymbol{\theta}}_r) + \left(\dot{\boldsymbol{p}}_i - \dot{\boldsymbol{p}}_{k-1} \right) \times \Delta\boldsymbol{\omega}_k(\boldsymbol{\theta}, \dot{\boldsymbol{\theta}}_r) \right\} \\ &= \sum_{k=1}^{i} \left\{ \left(\left[\dot{\boldsymbol{\omega}}_k(\boldsymbol{\theta}, \dot{\boldsymbol{\theta}}, \dot{\boldsymbol{\theta}}_r, \ddot{\boldsymbol{\theta}}_r)\Big|_{\ddot{\boldsymbol{\theta}}_{r,i}=\mathbf{o}} \times \right] + \left[\boldsymbol{\omega}_k(\boldsymbol{\theta}, \dot{\boldsymbol{\theta}}_r) \times \right] \left[\boldsymbol{\omega}_k(\boldsymbol{\theta}, \dot{\boldsymbol{\theta}}) \times \right] \right) \boldsymbol{\Phi}_k \boldsymbol{l}_k \right\} \\ &= -\ddot{\boldsymbol{p}}(\boldsymbol{\theta}, \dot{\boldsymbol{\theta}}, \dot{\boldsymbol{\theta}}_r, \ddot{\boldsymbol{\theta}}_r)\Big|_{\ddot{\boldsymbol{\theta}}_{r,i}=\mathbf{o}}, \end{aligned} \tag{5.69}$$

we finally obtain the following recursive expression of $\ddot{\tilde{\boldsymbol{q}}}_{r,i}$:

$$\begin{aligned}
\ddot{\tilde{\boldsymbol{q}}}_{r,i} &= \begin{bmatrix} \ddot{\boldsymbol{\theta}}_{r,i} \\ \ddot{\sigma}_{r,i} \end{bmatrix} \\
&= \bar{\boldsymbol{J}}_{ii}^{-1} \left\{ \ddot{\boldsymbol{c}}(\hat{\sigma}_i, \dot{\hat{\sigma}}_i, \dot{\hat{\sigma}}_{r,i}, 0, t) - \ddot{\boldsymbol{p}}(\boldsymbol{\theta}, \dot{\boldsymbol{\theta}}, \dot{\boldsymbol{\theta}}_r, \ddot{\boldsymbol{\theta}}_r)\big|_{\ddot{\boldsymbol{\theta}}_{r,i}=\mathbf{o}} - \boldsymbol{\Lambda}_i \dot{\hat{\boldsymbol{e}}}_i \right\} \\
&= -\bar{\boldsymbol{J}}_{ii}^{-1} \left\{ \ddot{\hat{\boldsymbol{e}}}_i(\boldsymbol{q}, \dot{\boldsymbol{q}}, \dot{\boldsymbol{q}}_r, \ddot{\boldsymbol{q}}_r)\big|_{\ddot{\boldsymbol{q}}_{r,i}=\mathbf{o}} + \boldsymbol{\Lambda}_i \dot{\hat{\boldsymbol{e}}}_i \right\}. \qquad (5.70)
\end{aligned}$$

Computational burden is not so heavy in the both cases since the obtained recursive expressions, (5.55) and (5.64), (5.70) have very simple structures. Since all the calculations are performed recursively with respect to the link number, the asymptotic complexity is of $\mathcal{O}(n)$.

5.5 Simulation

In this section, the simulation results of shape tracking are shown. The simulation environment is exactly same as the simulation in the previous section.

We give the following contracting and expanding helix with a constant period as a target:

$$\boldsymbol{c}(\sigma, t) = \begin{bmatrix} \alpha(t)\sigma \\ R\cos(u(\sigma,t)) + C_y \\ R\sin(u(\sigma,t)) + C_z \end{bmatrix}, \qquad (5.71)$$

where $\alpha : \Re_+ \to \Re$, $u : \Re \times \Re_+ \to \Re$ and $C_y, C_z \in \Re$ are defined by

$$\begin{aligned}
\alpha(t) &:= A\cos(Bt) + C, \\
u(\sigma, t) &:= \frac{\sqrt{1-\alpha^2(t)}}{R}\sigma + \phi, \\
C_y &:= -R\cos(\phi), \\
C_z &:= -R\sin(\phi). \qquad (5.72)
\end{aligned}$$

Parameters A, B, C, R and ϕ are all constants and we assume $A = 0.20$, $B = 1.00\pi$, $C = 0.50$, $R = 0.10$, and $\phi = -0.50\pi$.

ID-based Shape Tracking

Suppose $\boldsymbol{K} = k_p\boldsymbol{I}$ and $\boldsymbol{K}_d = k_d\boldsymbol{I}$, and we set $k_p = 25.0$ and $k_d = 10.0$ in this simulation.

Figure 5.1 shows the manipulator movement from the initial time $0.00\,[\mathrm{s}]$ to the final time $5.00\,[\mathrm{s}]$ every a half second from two different standpoints. We can see that the manipulator smoothly follow the moving helix. Figure 5.2 and Figure 5.3 show the time responses of the root mean square of the estimated shape error $\hat{\boldsymbol{e}}$ and its velocity $\dot{\hat{\boldsymbol{e}}}$. We can see rapid convergence to zero from these figures. In this case, exponential convergence with respect to $\hat{\boldsymbol{e}}$ and $\dot{\hat{\boldsymbol{e}}}$ is assured.

Lyapunov-based Shape Tracking

Suppose $\boldsymbol{K} = k_p\boldsymbol{I}$, $\boldsymbol{K}_v = k_v\boldsymbol{I}$, $\boldsymbol{K}_\sigma = k_\sigma\boldsymbol{I}$ and $\boldsymbol{\Lambda} = \lambda\boldsymbol{I}$, and we set $k_p = 15.0$, $k_v = 0.05$, $k_\sigma = 1.00$ and $\lambda = 5.00$ in this simulation.

We can also see good convergence from Figure 5.7 and Figure 5.8, Figure 5.9, although the bigger control input than the ID-based controller is needed in this case.

In both cases, the control objective of the shape tracking is achieved, although the motions of two control laws are different.

Summary

Shape tracking was achieved by using the desired curve parameter estimator with 2nd-order dynamics. The coupled dynamics of manipulator and the estimator has the same form as the original one, and in addition, the important properties are preserved. That was why we could apply familiar design methods for tracking to the shape tracking problem. Two shape tracking control laws were derived and recursive expressions were given. Then the simulation results were also shown for both.

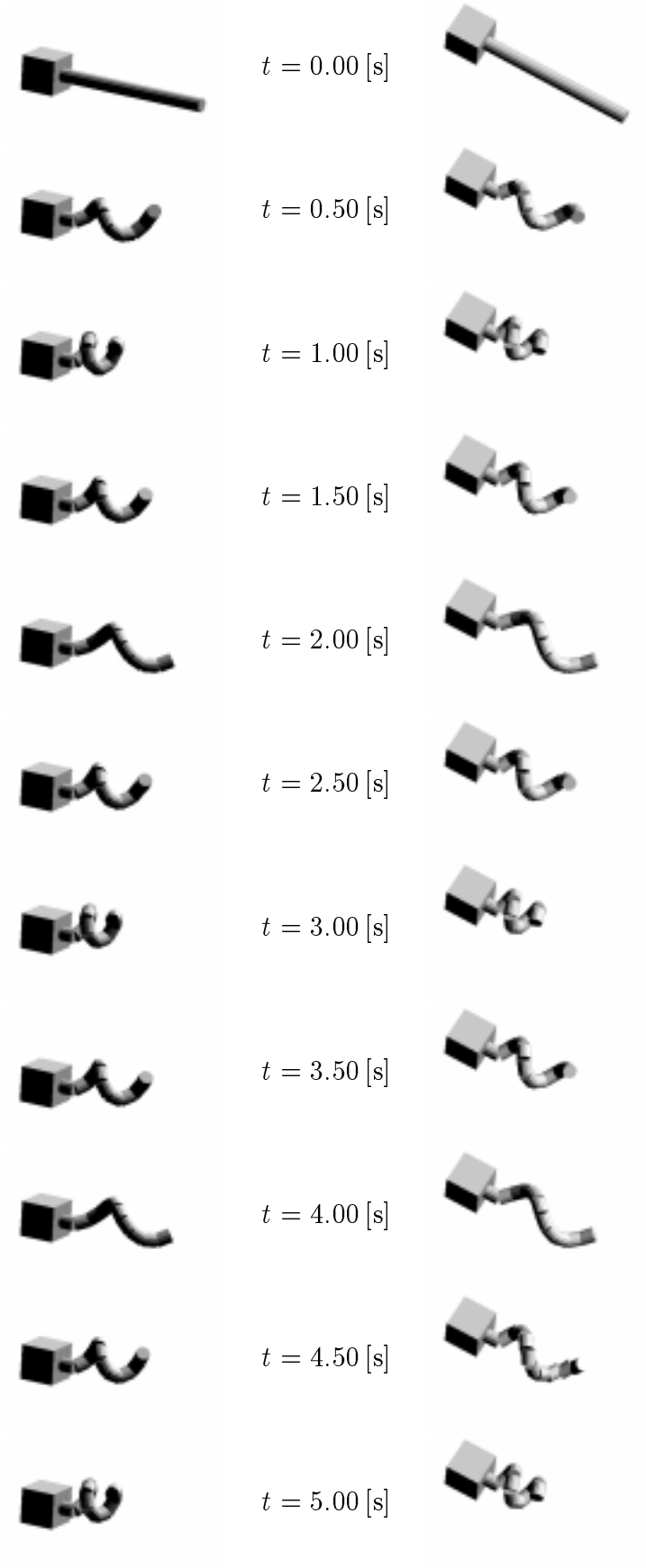

Figure 5.1: Manipulator movement (ID-based shape tracking)

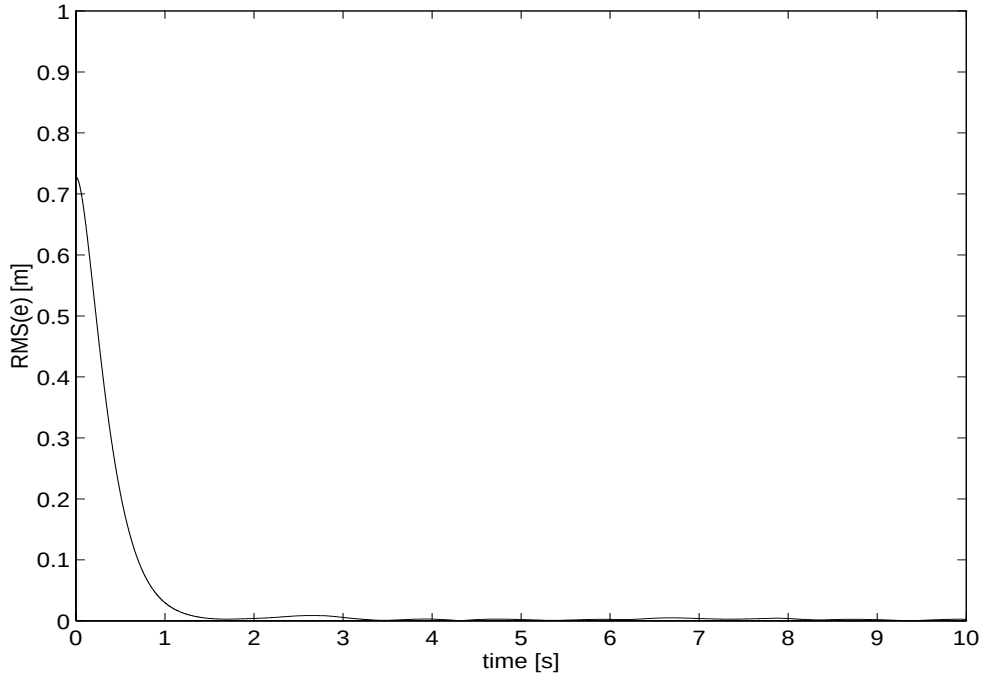

Figure 5.2: Error (ID-based shape tracking)

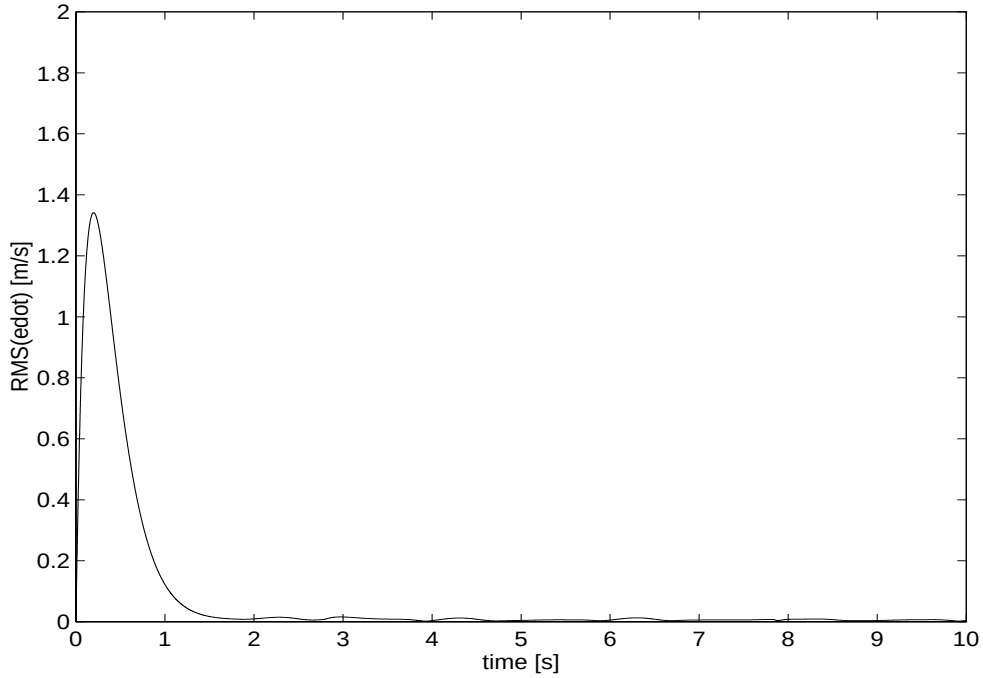

Figure 5.3: Derivative of error (ID-based shape tracking)

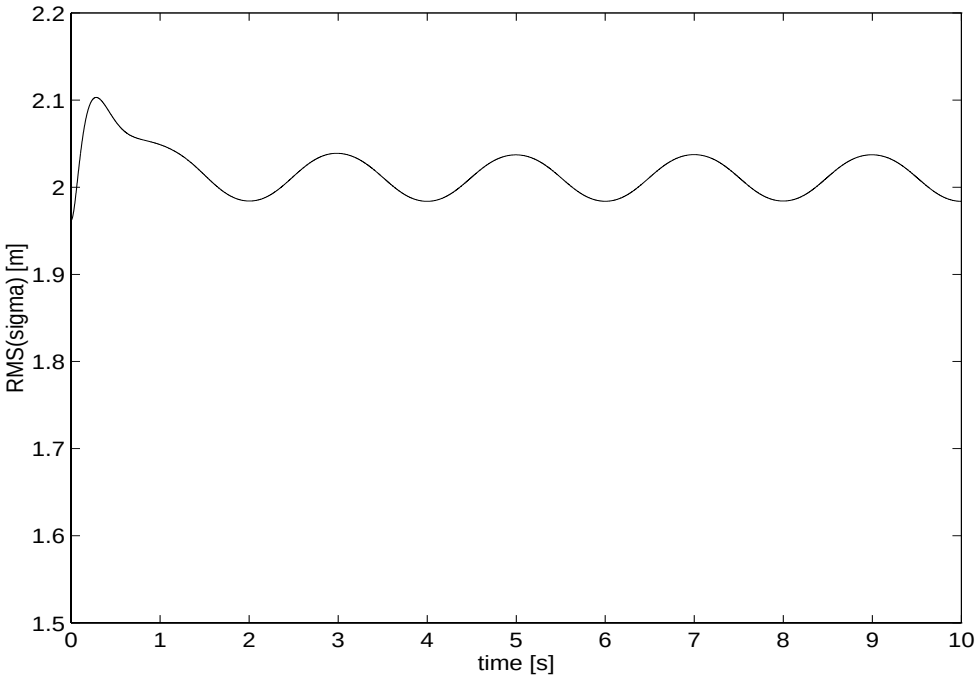

Figure 5.4: Estimated curve parameter (ID-based shape tracking)

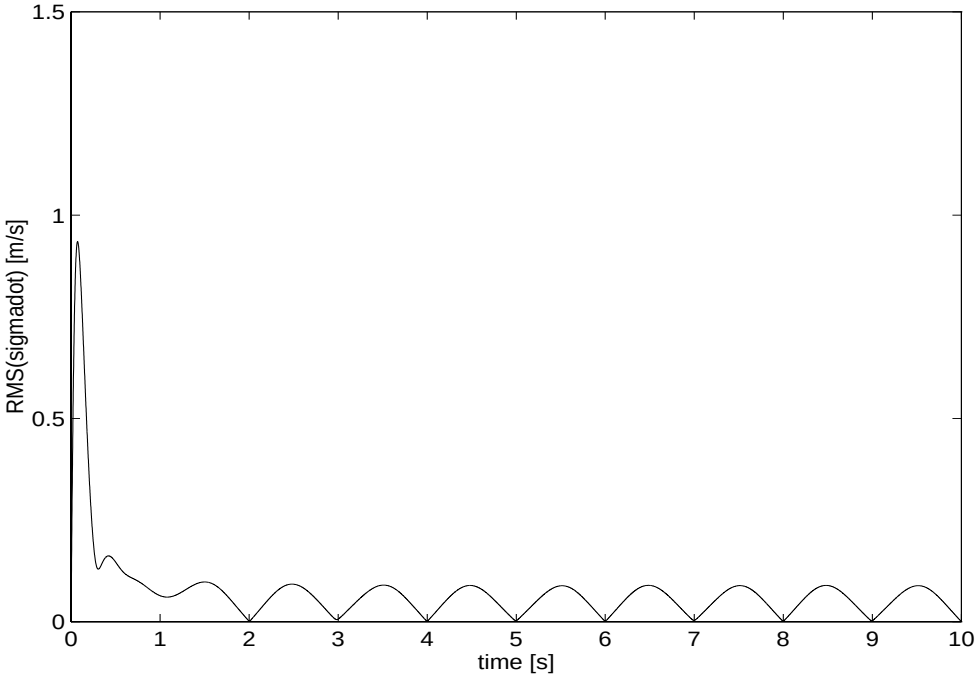

Figure 5.5: Derivative of estimated curve parameter (ID-based shape tracking)

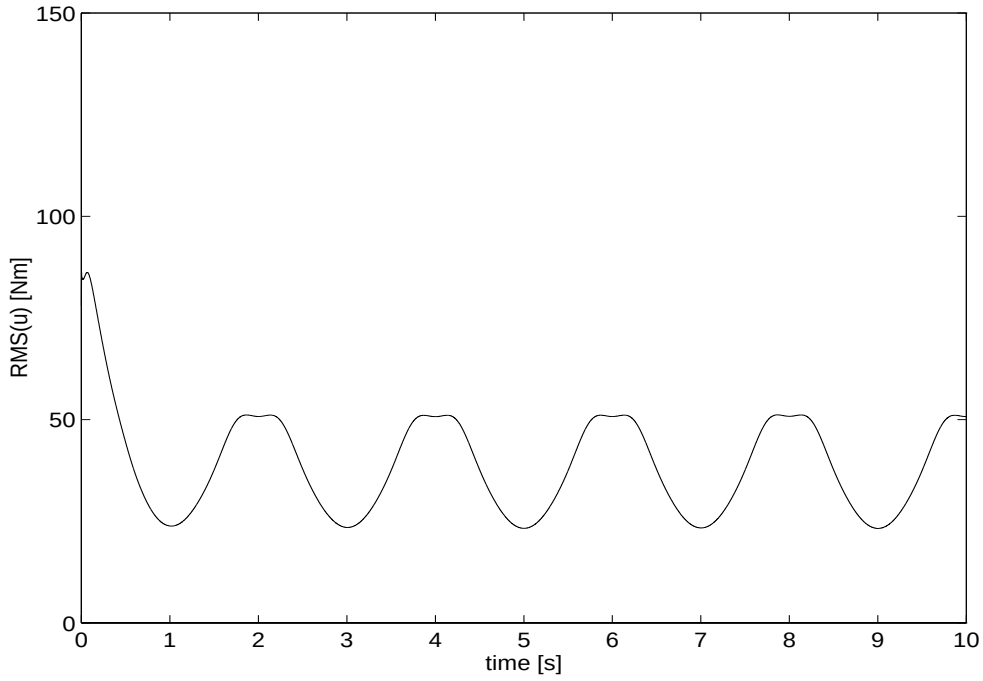

Figure 5.6: Input torgue (ID-based shape tracking)

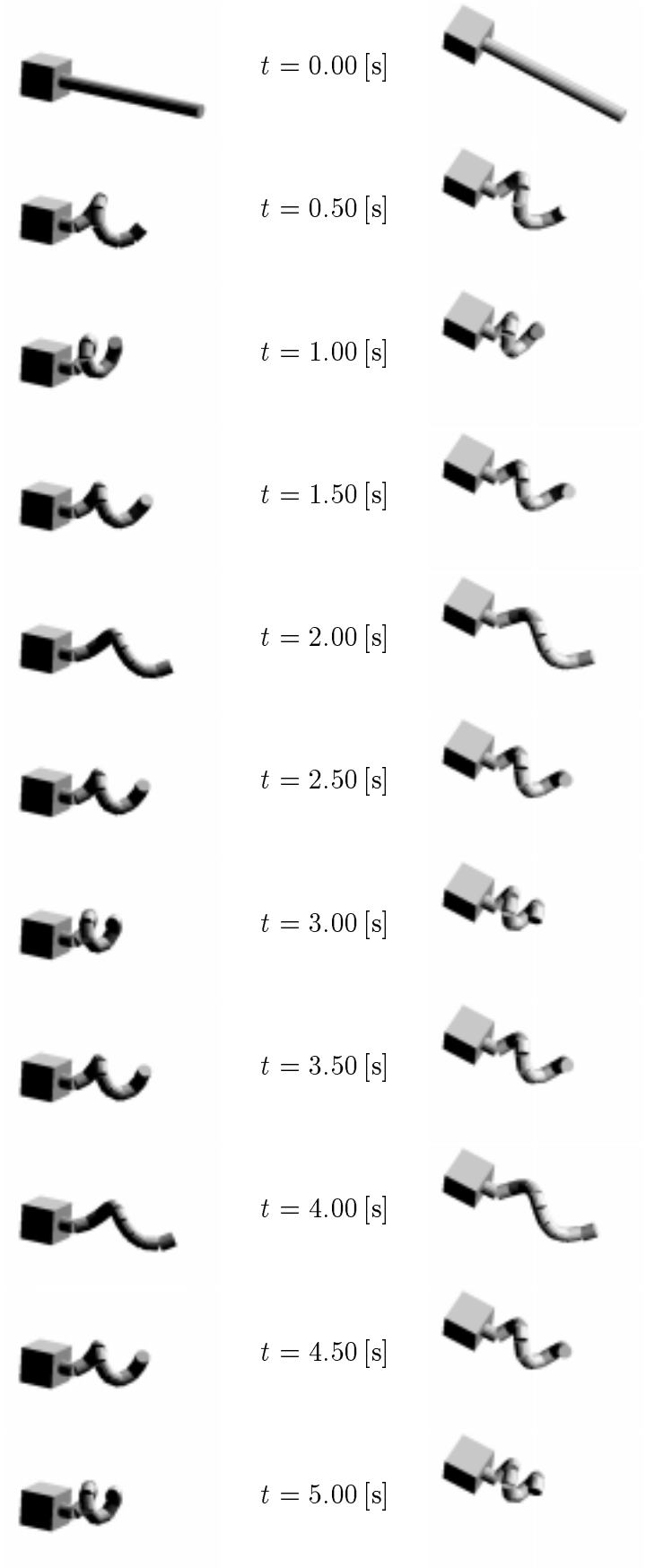

Figure 5.7: Manipulator movement (Lyapunov-based shape tracking)

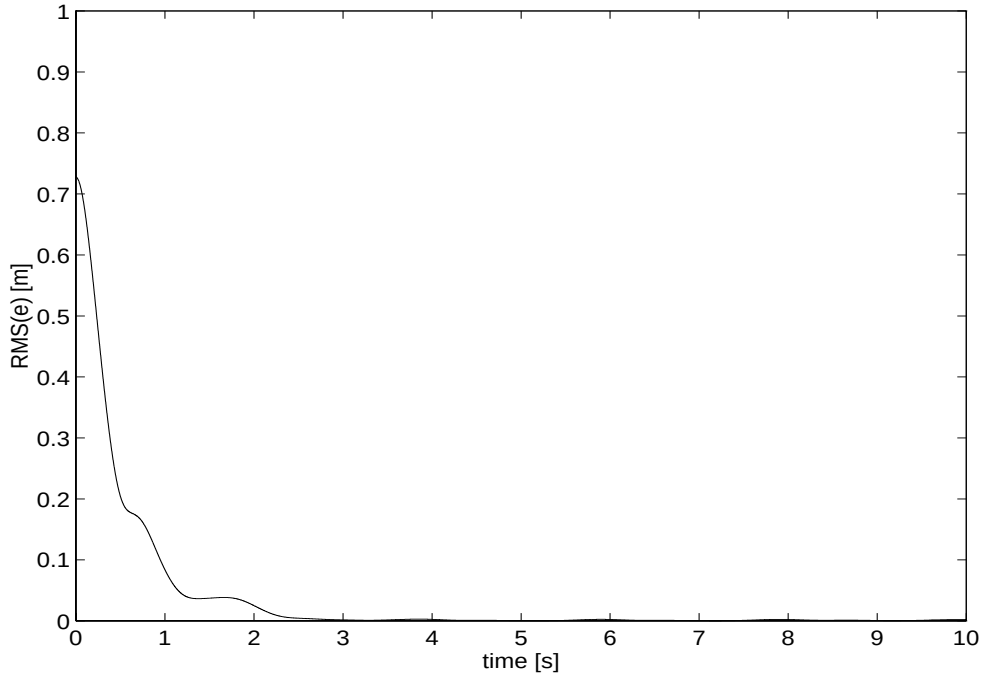

Figure 5.8: Error (Lyapunov-based shape tracking)

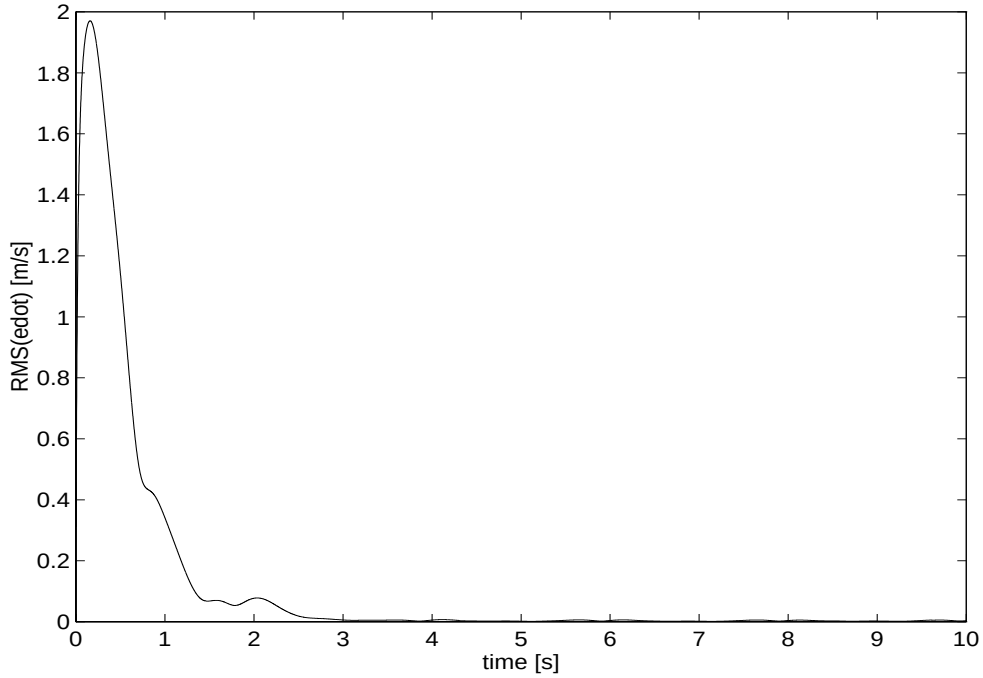

Figure 5.9: Derivative of error (Lyapunov-based shape tracking)

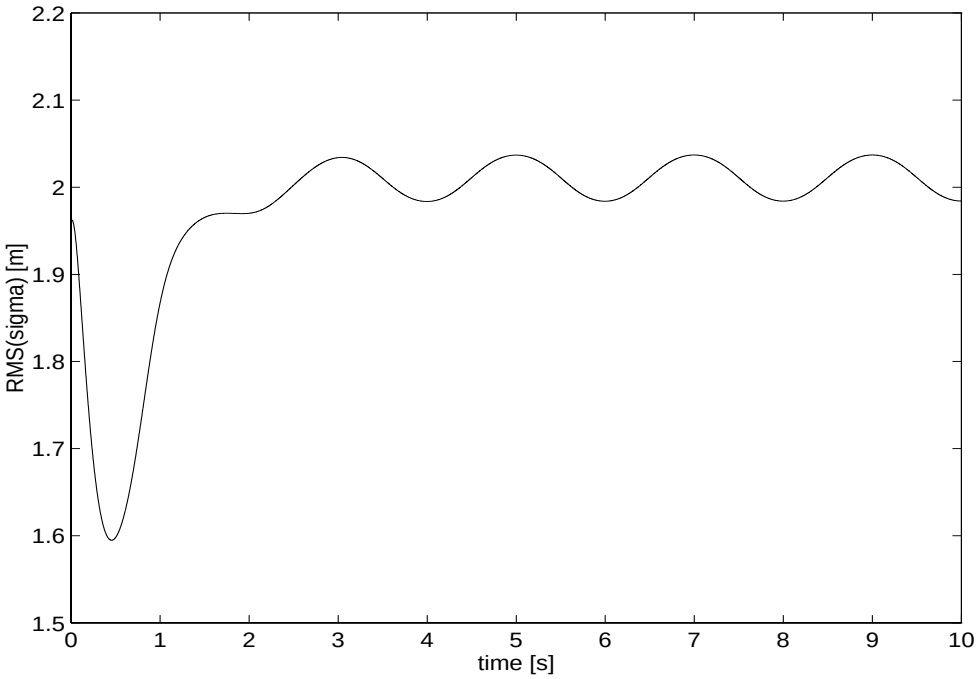

Figure 5.10: Estimated curve parameter (Lyapunov-based shape tracking)

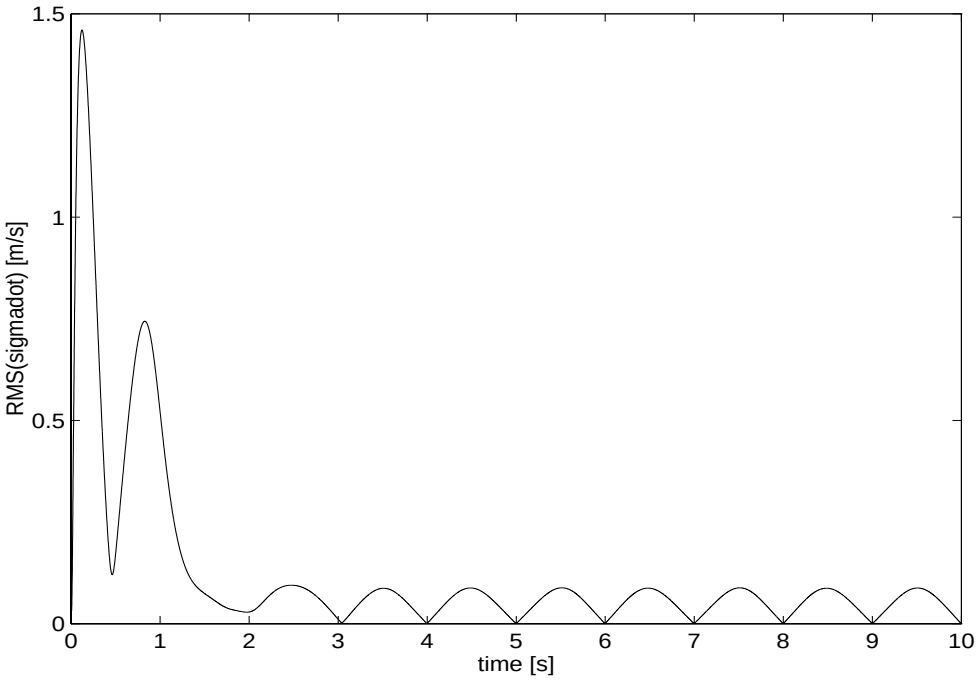

Figure 5.11: Derivative of estimated curve parameter (Lyapunov-based shape tracking)

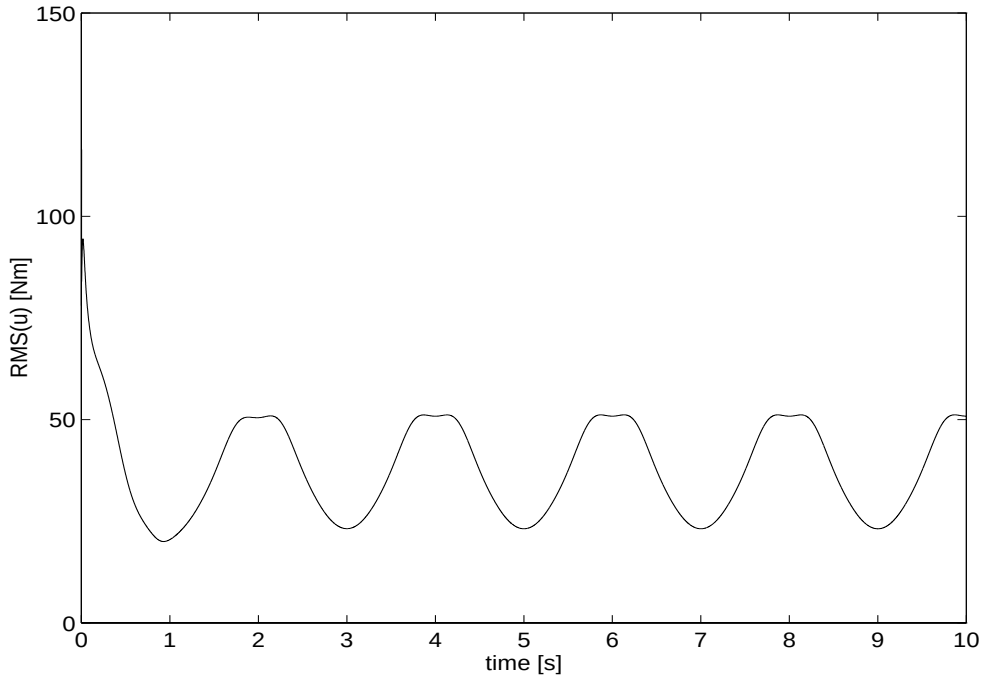

Figure 5.12: Input torgue (Lyapunov-based shape tracking)

Chapter 6

Shape Tracking Using Only Joint Angle Information

In this chapter, we consider shape tracking control using only joint angle information. Shape tracking control laws were derived in the previous chapter. However, those control laws need joint angle velocity signals, and we usually have difficulty to obtain them. To solve this problem, we use a shape velocity observer which has the closed-loop dynamics dual to that of a shape tracking controller. This duality between the controller and the observer brings us a successful result to solve this problem by using Lyapunov stability theory.

In Section **6.1**, the shape tracking problem using only joint angle information is stated and a strategy to solve the problem is shown. A shape velocity observer with closed-loop dynamics dual to a shape tracking controller is proposed in Section **6.2**. In Section **6.3**, it is shown that the simply tuned shape tracking controller and the shape velocity observer assure local asymptotic stability of the closed-loop system under some reasonable assumptions on a given spatial curve.

6.1 Problem Statement

We have already proposed the shape tracking controllers to control the shape of an HDOF manipulator to follow a given time-varying curve. The proposed shape tracking controllers need the joint angle velocity feedback. However, it is undesirable to attach any velocity sensors, such as tachometers, to all the joints since it causes heavy weight and high cost. Especially for an HDOF manipulator that has many joints, it is essential to avoid this undesirable equipment. One of the simplest method for this problem is the use of the first-order numerical differentiation of joint angle data instead of joint velocity measurement. Nevertheless, this method has been indicated to be inadequate because of

inaccuracy for low and high velocities, undesirable quantization effects and no theoretical justification [2].

Several velocity observers for robot systems that reconstruct the joint angle velocity signals using the high-quality joint angle information have been proposed [17, 3]. Lack of the separation principle for general nonlinear systems does not allow us to apply directly these velocity observers to our shape tracking controllers. To make nonlinear observer design more systematic, Berghuis et al. have proposed a combined controller-observer design scheme for robot systems where controller and observer structures are properly tuned to each other after designing them separately [1]. In this scheme, the duality between a controller and an observer plays an important role.

Following this idea, we derive an observer that does not directly estimate joint angle velocity signals, but *shape velocities*. After properly tuned, the modified shape tracking controller and shape velocity observer assure local asymptotic stability of the closed-loop system under some reasonable assumptions for a given curve.

A shape tracking control problem using only joint angle information is stated as follows:

Problem 5 (Shape Tracking Using Only Joint Angle Information)

Consider

1. an HDOF manipulator with dynamics (2.34), and
2. a time-varying curve $\boldsymbol{c} : \Re \times \Re_+ \to E^3$ satisfying **Assumption 2**.

Moreover, suppose that **Assumption 5** holds. Then, find a control input, $\boldsymbol{u}$, in (2.34) achieving that

$$\boldsymbol{\theta}(t) \;\to\; \boldsymbol{\theta}^*(t), \tag{6.1}$$

$$\dot{\boldsymbol{\theta}}(t) \;\to\; \dot{\boldsymbol{\theta}}^*(t), \tag{6.2}$$

as $t \to \infty$ without using joint angle velocity $\dot{\boldsymbol{\theta}}$. □

Clearly from the same discussion in the previous chapter, the control objective in this chapter can be restated as

$$\hat{\boldsymbol{e}}(\boldsymbol{\theta}, \hat{\boldsymbol{\sigma}}) \;\to\; \mathbf{o}, \tag{6.3}$$

$$\dot{\hat{\boldsymbol{e}}}(\boldsymbol{\theta}, \hat{\boldsymbol{\sigma}}, \dot{\boldsymbol{\theta}}, \dot{\hat{\boldsymbol{\sigma}}}) \;\to\; \mathbf{o}, \tag{6.4}$$

$$(\boldsymbol{\theta}, \hat{\boldsymbol{\sigma}}) \;\in\; \mathcal{D}_\delta, \tag{6.5}$$

without using $\dot{\boldsymbol{\theta}}$, instead of objectives (6.1) and (6.2) under the condition of non-singularity of shape Jacobian for any t.

If joint angle velocity $\dot{\boldsymbol{\theta}}$ are available from the measurement in addition to joint angles, we can achieve the shape tracking control using the control laws shown in the previous chapter. Figure 6.1 shows the structure of the Lyapunov-based shape tracking controller. We can see that there are four flows of joint angle velocity $\dot{\boldsymbol{\theta}}$ (dotted lines).

We take a strategy not to break the structure of this shape tracking controller, that is, to replace signals with their estimates. Due to the lack of the separation principle for general nonlinear systems, however, the proposed angle velocity observers do not work for this shape tracking controller. In obeserver design for nonlinear systems, duality between a controller and an observer plays an important role [1]. That is why we do not look for an joint angle velocity observer directly, but a shape velocity observer in the next section.

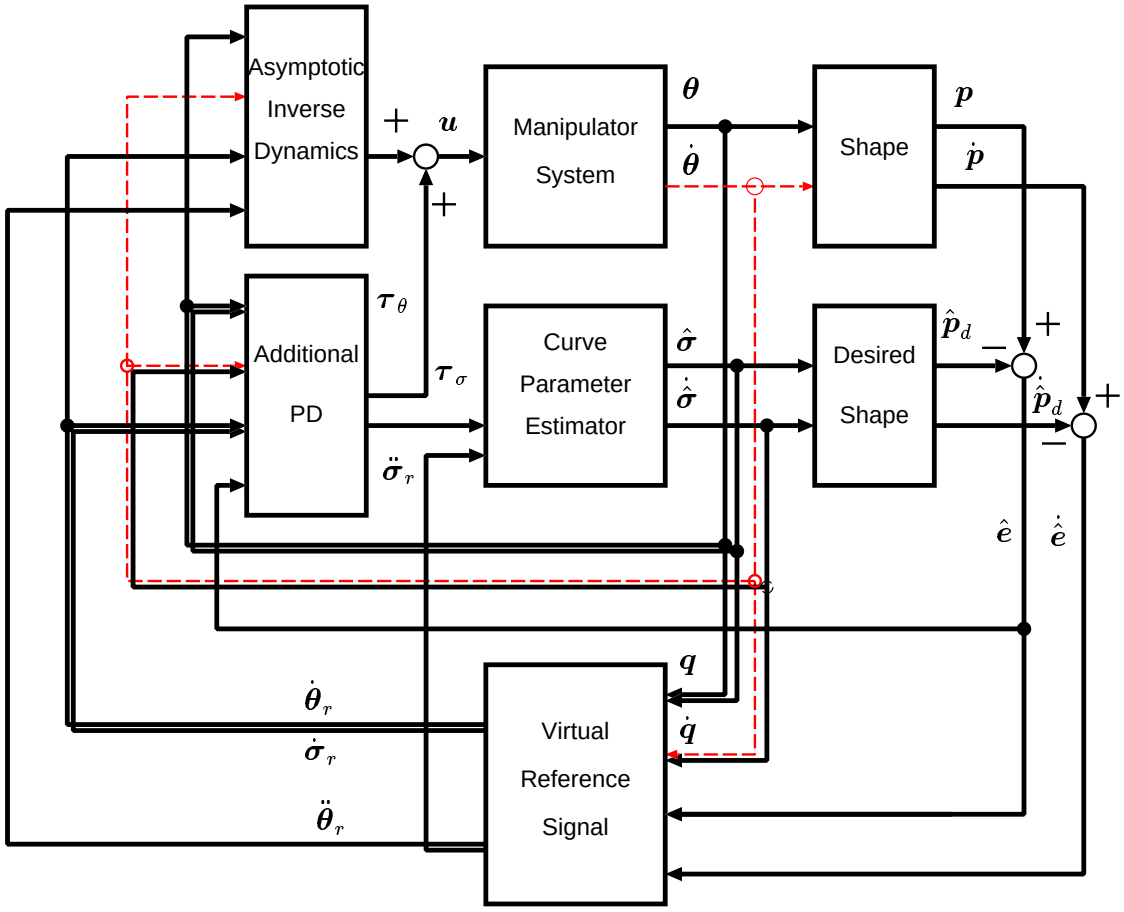

Figure 6.1: Structure of the shape tracking controller

6.2 Shape Velocity Observer

Let $\hat{\boldsymbol{p}} \in \Re^{3n}$ be an estimate of a shape, and $\tilde{\boldsymbol{p}} \in \Re^{3n}$ be a shape estimation error which is defined as the difference between a shape and its estimate:

$$\tilde{\boldsymbol{p}} := \boldsymbol{p} - \hat{\boldsymbol{p}}. \tag{6.6}$$

The objective in this section is to find an observer achieving that $\tilde{\boldsymbol{p}} \to \mathbf{o}, \dot{\tilde{\boldsymbol{p}}} \to \mathbf{o}$. To do this, we consider a sliding surface:

$$\dot{\tilde{\boldsymbol{p}}} + \boldsymbol{\Lambda}\tilde{\boldsymbol{p}} = \mathbf{o}, \tag{6.7}$$

where $\boldsymbol{\Lambda} \in \Re^{3n \times 3n}$ is a symmetric positive definite matrix. The surface:

$$\boldsymbol{J}^{-1}(\boldsymbol{q}, t)\left(\dot{\tilde{\boldsymbol{p}}} + \boldsymbol{\Lambda}\tilde{\boldsymbol{p}}\right) = \mathbf{o}, \tag{6.8}$$

is a sliding surface in joint space. Thus, define a new sliding variable $\boldsymbol{s}_o \in \Re^{3n}$ as

$$\boldsymbol{s}_o := \boldsymbol{J}^{-1}(\boldsymbol{q}, t)\left(\dot{\tilde{\boldsymbol{p}}} + \boldsymbol{\Lambda}\tilde{\boldsymbol{p}}\right). \tag{6.9}$$

Define also $\dot{\boldsymbol{q}}_o \in \Re^{3n}$, composed by $\dot{\boldsymbol{\theta}}_o \in \Re^{2n}$ and $\dot{\hat{\boldsymbol{\sigma}}}_o \in \Re^{n}$ like $\dot{\boldsymbol{q}}_r$, as

$$\begin{aligned}
\dot{\boldsymbol{q}}_o &= \begin{bmatrix} \dot{\boldsymbol{\theta}}_o \\ \dot{\hat{\boldsymbol{\sigma}}}_o \end{bmatrix} \qquad (6.10)\\
&:= \dot{\boldsymbol{q}} - \boldsymbol{s}_o \\
&= \dot{\boldsymbol{q}} - \boldsymbol{J}^{-1}(\boldsymbol{q}, t)\left(\dot{\tilde{\boldsymbol{p}}} + \boldsymbol{\Lambda}\tilde{\boldsymbol{p}}\right) \\
&= \boldsymbol{J}^{-1}(\boldsymbol{q}, t)\left\{\boldsymbol{J}(\boldsymbol{q}, t)\dot{\boldsymbol{q}} - \dot{\tilde{\boldsymbol{p}}} + \boldsymbol{\Lambda}\tilde{\boldsymbol{p}}\right\} \\
&= \boldsymbol{J}^{-1}(\boldsymbol{q}, t)\left\{\dot{\boldsymbol{p}} - \frac{\partial \boldsymbol{p}_d}{\partial \boldsymbol{\sigma}}(\hat{\boldsymbol{\sigma}}, t)\dot{\hat{\boldsymbol{\sigma}}} - \dot{\boldsymbol{p}} + \dot{\hat{\boldsymbol{p}}} + \boldsymbol{\Lambda}\tilde{\boldsymbol{p}}\right\} \\
&= \boldsymbol{J}^{-1}(\boldsymbol{q}, t)\left\{\dot{\hat{\boldsymbol{p}}} - \frac{\partial \boldsymbol{p}_d}{\partial \boldsymbol{\sigma}}(\hat{\boldsymbol{\sigma}}, t)\dot{\hat{\boldsymbol{\sigma}}} - \boldsymbol{\Lambda}\tilde{\boldsymbol{p}}\right\}. \qquad (6.11)
\end{aligned}$$

The following theorem states that shape velocity observation can be achieved:

Theorem 8 (Shape Velocity Observer)

Consider the following observer:

$$\dot{\hat{\boldsymbol{p}}} = \boldsymbol{z} + (l_d \boldsymbol{I} + \boldsymbol{\Lambda})(\boldsymbol{p} - \hat{\boldsymbol{p}}) + \frac{\partial \boldsymbol{p}_d}{\partial \boldsymbol{\sigma}}(\hat{\boldsymbol{\sigma}}, t)\dot{\hat{\boldsymbol{\sigma}}}, \tag{6.12}$$

$$\begin{aligned}
\dot{\boldsymbol{z}} &= l_d \boldsymbol{\Lambda}(\boldsymbol{p} - \hat{\boldsymbol{p}}) + \dot{\boldsymbol{J}}(\boldsymbol{q}, \dot{\boldsymbol{q}}, t)\dot{\boldsymbol{q}}_o \\
&\quad + \boldsymbol{J}(\boldsymbol{q}, t)\bar{\boldsymbol{M}}^{-1}(\boldsymbol{q})\left\{\bar{\boldsymbol{u}} - \bar{\boldsymbol{C}}(\boldsymbol{q}, \dot{\boldsymbol{q}})\dot{\boldsymbol{q}}_o - \bar{\boldsymbol{g}}(\boldsymbol{q}) + \boldsymbol{J}^T(\boldsymbol{q}, t)\boldsymbol{K}_p(\boldsymbol{p} - \hat{\boldsymbol{p}}) - \boldsymbol{\Delta}_o \boldsymbol{s}_o\right\},
\end{aligned} \tag{6.13}$$

where $\dot{\boldsymbol{q}}_o \in \Re^{3n}$ is defined as

$$\dot{\boldsymbol{q}}_o \;:=\; \boldsymbol{J}^{-1}(\boldsymbol{q},t)\left\{\dot{\hat{\boldsymbol{p}}} - \frac{\partial \boldsymbol{p}_d}{\partial \boldsymbol{\sigma}}(\hat{\boldsymbol{\sigma}},t)\dot{\hat{\boldsymbol{\sigma}}} - \boldsymbol{\Lambda}\tilde{\boldsymbol{p}}\right\}, \tag{6.14}$$

and $\left[\hat{\boldsymbol{p}}^T \boldsymbol{z}^T\right]^T \in \Re^{6n}$ is the observer state, l_d is a positive constant, $\boldsymbol{\Lambda}, \boldsymbol{K}_p \in \Re^{3n\times 3n}$ are symmetric postive definite matrices with the relation $\boldsymbol{\Lambda}^T\boldsymbol{K}_p = \boldsymbol{K}_p^T\boldsymbol{\Lambda}$ and $\boldsymbol{\Delta}_o \in \Re^{3n\times 3n}$ is a matrix with norm bound $\delta_o > 0$, i.e.,

$$\|\boldsymbol{\Delta}_o\| \;\leq\; \delta_o. \tag{6.15}$$

Assume that l_d is chosen to satisfy

$$l_d\bar{M}_m - \delta_o \;>\; 0. \tag{6.16}$$

Then, the closed loop system with the observer above is locally asymptotically stable for the equilibrium point, $(\tilde{\boldsymbol{p}}, \dot{\tilde{\boldsymbol{p}}}) = (\mathbf{o}, \mathbf{o})$, that is, asymptotic convergences of $\tilde{\boldsymbol{p}}$ and $\dot{\tilde{\boldsymbol{p}}}$ to zero are achieved locally. □

Proof. Eliminating $\boldsymbol{z}$ and $\bar{\boldsymbol{u}}$ from the observer in considering the effect of coupled dynamics (5.9), we obatain the following closed-loop dynamics for the shape velocity observer

$$\bar{\boldsymbol{M}}(\boldsymbol{q})\dot{\boldsymbol{s}}_o + \bar{\boldsymbol{C}}(\boldsymbol{q},\dot{\boldsymbol{q}})\boldsymbol{s}_o + \left(l_d\bar{\boldsymbol{M}}(\boldsymbol{q}) - \boldsymbol{\Delta}_o\right)\boldsymbol{s}_o + \boldsymbol{J}^T(\boldsymbol{q},t)\boldsymbol{K}_p\tilde{\boldsymbol{p}} \;=\; \mathbf{o}. \tag{6.17}$$

Note that this closed-loop dynamics has the substantially dual form to the closed-loop dynamics of the shape tracking controller in the previous section, (5.37).

Consider the following scalar function V_o positive definite with respect to $(\boldsymbol{s}_o, \tilde{\boldsymbol{p}})$:

$$V_o(\boldsymbol{s}_o, \tilde{\boldsymbol{p}}) = \frac{1}{2}{\boldsymbol{s}_o}^T\bar{\boldsymbol{M}}(\boldsymbol{q})\boldsymbol{s}_o + \frac{1}{2}\tilde{\boldsymbol{p}}^T\boldsymbol{K}_p\tilde{\boldsymbol{p}}. \tag{6.18}$$

Due to **Property 1**-4, the time derivative of V_o becomes

$$\begin{aligned}
\dot{V}_o(\boldsymbol{s}_o, \tilde{\boldsymbol{p}}) \;&=\; {\boldsymbol{s}_o}^T\bar{\boldsymbol{M}}(\boldsymbol{q})\dot{\boldsymbol{s}}_o + \frac{1}{2}{\boldsymbol{s}_o}^T\dot{\bar{\boldsymbol{M}}}(\boldsymbol{q})\boldsymbol{s}_o + \tilde{\boldsymbol{p}}^T\boldsymbol{K}_p\dot{\tilde{\boldsymbol{p}}} \\
&=\; -{\boldsymbol{s}_o}^T\left\{l_d\bar{\boldsymbol{M}}(\boldsymbol{q}) - \boldsymbol{\Delta}_o\right\}\boldsymbol{s}_o + \frac{1}{2}{\boldsymbol{s}_o}^T\left\{\dot{\bar{\boldsymbol{M}}}(\boldsymbol{q}) - 2\bar{\boldsymbol{C}}(\boldsymbol{q},\dot{\boldsymbol{q}})\right\}\boldsymbol{s}_o \\
&\quad -{\boldsymbol{s}_o}^T\boldsymbol{J}^T(\boldsymbol{q},t)\boldsymbol{K}_p\tilde{\boldsymbol{p}} + \tilde{\boldsymbol{p}}^T\boldsymbol{K}_p\dot{\tilde{\boldsymbol{p}}} \\
&=\; -{\boldsymbol{s}_o}^T\left\{l_d\bar{\boldsymbol{M}}(\boldsymbol{q}) - \boldsymbol{\Delta}_o\right\}\boldsymbol{s}_o - \tilde{\boldsymbol{p}}^T\boldsymbol{\Lambda}^T\boldsymbol{K}_p\tilde{\boldsymbol{p}}.
\end{aligned} \tag{6.19}$$

Therefore, condition (6.16) assures the negative definiteness of $\dot{V}_o$. Applying Lyapunov theorem completes the proof. (Q.E.D.)

This observer is a kind of task space version of the observer proposed in [1]. If we choose $\boldsymbol{\Delta}_o$ as

$$\boldsymbol{\Delta}_o \;=\; -\bar{\boldsymbol{C}}(\boldsymbol{q},\dot{\boldsymbol{q}}_o)+\bar{\boldsymbol{M}}(\boldsymbol{q})\boldsymbol{J}^{-1}(\boldsymbol{q},t)\dot{\boldsymbol{J}}_q(\boldsymbol{q},\dot{\boldsymbol{q}}_o,t), \tag{6.20}$$

then there appears no joint angle velocity signal in the proposed observer. We need the condition that $\dot{\boldsymbol{q}}$ is bounded to assure the boundedness of $\boldsymbol{\Delta}_o$ as same as the case in [1]. This condition is undesirable because we can not check whether this assumption holds or not in advance. However, in the next section, it will not be necessary to assume the boundedness of joint velocity signals directly. It is due to a shape tracking controller and a mild assumption for a given time-varying curve prescribing a desired shape.

6.3 Shape Tracking Controller with Shape Velocity Observer

In this section, we combine the controller and the observer derived in the previous section not to break the stability.

In order to get rid of joint angle velocity information from the shape trakcing control law, first define $\dot{\boldsymbol{q}}_r$ as follows:

$$\dot{\boldsymbol{q}}_r \;:=\; \boldsymbol{J}^{-1}(\boldsymbol{q},t)\left\{\frac{\partial \boldsymbol{p}_d}{\partial t}(\hat{\boldsymbol{\sigma}},t)-\boldsymbol{\Lambda}(\hat{\boldsymbol{p}}-\hat{\boldsymbol{p}}_d)\right\}, \tag{6.21}$$

that is, replace $\boldsymbol{p}$ in $\hat{\boldsymbol{e}}:=\boldsymbol{p}-\hat{\boldsymbol{p}}_d$ with its observed value, $\hat{\boldsymbol{p}}$. In the above expression, we abbreviate $\boldsymbol{p}_d(\hat{\boldsymbol{\sigma}},t)$ as $\hat{\boldsymbol{p}}_d$. This refinement of $\dot{\boldsymbol{q}}_r$ is reasonable, because the surface:

$$\begin{bmatrix}\boldsymbol{s}_c\\ \boldsymbol{s}_o\end{bmatrix} \;=\; \mathbf{o}, \tag{6.22}$$

still means the sliding surface of the purpose here under this refinement. Moreover, $\dot{\hat{\boldsymbol{e}}}$, which needs $\dot{\boldsymbol{q}}$ for the calculation, does not appear any longer in $\ddot{\boldsymbol{q}}_r$.

Furthermore, modify the shape tracking controller as follows:

1. Replace $\ddot{\boldsymbol{q}}_r$ with $\ddot{\boldsymbol{q}}_{ro}$ which is defined as

$$\ddot{\boldsymbol{q}}_{ro} \;:=\; \ddot{\boldsymbol{q}}_r(\boldsymbol{q},\dot{\boldsymbol{q}}_o,\hat{\boldsymbol{p}}-\hat{\boldsymbol{p}}_d,\dot{\hat{\boldsymbol{p}}}-\dot{\hat{\boldsymbol{p}}}_d). \tag{6.23}$$

2. Replace $\boldsymbol{C}(\boldsymbol{\theta},\dot{\boldsymbol{\theta}})\dot{\boldsymbol{\theta}}_r$ in (5.41) with $\boldsymbol{C}(\boldsymbol{\theta},\dot{\boldsymbol{\theta}}_o)\,\dot{\boldsymbol{\theta}}_r$.

3. Replace $-\boldsymbol{K}_d(\dot{\boldsymbol{q}}-\dot{\boldsymbol{q}}_r)$ in (5.42) with $-\boldsymbol{K}_d(\dot{\boldsymbol{q}}_o-\dot{\boldsymbol{q}}_r)$.

These are simple replacements of unavailable values with their observed values.

The difference beween the new control input and the old one by these modifications is

$$\{\boldsymbol{K}_d + \boldsymbol{X}(\boldsymbol{q}, \dot{\boldsymbol{q}}_r, t)\}\, \boldsymbol{s}_o, \tag{6.24}$$

where

$$\boldsymbol{X}(\boldsymbol{q}, \dot{\boldsymbol{q}}_r, t) \;:=\; -\bar{\boldsymbol{C}}(\boldsymbol{q}, \dot{\boldsymbol{q}}_r) + \bar{\boldsymbol{M}}(\boldsymbol{q})\boldsymbol{J}^{-1}(\boldsymbol{q}, t)\dot{\boldsymbol{J}}(\boldsymbol{q}, \dot{\boldsymbol{q}}_r, t). \tag{6.25}$$

The closed-loop dynamics for the new controller is as follows:

$$\bar{\boldsymbol{M}}(\boldsymbol{q})\, \dot{\boldsymbol{s}}_c + \bar{\boldsymbol{C}}(\boldsymbol{q}, \dot{\boldsymbol{q}})\boldsymbol{s}_c + \boldsymbol{K}_d\boldsymbol{s}_c + \boldsymbol{J}^T(\boldsymbol{q}, t)\boldsymbol{K}_p\hat{\boldsymbol{e}} = \{\boldsymbol{K}_d + \boldsymbol{X}(\boldsymbol{q}, \dot{\boldsymbol{q}}_r, t)\}\, \boldsymbol{s}_o. \tag{6.26}$$

When we compare the above closed-loop dynamics with (5.37), we find that the effect of the modification appears in the right-hand side.

On the other hand, the observer for the new controller becomes

$$\dot{\hat{\boldsymbol{p}}} \;=\; \boldsymbol{z} + \dot{\hat{\boldsymbol{p}}}_d + (l_d\boldsymbol{I} + \boldsymbol{\Lambda})\,(\boldsymbol{p} - \hat{\boldsymbol{p}}) - \boldsymbol{\Lambda}\,(\hat{\boldsymbol{p}} - \hat{\boldsymbol{p}}_d)\,, \tag{6.27}$$

$$\begin{aligned}\dot{\boldsymbol{z}} \;=\;& l_d\boldsymbol{\Lambda}\,(\boldsymbol{p} - \hat{\boldsymbol{p}}) - \boldsymbol{J}(\boldsymbol{q}, t)\bar{\boldsymbol{M}}^{-1}(\boldsymbol{q})\boldsymbol{J}^T(\boldsymbol{q}, t)\boldsymbol{K}_p\,(\hat{\boldsymbol{p}} - \hat{\boldsymbol{p}}_d) \\ &+ \boldsymbol{J}(\boldsymbol{q}, t)\bar{\boldsymbol{M}}^{-1}(\boldsymbol{q})\,\{\boldsymbol{X}(\boldsymbol{q}, \dot{\boldsymbol{q}}_o, t) - \boldsymbol{K}_d\}\,\boldsymbol{s}_c + \boldsymbol{J}(\boldsymbol{q}, t)\bar{\boldsymbol{M}}^{-1}(\boldsymbol{q})\,(\boldsymbol{\Delta}_o + \boldsymbol{K}_d)\,\boldsymbol{s}_o.\end{aligned} \tag{6.28}$$

Note that this observer has the same closed-loop dynamics as (6.17) since any modifications about control inputs do not affect the closed-loop dynamics for the observer, which can be seen from (6.13). If we neglect the third term in (6.28) and make the choice that $\boldsymbol{\Delta}_o = -\boldsymbol{K}_d$ we obtain the following closed-loop dynamics for the observer:

$$\bar{\boldsymbol{M}}(\boldsymbol{q})\, \dot{\boldsymbol{s}}_o + \bar{\boldsymbol{C}}(\boldsymbol{q}, \dot{\boldsymbol{q}})\boldsymbol{s}_o + l_d\bar{\boldsymbol{M}}(\boldsymbol{q})\boldsymbol{s}_o + \boldsymbol{J}^T(\boldsymbol{q}, t)\boldsymbol{K}_p\tilde{\boldsymbol{p}} = \{\boldsymbol{X}(\boldsymbol{q}, \dot{\boldsymbol{q}}_o, t) - \boldsymbol{K}_d\}\, \boldsymbol{s}_c, \tag{6.29}$$

which has the dual structure to closed-loop dynamics (6.26).

Consider the scalar function $V := V_c + V_o$, i.e.,

$$V(\boldsymbol{s}_c, \hat{\boldsymbol{e}}, \boldsymbol{s}_o, \tilde{\boldsymbol{p}}) \;=\; \frac{1}{2}\hat{\boldsymbol{e}}^T\boldsymbol{K}_p\hat{\boldsymbol{e}} + \frac{1}{2}\boldsymbol{s}_c{}^T\bar{\boldsymbol{M}}(\boldsymbol{q})\boldsymbol{s}_c + \frac{1}{2}\tilde{\boldsymbol{p}}^T\boldsymbol{K}_p\tilde{\boldsymbol{p}} + \frac{1}{2}\boldsymbol{s}_o{}^T\bar{\boldsymbol{M}}(\boldsymbol{q})\boldsymbol{s}_o. \tag{6.30}$$

By using **Property 1**-4, the time derivative of V along the trajectory becomes

$$\begin{aligned}\dot{V}(\boldsymbol{s}_c, \hat{\boldsymbol{e}}, \boldsymbol{s}_o, \tilde{\boldsymbol{p}}) \;=\;& \boldsymbol{s}_c{}^T\bar{\boldsymbol{M}}(\boldsymbol{q})\, \dot{\boldsymbol{s}}_c + \frac{1}{2}\boldsymbol{s}_c{}^T\dot{\bar{\boldsymbol{M}}}(\boldsymbol{q})\, \boldsymbol{s}_c + \hat{\boldsymbol{e}}^T\boldsymbol{K}_p\dot{\hat{\boldsymbol{e}}} \\ &+ \boldsymbol{s}_o{}^T\bar{\boldsymbol{M}}(\boldsymbol{q})\, \dot{\boldsymbol{s}}_o + \frac{1}{2}\boldsymbol{s}_o{}^T\dot{\bar{\boldsymbol{M}}}(\boldsymbol{q})\, \boldsymbol{s}_o + \tilde{\boldsymbol{p}}^T\boldsymbol{K}_p\dot{\tilde{\boldsymbol{p}}}\end{aligned}$$

$$
\begin{aligned}
= & -\boldsymbol{s}_c{}^T \boldsymbol{K}_d \boldsymbol{s}_c + \frac{1}{2}\boldsymbol{s}_c{}^T \left\{\dot{\bar{\boldsymbol{M}}}(\boldsymbol{q}) - 2\bar{\boldsymbol{C}}(\boldsymbol{q},\dot{\boldsymbol{q}})\right\}\boldsymbol{s}_c \\
& -\boldsymbol{s}_c{}^T \boldsymbol{J}^T(\boldsymbol{q},t)\boldsymbol{K}_p\hat{\boldsymbol{e}} + \hat{\boldsymbol{e}}^T\boldsymbol{K}_p\dot{\hat{\boldsymbol{e}}} + \boldsymbol{s}_c{}^T\left\{\boldsymbol{K}_d + \boldsymbol{X}(\boldsymbol{q},\dot{\boldsymbol{q}}_r,t)\right\}\boldsymbol{s}_o \\
& -\boldsymbol{s}_o{}^T l_d \bar{\boldsymbol{M}}(\boldsymbol{q})\boldsymbol{s}_o + \frac{1}{2}\boldsymbol{s}_o{}^T\left\{\dot{\bar{\boldsymbol{M}}}(\boldsymbol{q}) - 2\bar{\boldsymbol{C}}(\boldsymbol{q},\dot{\boldsymbol{q}})\right\}\boldsymbol{s}_o \\
& -\boldsymbol{s}_o{}^T \boldsymbol{J}^T(\boldsymbol{q},t)\boldsymbol{K}_p\tilde{\boldsymbol{p}} + \tilde{\boldsymbol{p}}^T\boldsymbol{K}_p\dot{\tilde{\boldsymbol{p}}} + \boldsymbol{s}_o{}^T\left\{\boldsymbol{X}(\boldsymbol{q},\dot{\boldsymbol{q}}_o,t) - \boldsymbol{K}_d\right\}\boldsymbol{s}_c \\
= & -\boldsymbol{s}_c{}^T \boldsymbol{K}_d \boldsymbol{s}_c - (\hat{\boldsymbol{e}} - \tilde{\boldsymbol{p}})^T \boldsymbol{\Lambda}^T\boldsymbol{K}_p\hat{\boldsymbol{e}} + \boldsymbol{s}_c{}^T\boldsymbol{X}(\boldsymbol{q},\dot{\boldsymbol{q}}_r,t)\boldsymbol{s}_o \\
& -\boldsymbol{s}_o{}^T l_d \bar{\boldsymbol{M}}(\boldsymbol{q})\boldsymbol{s}_o - \tilde{\boldsymbol{p}}^T\boldsymbol{\Lambda}^T\boldsymbol{K}_p\tilde{\boldsymbol{p}} + \boldsymbol{s}_o{}^T\boldsymbol{X}(\boldsymbol{q},\dot{\boldsymbol{q}}_o,t)\boldsymbol{s}_c. \qquad (6.31)
\end{aligned}
$$

Here we make the following assumption:

Assumption 7 (Boundedness of the Change of the Desired Shape)

There exist some positive constants v_c and v_t such that

$$
v_c = \sup_{t\in\Re_+,\dot{\boldsymbol{\sigma}}\in\Re^n}\left\|\frac{\partial \boldsymbol{p}_d}{\partial t}(\hat{\boldsymbol{\sigma}},t)\right\|, \qquad (6.32)
$$

$$
v_t = \sup_{t\in\Re_+,\dot{\boldsymbol{\sigma}}\in\Re^n}\left\|\frac{\partial^2 \boldsymbol{p}_d}{\partial \boldsymbol{\sigma}\partial t}(\hat{\boldsymbol{\sigma}},t)\right\|. \qquad (6.33)
$$

□

This assumption requires only that given time-varying curves do not vary very rapidly.

Under this assumption, we can evaluate $\|\boldsymbol{X}\|$ as

$$
\|\boldsymbol{X}(\boldsymbol{q},\dot{\boldsymbol{q}},t)\| \leq \alpha\|\dot{\boldsymbol{q}}\| + \beta, \qquad (6.34)
$$

where α and β are defined as

$$
\alpha := \bar{M}_M {J_m}^{-1} J_H + \bar{C}_M, \qquad (6.35)
$$

$$
\beta := \bar{M}_M {J_m}^{-1} v_t. \qquad (6.36)
$$

Using α, β, we can evaluate the cross terms of $\boldsymbol{s}_c$ and $\boldsymbol{s}_o$ in (6.31) as

$$
\begin{aligned}
& \boldsymbol{s}_c{}^T\boldsymbol{X}(\boldsymbol{q},\dot{\boldsymbol{q}}_r,t)\boldsymbol{s}_o + \boldsymbol{s}_o{}^T\boldsymbol{X}(\boldsymbol{q},\dot{\boldsymbol{q}}_o,t)\boldsymbol{s}_c \\
& \quad \leq \{\alpha(\|\dot{\boldsymbol{q}}_r\| + \|\dot{\boldsymbol{q}}_o\|) + 2\beta\}\|\boldsymbol{s}_c\|\|\boldsymbol{s}_o\| \\
& \quad \leq \{\alpha(\|\dot{\boldsymbol{q}}_r\| + \|\boldsymbol{s}_c\| + \|\dot{\boldsymbol{q}}_r\| + \|\boldsymbol{s}_o\|) + 2\beta\}\|\boldsymbol{s}_c\|\|\boldsymbol{s}_o\| \\
& \quad \leq \{\alpha(\|\dot{\boldsymbol{q}}_r\| + \|\boldsymbol{s}_o\|) + \beta\}\|\boldsymbol{s}_c\|^2 + \{\alpha(\|\dot{\boldsymbol{q}}_r\| + \|\boldsymbol{s}_c\|) + \beta\}\|\boldsymbol{s}_o\|^2. \qquad (6.37)
\end{aligned}
$$

Moreover, **Property 3**-1 allows us to evaluate $\|\dot{\boldsymbol{q}}_r\|$ as

$$\begin{aligned}\|\dot{\boldsymbol{q}}_r\| &= \left\| \boldsymbol{J}^{-1}(\boldsymbol{q},t)\left\{\frac{\partial \boldsymbol{p}_d}{\partial t}(\hat{\boldsymbol{\sigma}},t) - \boldsymbol{\Lambda}(\hat{\boldsymbol{e}}-\tilde{\boldsymbol{p}})\right\}\right\| \\ &\leq {J_m}^{-1}\left(v_c + \lambda_M(\boldsymbol{\Lambda})\|\hat{\boldsymbol{e}}\| + \lambda_M(\boldsymbol{\Lambda})\|\tilde{\boldsymbol{p}}\|\right). \end{aligned} \tag{6.38}$$

Thus, $\dot{V}$ is evaluated as

$$\begin{aligned}&\dot{V}(\boldsymbol{s}_c,\hat{\boldsymbol{e}},\boldsymbol{s}_o,\tilde{\boldsymbol{p}}) \\ &\leq -\left[\lambda_m(\boldsymbol{K}_d) - \beta - \alpha\left\{{J_m}^{-1}\left(v_c + \lambda_M(\boldsymbol{\Lambda})\|\hat{\boldsymbol{e}}\| + \lambda_M(\boldsymbol{\Lambda})\|\tilde{\boldsymbol{p}}\|\right) + \|\boldsymbol{s}_o\|\right\}\right]\|\boldsymbol{s}_c\|^2 \\ &\quad -\left[l_d\bar{M}_m - \beta - \alpha\left\{{J_m}^{-1}\left(v_c + \lambda_M(\boldsymbol{\Lambda})\|\hat{\boldsymbol{e}}\| + \lambda_M(\boldsymbol{\Lambda})\|\tilde{\boldsymbol{p}}\|\right) + \|\boldsymbol{s}_c\|\right\}\right]\|\boldsymbol{s}_o\|^2 \\ &\quad -\frac{1}{2}\lambda_m(\boldsymbol{\Lambda}^T\boldsymbol{K}_p)\|\hat{\boldsymbol{e}}\|^2 - \frac{1}{2}\lambda_m(\boldsymbol{\Lambda}^T\boldsymbol{K}_p)\|\tilde{\boldsymbol{p}}\|^2. \end{aligned} \tag{6.39}$$

If a part of coordinates $(\hat{\boldsymbol{e}},\boldsymbol{s}_o,\tilde{\boldsymbol{p}})$ satisfies the condition:

$$\frac{1}{2}\max^{-1}(\lambda_M(\boldsymbol{\Lambda}),J_m)\left\{J_m\alpha^{-1}\left(\lambda_m(\boldsymbol{K}_d)-\beta\right) - v_c\right\} \geq \left\|\begin{bmatrix}\hat{\boldsymbol{e}}\\ \boldsymbol{s}_o\\ \tilde{\boldsymbol{p}}\end{bmatrix}\right\|, \tag{6.40}$$

then negativeness of the coefficient of $\|\boldsymbol{s}_c\|^2$ is assured. On the other hand, if a part of coordinates $(\boldsymbol{s}_c,\hat{\boldsymbol{e}},\tilde{\boldsymbol{p}})$ satisfies the condition:

$$\frac{1}{2}\max^{-1}(\lambda_M(\boldsymbol{\Lambda}),J_m)\left\{J_m\alpha^{-1}\left(l_d\bar{M}_m-\beta\right) - v_c\right\} \geq \left\|\begin{bmatrix}\boldsymbol{s}_c\\ \hat{\boldsymbol{e}}\\ \tilde{\boldsymbol{p}}\end{bmatrix}\right\|, \tag{6.41}$$

then negativeness of the coefficient of $\|\boldsymbol{s}_o\|^2$ is assured. Thus, if the set of full coordinates $(\boldsymbol{s}_c,\hat{\boldsymbol{e}},\boldsymbol{s}_o,\tilde{\boldsymbol{p}})$ satisfies the condition:

$$\frac{1}{2}\max^{-1}(\lambda_M(\boldsymbol{\Lambda}),J_m)\left[J_m\alpha^{-1}\left\{\min\left(\lambda_m(\boldsymbol{K}_d),l_d\bar{M}_m\right)-\beta\right\} - v_c\right] \geq \left\|\begin{bmatrix}\boldsymbol{s}_c\\ \hat{\boldsymbol{e}}\\ \boldsymbol{s}_o\\ \tilde{\boldsymbol{p}}\end{bmatrix}\right\|, \tag{6.42}$$

then negative definiteness of $\dot{V}$ is assured. Thus, if the gain condition

$$J_m\alpha^{-1}\left\{\min\left(\lambda_m(\boldsymbol{K}_d),l_d\bar{M}_m\right)-\beta\right\} - v_c > 0 \tag{6.43}$$

is satisfied, there exists a region to satisfy (6.42).

We summarize the above discussion in the following theorem:

Theorem 9 (Shape Tracking Controller with Shape Velocity Observer)

Consider the following controller based on curve parameter estimation:

$$\boldsymbol{u} = \boldsymbol{M}(\boldsymbol{\theta})\ddot{\boldsymbol{\theta}}_{ro} + \boldsymbol{C}(\boldsymbol{\theta}, \dot{\boldsymbol{\theta}}_o)\dot{\boldsymbol{\theta}}_r + \boldsymbol{g}(\boldsymbol{\theta}) + \boldsymbol{\tau}_\theta, \tag{6.44}$$

$$\ddot{\hat{\boldsymbol{\sigma}}} = \ddot{\hat{\boldsymbol{\sigma}}}_{ro} + \boldsymbol{K}_\sigma \boldsymbol{\tau}_\sigma, \tag{6.45}$$

$$\begin{bmatrix} \boldsymbol{\tau}_\theta \\ \boldsymbol{\tau}_\sigma \end{bmatrix} = -\boldsymbol{J}^T(\boldsymbol{q}, t)\boldsymbol{K}_p\hat{\boldsymbol{e}} - \boldsymbol{K}_d(\dot{\boldsymbol{q}}_o - \dot{\boldsymbol{q}}_r), \tag{6.46}$$

with the following shape velocity observer:

$$\dot{\hat{\boldsymbol{p}}} = \boldsymbol{z} + \dot{\hat{\boldsymbol{p}}}_d + (l_d\boldsymbol{I} + \boldsymbol{\Lambda})(\boldsymbol{p} - \hat{\boldsymbol{p}}) - \boldsymbol{\Lambda}(\hat{\boldsymbol{p}} - \hat{\boldsymbol{p}}_d), \tag{6.47}$$

$$\dot{\boldsymbol{z}} = l_d\boldsymbol{\Lambda}(\boldsymbol{p} - \hat{\boldsymbol{p}}) - \boldsymbol{J}(\boldsymbol{q}, t)\bar{\boldsymbol{M}}^{-1}(\boldsymbol{q})\boldsymbol{J}^T(\boldsymbol{q}, t)\boldsymbol{K}_p(\hat{\boldsymbol{p}} - \hat{\boldsymbol{p}}_d), \tag{6.48}$$

where $\dot{\boldsymbol{q}}_r, \dot{\boldsymbol{q}}_o \in \Re^{3n}$ and $\ddot{\boldsymbol{q}}_{ro} \in \Re^{3n}$ are defined as

$$\dot{\boldsymbol{q}}_r = \begin{bmatrix} \dot{\boldsymbol{\theta}}_r \\ \dot{\hat{\boldsymbol{\sigma}}}_r \end{bmatrix} := \boldsymbol{J}^{-1}(\boldsymbol{q}, t)\left\{\frac{\partial \boldsymbol{p}_d}{\partial t}(\hat{\boldsymbol{\sigma}}, t) - \boldsymbol{\Lambda}(\hat{\boldsymbol{p}} - \hat{\boldsymbol{p}}_d)\right\}, \tag{6.49}$$

$$\dot{\boldsymbol{q}}_o = \begin{bmatrix} \dot{\boldsymbol{\theta}}_o \\ \dot{\hat{\boldsymbol{\sigma}}}_o \end{bmatrix} := \boldsymbol{J}^{-1}(\boldsymbol{q}, t)\left\{\dot{\hat{\boldsymbol{p}}} - \frac{\partial \boldsymbol{p}_d}{\partial \boldsymbol{\sigma}}(\hat{\boldsymbol{\sigma}}, t)\dot{\hat{\boldsymbol{\sigma}}} - \boldsymbol{\Lambda}(\boldsymbol{p} - \hat{\boldsymbol{p}})\right\}, \tag{6.50}$$

$$\ddot{\boldsymbol{q}}_{ro} = \begin{bmatrix} \ddot{\boldsymbol{\theta}}_{ro} \\ \ddot{\hat{\boldsymbol{\sigma}}}_{ro} \end{bmatrix} := \ddot{\boldsymbol{q}}_r(\boldsymbol{q}, \dot{\boldsymbol{q}}_o, \hat{\boldsymbol{p}} - \hat{\boldsymbol{p}}_d, \dot{\hat{\boldsymbol{p}}} - \dot{\hat{\boldsymbol{p}}}_d), \tag{6.51}$$

and $\left[\hat{\boldsymbol{p}}^T \boldsymbol{z}^T\right]^T \in \Re^{6n}$ is the observer state, $\boldsymbol{\Lambda}, \boldsymbol{K}_p \in \Re^{3n\times 3n}$ are symmetric postive definite matrices with the relation $\boldsymbol{\Lambda}^T\boldsymbol{K}_p = \boldsymbol{K}_p^T\boldsymbol{\Lambda}$, $\boldsymbol{K}_d \in \Re^{2n\times 2n}$ and $\boldsymbol{K}_\sigma \in \Re^{n\times n}$ are symmetric positive definite matrices and l_d is a positive constant. Under **Assumption 7**, suppose l_d and $\boldsymbol{K}_d$ are chosen to satisfy

$$J_m\alpha^{-1}\left\{\min\left(\lambda_m(\boldsymbol{K}_d), l_d\bar{M}_m\right) - \beta\right\} - v_c > 0, \tag{6.52}$$

where α, β are

$$\alpha := \bar{C}_M + \bar{M}_M {J_m}^{-1} J_H., \tag{6.53}$$

$$\beta := \bar{M}_M {J_m}^{-1} v_t. \tag{6.54}$$

Then, shape tracking using only joint angle information is achieved locally. □

Proof. It is clear from the above discussion. (Q.E.D.)

Figure 6.2 shows the block diagram of the modified shape tracking controller. As stated before, we never change the controller structure. Instead, we replace the unavailable signals with their estimated values. The dual structure between the controller and the observer is the crucial key to solve this problem by Lyapunov theorem.

Summary

It was shown that shape tracking using only joint angles was attained by utilizing a shape velocity observer. This observer has a Lyapunov function dual to that of a shape tracking controller. It was proved that the simply tuned shape tracking controller and the shape velocity observer assured local asymptotic stability of the closed-loop system under some reasonable assumptions for a given spatial curve.

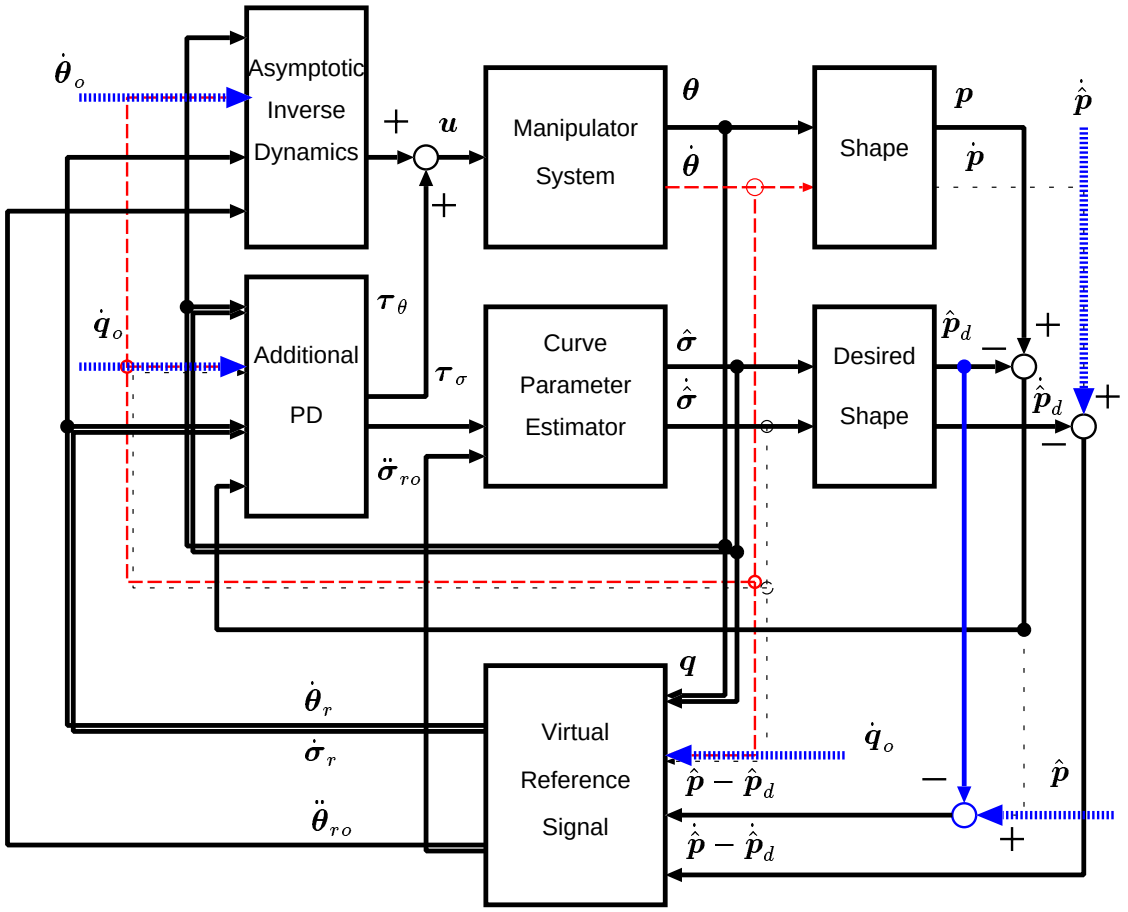

Figure 6.2: Modified shape tracking controller

Chapter 7

Obstacle Avoidance Based on Shape Control

In this chapter, we consider new task accomplishment from the viewpoint of shape control. An HDOF manipulator is expected to move in a highly constrained environment, especially to go into a very narrow space like a tube in order to look the deep inside among obstacles that can never be observed from the outside. Any conventional control methods for manipulators do not give any solution of this kind of obstacle avoidance problems. If we achieve a motion control along the curve which never collides any obstacles, then it is useful for the obstacle avoidance. It is shown that this motion control problem is successfully solved through the shape control concept.

In Section **7.1**, the main idea for utilizing shape control to the obstacle avoidance is shown. In Section **7.2**, a motion control problem is stated. This problem is to find a control to move the manipulator along a collision-free curve specified in advance. In Section **7.3**, two control laws are given as the counterparts of two tracking controllers in Chapter **5**.

7.1 Strategy for Obstacle Avoidance

Going into a narrow space is one of typical and useful obstacle avoidance tasks for an HDOF manipulator. For example, an HDOF manipulator with a camera at the tip is expected to look inside objects without any collisions. (See Figure 7.1.) It is also possible to affect forces to the point in deep inside of objects where one can never reach.

One of the simplest strategies to accomplish this task is the "follow the leader" method [20]. This is a literally ad hoc method that the previous target position of the next link (leader's) position is given as the present target position of each link. In this method, however, manipulator dynamics is completely neglected so that there is no theoretical

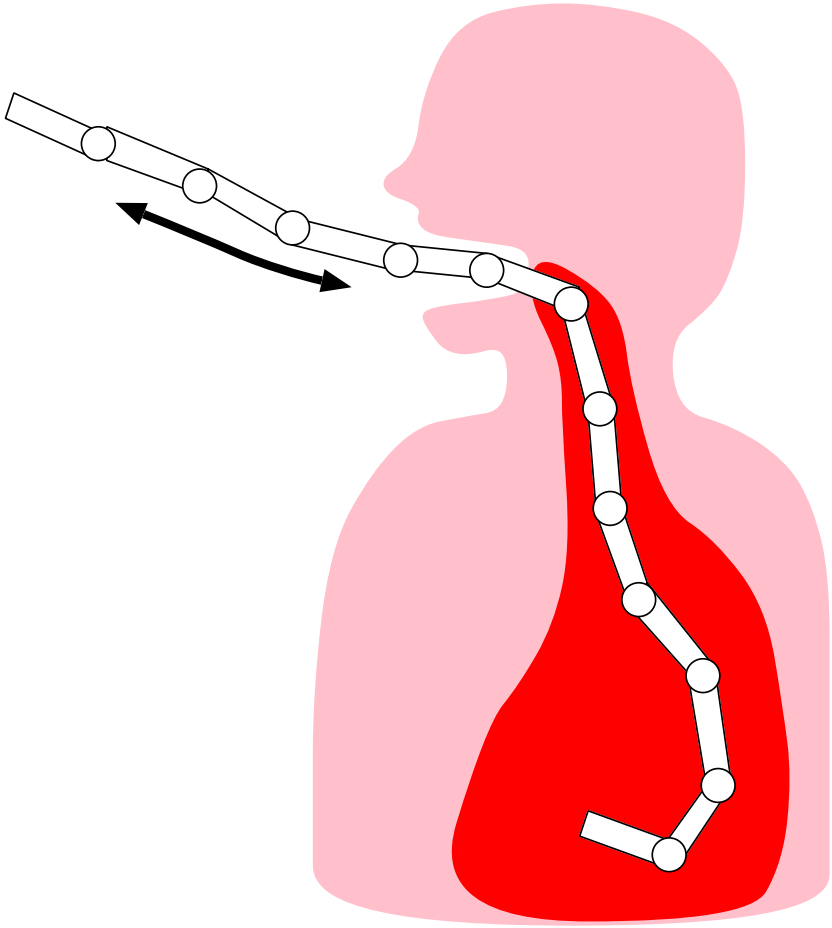

Figure 7.1: Going into a narrow space

assurance to avoid the obstacles, even if we completely know the desirable path that never crosses the obstacles in advance.

It is important to note that the motion along manipulator's length is essential to go into a narrow space. Then we consider a useful motion control problem for an obstacle avoidance, that is, to move along a specified curve. Before we formulate the problem, we have to observe that mobility is essential in order to attain the task. Because, we assume in this context that manipulator has only revolute joints. This type of joints basically generates the motion perpendicular to the manipulator's length direction. Mobility is introduced to make the motion of the direction along the length. Ma and Hirose developed a manipulator called the moray drive manipulator [9] that is an example to show that a manipulator with mobility is adequate for going into a narrow space, although they use a translational joint to make the motion of the manipulator's length direction.

There are some ways to give mobility to an HDOF manipulator: for example, to mount

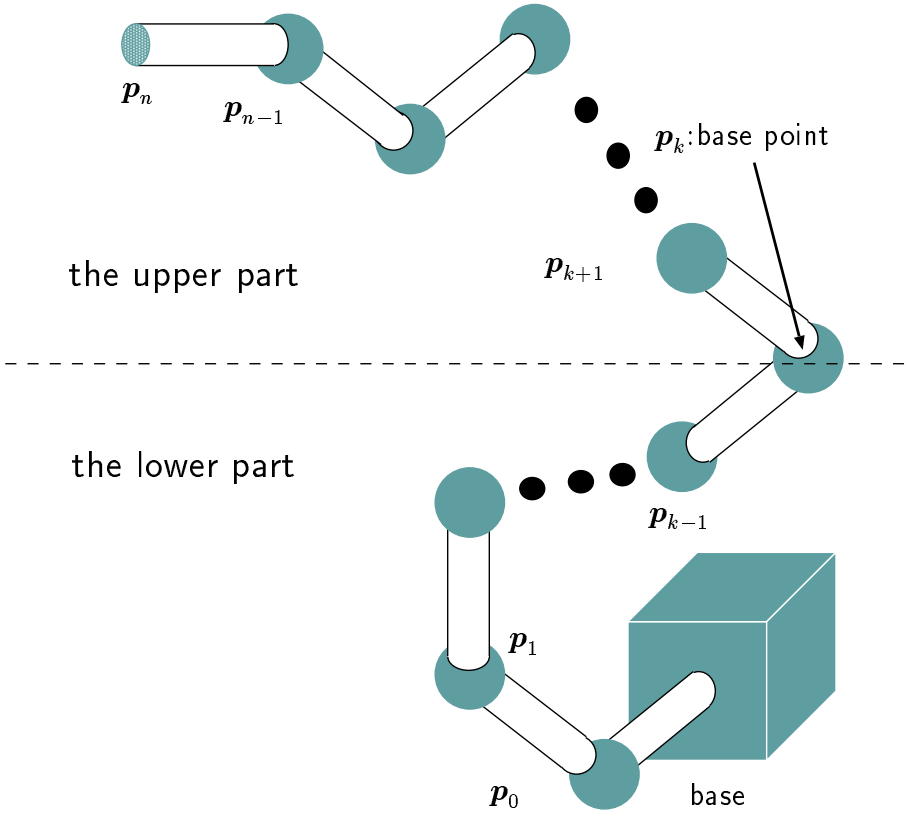

Figure 7.2: HDOF manipulator with mobility

it on a car, legs, plane and so on. Here we divide an HDOF manipulator into two parts, the upper one and the lower one. The lower part is used for mobility, while the shape of the upper part is controlled to avoid obstacles. The boundary point of two parts is called the *base point*. (See Figure 7.2.)

7.2 Problem Statement

Suppose that the base point is at $\boldsymbol{p}_k$, the k-th link position. Define $\boldsymbol{\theta}_L \in \Re^{2k}$ and $\boldsymbol{\theta}_U \in \Re^{2(n-k)}$ as

$$\boldsymbol{\theta}_L := \begin{bmatrix} \boldsymbol{\theta}_1 \\ \vdots \\ \boldsymbol{\theta}_k \end{bmatrix}, \tag{7.1}$$

$$\boldsymbol{\theta}_U = \begin{bmatrix} \boldsymbol{\theta}_{k+1} \\ \vdots \\ \boldsymbol{\theta}_n \end{bmatrix}. \tag{7.2}$$

We call $\boldsymbol{\theta}_L$ the *lower joint angles*, $\boldsymbol{\theta}_U$ the *upper joint angles*. Also define $\boldsymbol{p}_U \in \Re^{3(n-k)}$ as

$$\boldsymbol{p}_U = \begin{bmatrix} \boldsymbol{p}_{k+1} \\ \vdots \\ \boldsymbol{p}_n \end{bmatrix}. \tag{7.3}$$

We call $\boldsymbol{p}_U$ the *upper shape* of the manipulator.

Consider m obstacles, $\mathcal{O}_j, (j = 1, \cdots, m)$, in Euclidean space. Suppose that , for some positive real constant r, we know a curve $\check{\boldsymbol{c}} : \Re \to E^3$ satisfying the following condition:

$$\forall j \quad \mathcal{T}(\check{\boldsymbol{c}}, r) \cap O_j = \emptyset, \tag{7.4}$$

where $\mathcal{T} \subset E^3$ is defined as

$$\mathcal{T}(\check{\boldsymbol{c}}, r) := \left\{ \boldsymbol{p} \in E^3 \middle| \ \|\boldsymbol{p} - \check{\boldsymbol{c}}(\sigma)\| \leq r, \sigma \in \Re \right\}. \tag{7.5}$$

That is, $\check{\boldsymbol{c}}$ is a collision-free curve assured to be amount r apart from any obstacles (see Figure 7.3). Therefore, an HDOF manipulator never collides the obstacles if it moves along the curve. Then, we consider a control to move the upper part of an HDOF manipulator along this curve.

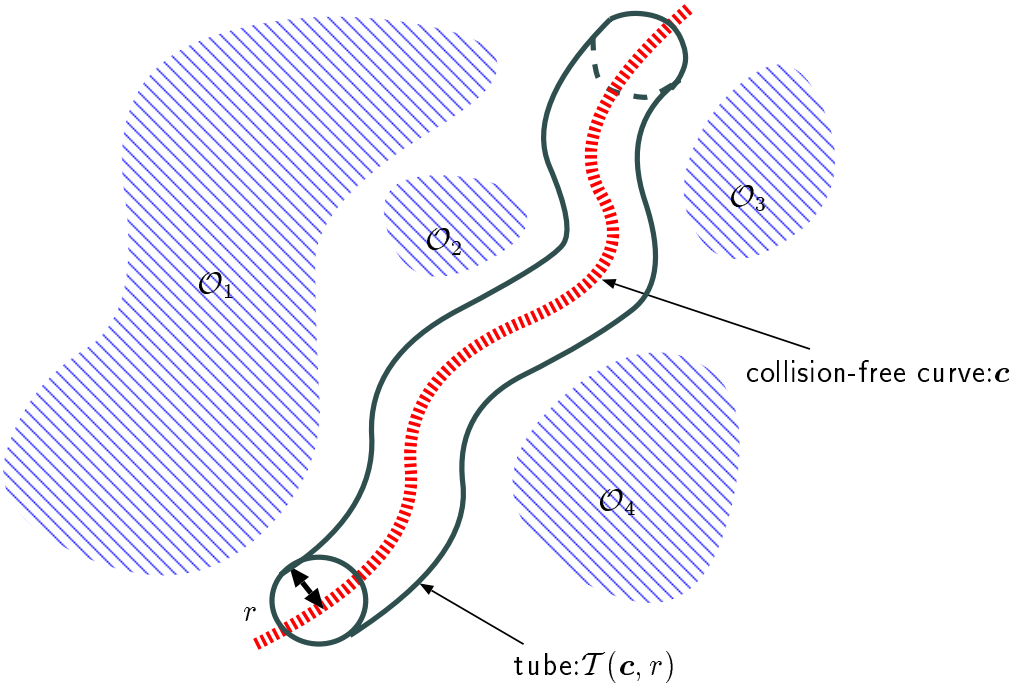

Figure 7.3: Collision-free curve

Let $\sigma_k{}^*$ be the desired curve parameter corresponding to the base point, $\boldsymbol{p}_k$. We will give this value $\sigma_k{}^*$ as a command to move it forward or backword along the curve. If $\dot{\sigma}_k^* > 0$, then the desired base position moves forward along the curve.

Consider a time-varying curve, $\boldsymbol{c} : \Re \times \Re_+ \to E^3$, defined by

$$\boldsymbol{c}(\sigma, t) \;:=\; \check{\boldsymbol{c}}(\sigma + \sigma_k{}^*(t)) - \check{\boldsymbol{c}}(\sigma_k{}^*(t)). \tag{7.6}$$

Let $\boldsymbol{\theta}_U{}^*(t)$ be the solution of the extended shape inverse problem for the upper part of the manipulator and time-varying curve (7.6). Then, a control problem achieving the motion along a collision-free curve is stated as follows:

Problem 6 (Motion Control along a Collision-free Curve)

Consider

1. an HDOF manipulator with dynamics (2.34) and the base point at $\boldsymbol{p}_k$,
2. a collision-free curve $\check{\boldsymbol{c}} : \Re \to E^3$ satisfying **Assumption 1**, and
3. a desired curve parameter corresponding to the desired base position, $\sigma_k{}^*(t)$, which is a continuously differentiable function of time.

Moreover, suppose that **Assumption 5** holds. Then, find a control input, $\boldsymbol{u}$, in (2.34) achieving that

$$\boldsymbol{\theta}_U(t) \;\to\; \boldsymbol{\theta}_U{}^*(t), \tag{7.7}$$

$$\dot{\boldsymbol{\theta}}_U(t) \;\to\; \dot{\boldsymbol{\theta}}_U^*(t), \tag{7.8}$$

and

$$\boldsymbol{p}_k(\boldsymbol{\theta}_L(t)) \;\to\; \check{\boldsymbol{c}}(\sigma_k{}^*(t)), \tag{7.9}$$

$$\dot{\boldsymbol{p}}_k(\boldsymbol{\theta}_L(t), \dot{\boldsymbol{\theta}}_L(t)) \;\to\; \dot{\check{\boldsymbol{c}}}(\sigma_k{}^*(t), \dot{\sigma}_k^*(t)), \tag{7.10}$$

as $t \to \infty$, where $\boldsymbol{\theta}_U{}^*(t)$ is the desired joint angle function for the upper part of the manipulator, that is, the solution of the extended shape inverse problem for the upper part and the time-varying curve $\boldsymbol{c}(\sigma, t) := \check{\boldsymbol{c}}(\sigma + \sigma_k{}^*(t)) - \check{\boldsymbol{c}}(\sigma_k{}^*(t))$. □

Control objective (7.7), (7.8) requires that the upper shape corresponds to the desired shape, while objective (7.9), (7.10) means the base point error to be zero. We need to see that the configuration of the upper part of the manipulator consists of not only its shape, but also its position and orientation [19].

Consider a part of the estimated curve parameter, $\hat{\boldsymbol{\sigma}}_U := [\hat{\sigma}_{k+1} \ \cdots \ \hat{\sigma}_n]^T \in \Re^{n-k}$ and define $\boldsymbol{p}_{U,d}(\hat{\boldsymbol{\sigma}}_U) \in \Re^{3(n-k)}$ as

$$\boldsymbol{p}_{U,d}(\hat{\boldsymbol{\sigma}}_U) := \begin{bmatrix} \boldsymbol{c}(\hat{\sigma}_{k+1}) \\ \vdots \\ \boldsymbol{c}(\hat{\sigma}_n) \end{bmatrix}. \tag{7.11}$$

This vector means the estimated desired upper shape. Define also $\boldsymbol{\xi} \in \Re^{3(n-k+1)}$ as

$$\hat{\boldsymbol{\xi}}(\boldsymbol{\theta}, \hat{\boldsymbol{\sigma}}_U; {\sigma_k}^*) := \begin{bmatrix} \boldsymbol{p}_k(\boldsymbol{\theta}) - \check{\boldsymbol{c}}({\sigma_k}^*) \\ \boldsymbol{p}_U(\boldsymbol{\theta}) - \boldsymbol{p}_{U,d}(\hat{\boldsymbol{\sigma}}_U) \end{bmatrix}, \tag{7.12}$$

which is called the *estimated configuration error*.

If we define $\boldsymbol{J}_\xi(\boldsymbol{\theta}, \boldsymbol{\sigma}_U) \in \Re^{3(n-k+1)\times(3n-k)}$ and $\boldsymbol{x} \in \Re^{3(n-k+1)}$ as

$$\boldsymbol{J}_\xi(\boldsymbol{\theta}, \boldsymbol{\sigma}_U) := \begin{bmatrix} \dfrac{\partial \boldsymbol{p}_k}{\partial \boldsymbol{\theta}}(\boldsymbol{\theta}) & \mathbf{o} \\ \dfrac{\partial \boldsymbol{p}_U}{\partial \boldsymbol{\theta}}(\boldsymbol{\theta}) & -\dfrac{\partial \boldsymbol{p}_{U,d}}{\partial \boldsymbol{\sigma}_U}(\boldsymbol{\sigma}_U) \end{bmatrix}, \tag{7.13}$$

$$\boldsymbol{x}^*({\sigma_k}^*) = \begin{bmatrix} \check{\boldsymbol{c}}({\sigma_k}^*) \\ \mathbf{o} \end{bmatrix}, \tag{7.14}$$

then the time derivative of $\hat{\boldsymbol{\xi}}$ can be written as

$$\dot{\hat{\boldsymbol{\xi}}}(\boldsymbol{\theta}, \boldsymbol{\sigma}_U, \dot{\boldsymbol{\theta}}, \dot{\boldsymbol{\sigma}}_U; \sigma_k, \dot{\sigma}_k) = \boldsymbol{J}_\xi(\boldsymbol{\theta}, \hat{\boldsymbol{\sigma}}_U)\dot{\boldsymbol{q}}_\xi - \dot{\boldsymbol{x}}^*({\sigma_k}^*, \dot{\sigma}_k^*), \tag{7.15}$$

where $\boldsymbol{q}_\xi := \begin{bmatrix} \boldsymbol{\theta}^T & \hat{\boldsymbol{\sigma}} \end{bmatrix}^T \in \Re^{3n-k}$.

Here we make the following assumption for $\boldsymbol{J}_\xi(\boldsymbol{\theta}, \hat{\boldsymbol{\sigma}}_U)$:

Assumption 8 (Time-varying Shape Jacobian)

The matrix $\boldsymbol{J}_\xi(\boldsymbol{\theta}, \hat{\boldsymbol{\sigma}}_U)$ is of full rank for any $(\boldsymbol{\theta}, \hat{\boldsymbol{\sigma}}_U)$ which satisfy $\hat{\boldsymbol{\xi}} = \mathbf{o}$. □

Define $\mathcal{D}_{U,\delta} \subset \Re^{3n-k}$ as

$$\mathcal{D}_{U,\delta} := \left\{ (\boldsymbol{\theta}_U, \boldsymbol{\sigma}_U) \in \Re^{3(n-k)} \,\middle|\, |\theta_{s,i}| < \pi, \ |\theta_{m,i}| < \pi, \ \delta < \sigma_i - \sigma_{i-1} < \frac{1}{\kappa_M} \right\}, \tag{7.16}$$

where $\delta \in [-l_M \ l_M]$ and $i = k+1, \cdots, n$. From **Theorem 4**, under **Assumption 8**, if

$$\hat{\boldsymbol{\xi}}(\boldsymbol{\theta}, \hat{\boldsymbol{\sigma}}_U; {\sigma_k}^*) \to \mathbf{o}, \tag{7.17}$$

$$\dot{\hat{\boldsymbol{\xi}}}(\boldsymbol{\theta}, \hat{\boldsymbol{\sigma}}_U, \dot{\boldsymbol{\theta}}, \dot{\hat{\boldsymbol{\sigma}}}_U; {\sigma_k}^*, \dot{\sigma}_k^*) \to \mathbf{o}, \tag{7.18}$$

$$(\boldsymbol{\theta}_U, \hat{\boldsymbol{\sigma}}_U) \in \mathcal{D}_{U,\delta}, \tag{7.19}$$

then, the control objective (7.7), (7.8), (7.9) and (7.10) is achieved.

7.3 Obstacle Avoidance Controllers

In the same manner as Chapter **5**, we show two controllers achieving the control objective in this chapter.

Theorem 10 (ID-based Obstacle Avoidance)

Consider a control law with a curve parameter estimation law as follows :

$$\boldsymbol{u} = \boldsymbol{M}(\boldsymbol{\theta})\ddot{\boldsymbol{\theta}}_d + \boldsymbol{C}(\boldsymbol{\theta}, \dot{\boldsymbol{\theta}})\dot{\boldsymbol{\theta}} + \boldsymbol{g}(\boldsymbol{\theta}), \tag{7.20}$$

$$\ddot{\hat{\boldsymbol{\sigma}}}_U = \ddot{\boldsymbol{\sigma}}_{U,d}, \tag{7.21}$$

where $\ddot{\boldsymbol{\theta}}_d \in \Re^{2n}$ and $\ddot{\boldsymbol{\sigma}}_{U,d} \in \Re^{n-k}$ are

$$\begin{bmatrix} \ddot{\boldsymbol{\theta}}_d \\ \ddot{\boldsymbol{\sigma}}_{U,d} \end{bmatrix} = \boldsymbol{J}_\xi{}^+(\boldsymbol{q}_\xi)\left\{\ddot{\boldsymbol{x}}^* - \dot{\boldsymbol{J}}_\xi(\boldsymbol{q}_\xi, \dot{\boldsymbol{q}}_\xi)\dot{\boldsymbol{q}}_\xi - \boldsymbol{L}_p\hat{\boldsymbol{\xi}} - \boldsymbol{L}_d\dot{\hat{\boldsymbol{\xi}}}\right\}. \tag{7.22}$$

and $\boldsymbol{L}_p, \boldsymbol{L}_d \in \Re^{3(n-k+1)\times 3(n-k+1)}$ are symmetric positive definite matrices, the symbol $'+'$ denotes the pseudo-inverse of a matrix. Then, under **Assumption 8**, the control objective of the motion control along a collision-free curve is achieved locally. □

Proof. From (7.20), (7.21), (7.22), we obtain the closed loop system

$$\ddot{\boldsymbol{q}} = \boldsymbol{J}_\xi{}^+(\boldsymbol{q}_\xi)\left\{\ddot{\boldsymbol{x}}^* - \dot{\boldsymbol{J}}_\xi(\boldsymbol{q}_\xi, \dot{\boldsymbol{q}}_\xi)\dot{\boldsymbol{q}}_\xi - \boldsymbol{L}_p\hat{\boldsymbol{\xi}} - \boldsymbol{L}_d\dot{\hat{\boldsymbol{\xi}}}\right\}. \tag{7.23}$$

Multiplying both sides of the expression above by $\boldsymbol{J}_\xi$ leads to

$$\ddot{\hat{\boldsymbol{\xi}}} + \boldsymbol{L}_d\dot{\hat{\boldsymbol{\xi}}} + \boldsymbol{L}_p\hat{\boldsymbol{\xi}} = \mathbf{o}, \tag{7.24}$$

which shows $\boldsymbol{\xi} \to \mathbf{o}$, $\dot{\boldsymbol{\xi}} \to \mathbf{o}$. (Q.E.D.)

Theorem 11 (Lyapunov-based Obstacle Avoidance)

Consider a control law with a curve parameter estimation law as follows:

$$\boldsymbol{u} = \boldsymbol{M}(\boldsymbol{\theta})\ddot{\boldsymbol{\theta}}_r + \boldsymbol{C}(\boldsymbol{\theta}, \dot{\boldsymbol{\theta}})\dot{\boldsymbol{\theta}}_r + \boldsymbol{g}(\boldsymbol{\theta}) + \boldsymbol{\tau}_\theta, \tag{7.25}$$

$$\ddot{\hat{\boldsymbol{\sigma}}}_U = \ddot{\boldsymbol{\sigma}}_{U,r} + \boldsymbol{L}_\sigma\boldsymbol{\tau}_{\sigma,U}, \tag{7.26}$$

where $\boldsymbol{\tau}_\theta \in \Re^{2n}$ and $\boldsymbol{\tau}_{\sigma,U} \in \Re^{n-k}$ are

$$\begin{bmatrix} \boldsymbol{\tau}_\theta \\ \boldsymbol{\tau}_{\sigma,U} \end{bmatrix} = -\boldsymbol{J}_\xi{}^T(\boldsymbol{q}_\xi)\boldsymbol{L}_p\hat{\boldsymbol{\xi}} - \boldsymbol{L}_d\left(\dot{\boldsymbol{q}}_\xi - \dot{\boldsymbol{q}}_{\xi,r}\right), \tag{7.27}$$

and $\dot{\boldsymbol{q}}_{\xi,r} \in \Re^{3n-k}$, $\dot{\boldsymbol{\theta}}_r \in \Re^{2n}$, $\dot{\hat{\boldsymbol{\sigma}}}_{U,r} \in \Re^{n-k}$, are defined by

$$\dot{\boldsymbol{q}}_{\xi,r} = \begin{bmatrix} \dot{\boldsymbol{\theta}}_r \\ \dot{\hat{\boldsymbol{\sigma}}}_{U,r} \end{bmatrix} := \left\{\boldsymbol{I} - \boldsymbol{J}_\xi^+(\boldsymbol{q}_\xi)\boldsymbol{J}_\xi(\boldsymbol{q}_\xi)\right\}\dot{\boldsymbol{q}}_\xi + \boldsymbol{J}_\xi{}^+(\boldsymbol{q}_\xi)\left(\dot{\boldsymbol{x}}^* - \boldsymbol{\Lambda}\hat{\boldsymbol{\xi}}\right), \tag{7.28}$$

and $\boldsymbol{L}_p, \boldsymbol{\Lambda} \in \Re^{3(n-k+1)\times 3(n-k+1)}$, $\boldsymbol{L}_d \in \Re^{3(n-k)\times 3(n-k)}$ and $\boldsymbol{L}_\sigma \in \Re^{(n-k)\times(n-k)}$ are all symmetric positive definite matrices. Then, under **Assumption 8**, the control objectives of the motion control along a collision-free curve are achieved locally. □

Proof. Define $\boldsymbol{s}_{\xi,c} := \dot{\boldsymbol{q}}_\xi - \dot{\boldsymbol{q}}_{\xi,r}$. Consider the following scalar function:

$$V(\boldsymbol{s}_{\xi,c}, \hat{\boldsymbol{\xi}}) = \frac{1}{2}\boldsymbol{s}_{\xi,c}{}^T \bar{\boldsymbol{M}}(\boldsymbol{q})\, \boldsymbol{s}_{\xi,c} + \frac{1}{2}\hat{\boldsymbol{\xi}}^T \boldsymbol{K}_p \hat{\boldsymbol{\xi}}. \tag{7.29}$$

This function has the following time-derivative:

$$\dot{V}(\boldsymbol{s}_{\xi,c}, \hat{\boldsymbol{\xi}}) \;=\; -\boldsymbol{s}_{\xi,c}{}^T \boldsymbol{K}_d \boldsymbol{s}_{\xi,c} - \hat{\boldsymbol{\xi}}^T \boldsymbol{\Lambda}^T \boldsymbol{K}_p \hat{\boldsymbol{\xi}}, \tag{7.30}$$

which completes the proof. (Q.E.D.)

Obviously, these controllers are the counterparts of tracking controllers in Chapter **5**.

Summary

One obstacle avoidance scheme was proposed as an example of new task accomplishment by shape control. This is based on a motion control along the curve which never collides any obstacles. Two controllers achieving this motion were shown as the counterparts of two shape tracking controller derived before.

Chapter 8

Limit Analysis via Increase in DOF

In the previous chapters, we mainly consider to control the shape of an HDOF manipulator. In this chapter, we discuss essentials of an HDOF manipulator from the viewpoint of shape control. The feature of an HDOF manipulator is its rich kinematic DOF. When we imagine to increase its DOF, we know by intuition that the "zig-zag" form of the manipulator approaches a smooth curve in shape, which is related to the idea of shape control. Thus, it is natural to expect that its essentials are getting clear as the DOF of a manipulator increases. Then we discuss asymptotic properties of an HDOF manipulator by increase in DOF.

In Section **8.1**, the operation of increase in DOF is defined. In Section **8.2**, we prove by using the operation that the "zig-zag" form of the manipulator on a smooth curve approaches the curve in shape. In Section **8.3**, as one trial to look for essentials by increase in DOF, a specific kinematic structure for an HDOF manipulator is considered. It is reasonable in the sense that its direct kinematics tends to Frenet-Serret formula of spatial curves.

8.1 Increase in DOF

First we define a special sequence of position vectors in order to represent increase in DOF.

Definition 3 (Chain)

A sequence of position vectors in E^3 , Δ, is said to be a *chain* if any distances between adjacent position vectors are constant. □

For a chain, Δ, let $\boldsymbol{p}_i(\Delta) \in E^3$ be the i-th position vector in Δ and $n(\Delta)$ denotes the number of position vectors in Δ. Define also the *chain fineness*, $\mathrm{mes}(\Delta)$, as the

maximum distance between any two adjacent position vectors in Δ:

$$\mathrm{mes}(\Delta) := \max_i \ l_i(\Delta), \tag{8.1}$$

where $l_i(\Delta) := \left\| \boldsymbol{p}_i(\Delta) - \boldsymbol{p}_{i-1}(\Delta) \right\|$. Define *sub-length of a chain*, $L_i(\Delta)$, by

$$L_i(\Delta) := \sum_{j=1}^{i} l_j(\Delta). \tag{8.2}$$

The *total length* of a chain is expressed by $L_{n(\Delta)}(\Delta)$.

By using chains, we define *increase in DOF* as follows:

Definition 4 (Increase in DOF)

Consider a sequence of chains, $\{\Delta_k\}_{k=0}^{\infty}$. An operation increasing k in the sequence is called *increase in DOF* if the sequence satisfies the following conditions:

1. The number of position vectors of a chain in the sequence increases strictly with respect to the indexes, i.e.,

$$\forall k_1, k_2 \in N \quad k_1 < k_2 \Rightarrow n(\Delta_{k_1}) < n(\Delta_{k_2}).$$

2. The total length of a chain in the sequence is invariant, i.e.,

$$\forall k_1, k_2 \in N \quad L_{n(\Delta_{k_1})}(\Delta_{k_1}) = L_{n(\Delta_{k_2})}(\Delta_{k_2}).$$

3. The sub-length of a chain is preserved, i.e.,

$$\forall k_1, k_2 \in N$$

$$k_1 < k_2 \Rightarrow \exists \iota(i, k_1, k_2) \in N \quad L_i(\Delta_{k_1}) = L_\iota(\Delta_{k_2}).$$

4. The fineness of a chain in the sequence converges to zero asymptotically, i.e.,

$$\lim_{k \to \infty} \mathrm{mes}(\Delta_k) = 0.$$

□

8.2 Convergence to a Smooth Curve

Using the operation defined by **Definition 4**, we can rigorously prove the intuitively clear fact that the "zig-zag" form of an HDOF manipulator on a curve converges to the curve.

Theorem 12 (Convergence to a Smooth Curve)

Consider

1. an HDOF manipulator whose direct kinematics is expressed by (2.20), (2.15) and (2.25),
2. a continuously differentiable curve $\boldsymbol{c} : \Re \to E^3$, and
3. a chain sequence $\{\Delta_k\}_{k=0}^{\infty}$, generated by increase in DOF, which has link positions of the manipulator as the initial chain:

$$\Delta_0 = \{\boldsymbol{p}_i\}_{i=0}^{n}. \tag{8.3}$$

Suppose that any position vectors in any chains in the chain sequence are on the curve, i.e.,

$$\begin{aligned} &\forall k \in N \quad \forall i \in \{0, \cdots, n(\Delta_k)\} \quad \exists \sigma_i(\Delta_k) \in \Re \\ &\boldsymbol{p}_i(\Delta_k) = \boldsymbol{c}(\sigma_i(\Delta_k)). \end{aligned} \tag{8.4}$$

Then, the following equation holds:

$$\lim_{k\to\infty} \boldsymbol{p}_i = \boldsymbol{c}(L_i), \tag{8.5}$$

where $L_i := \sum_{j}^{i} l_j$. This means that link position $\boldsymbol{p}_i$ on a curve converges to $\boldsymbol{c}(L_i)$ by increase in DOF. □

Proof. The left-hand side of (8.5) is

$$\begin{aligned} \lim_{k\to\infty} \boldsymbol{p}_i &= \lim_{k\to\infty} \boldsymbol{p}_{\iota(i,0,k)}(\Delta_k) \\ &= \lim_{k\to\infty} \boldsymbol{c}(\sigma_{\iota(i,0,k)}(\Delta_k)) \\ &= \boldsymbol{c}(\lim_{k\to\infty} \sigma_{\iota(i,0,k)}(\Delta_k)). \end{aligned} \tag{8.6}$$

On the other hand, the right-hand side of (8.5) is

$$\boldsymbol{c}(L_i) = \boldsymbol{c}(\lim_{k\to\infty} L_{\iota(i,0,k)}(\Delta_k)). \tag{8.7}$$

Then it is enough to show that

$$\lim_{k\to\infty} \left(\sigma_{\iota(i,0,k)} - L_{\iota(i,0,k)}\right) = 0, \tag{8.8}$$

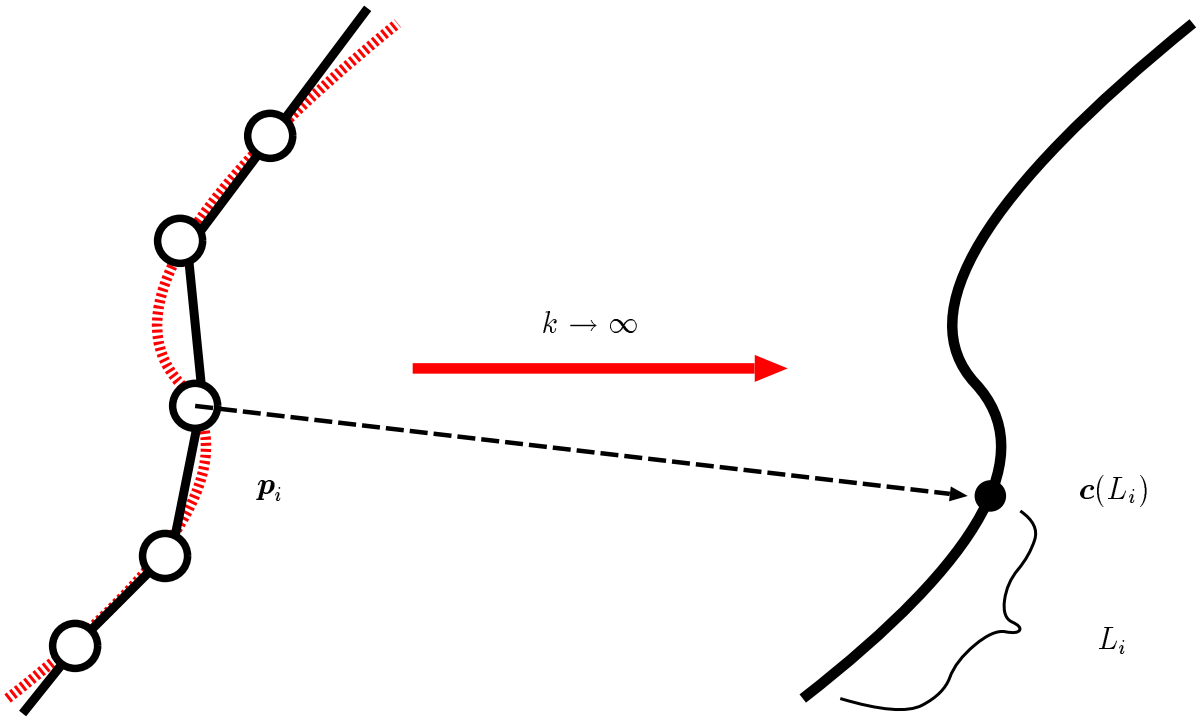

Figure 8.1: Convergence to a smooth curve

for the proof.

$$\lim_{k\to\infty}\left(\sigma_{\iota(i,0,k)} - L_{\iota(i,0,k)}\right) = \lim_{k\to\infty}\left(\int_0^{\sigma_\iota}\left\|\frac{d\boldsymbol{c}}{d\sigma}(\sigma)\right\| d\sigma - \sum_{s=1}^{\iota} l_s(\Delta_k)\right), \tag{8.9}$$

where we abbreviate $\iota(i,0,k)$ just as ι. If we write $\dfrac{d\boldsymbol{c}}{d\sigma}(\sigma)$ as

$$\frac{d\boldsymbol{c}}{d\sigma}(\sigma) = \begin{bmatrix} \dot{c}_x(\sigma) \\ \dot{c}_y(\sigma) \\ \dot{c}_z(\sigma) \end{bmatrix}, \tag{8.10}$$

then by the mean value theorem, there exist $\sigma_{x,s}, \sigma_{y,s}, \sigma_{z,s} \in [\sigma_{i-1}\ \sigma_i]$ such that

$$l_s(\Delta_k) = \left\{\dot{c}_x^2(\sigma_{x,s}) + \dot{c}_y^2(\sigma_{y,s}) + \dot{c}_z^2(\sigma_{z,s})\right\}^{\frac{1}{2}}(\sigma_s - \sigma_{s-1}). \tag{8.11}$$

Therefore, we obtain

$$\begin{aligned}\lim_{k\to\infty}\left(\sigma_{\iota(i,0,k)} - L_{\iota(i,0,k)}\right) = \lim_{k\to\infty}\sum_{s=1}^{\iota}\Bigg[\Big(&\left\{\dot{c}_x^2(\sigma_s) + \dot{c}_y^2(\sigma_s) + \dot{c}_z^2(\sigma_s)\right\}^{\frac{1}{2}} \\ &- \left\{\dot{c}_x^2(\sigma_{x,s}) + \dot{c}_y^2(\sigma_{y,s}) + \dot{c}_z^2(\sigma_{z,s})\right\}^{\frac{1}{2}}\Big)(\sigma_s - \sigma_{s-1})\Bigg].\end{aligned} \tag{8.12}$$

Since $\dot{c}_x, \dot{c}_y, \dot{c}_z$ are uniformly continuous because of their continuity, for any positive constant ϵ, we can find k such that

$$\begin{aligned} |\dot{c}_x(\sigma_s) - \dot{c}_x(\sigma_{x,s})| &< \epsilon, \\ |\dot{c}_y(\sigma_s) - \dot{c}_y(\sigma_{y,s})| &< \epsilon, \\ |\dot{c}_z(\sigma_s) - \dot{c}_z(\sigma_{z,s})| &< \epsilon. \end{aligned} \tag{8.13}$$

Thus, we obtain

$$\begin{aligned} &\left\{\dot{c}_x^2(\sigma_s) + \dot{c}_y^2(\sigma_s) + \dot{c}_z^2(\sigma_s)\right\}^{\frac{1}{2}} - \left\{\dot{c}_x^2(\sigma_{x,s}) + \dot{c}_y^2(\sigma_{y,s}) + \dot{c}_z^2(\sigma_{z,s})\right\}^{\frac{1}{2}} \\ &\quad\leq |\dot{c}_x(\sigma_s) - \dot{c}_x(\sigma_{x,s})| + |\dot{c}_y(\sigma_s) - \dot{c}_y(\sigma_{y,s})| + |\dot{c}_z(\sigma_s) - \dot{c}_z(\sigma_{z,s})| \\ &\quad< 3\epsilon. \end{aligned} \tag{8.14}$$

Therefore,

$$\begin{aligned} \left|\sigma_{\iota(i,0,k)} - L_{\iota(i,0,k)}\right| &< 3\epsilon \left|\sum_{s=1}^{\iota}(\sigma_s - \sigma_{s-1})\right| \\ &= 3\epsilon\sigma_{\iota(i,0,k)}, \end{aligned} \tag{8.15}$$

which concludes (8.8) since $\sigma_{\iota(i,0,k)}$ is bounded from above and we can make ϵ be arbitrarily small by taking sufficiently large k. (Q.E.D.)

8.3 Kinematic Structure for HDOF Manipulators

Up to here, we have said nothing about a kinematic structure of the 2DOF joint. Increase in DOF enables us to consider the kinematic structure deeply. The conditions for a specific kinematic structure are derived from the geometrically natural requirement that its direct kinematics tends to Frenet-Serret formula by increase in DOF.

Let $\boldsymbol{\Phi}_i(\Delta_k) \in SO(3)$ be the i-th link coordinate in chain Δ_k. By increase in DOF, $\boldsymbol{\Phi}_i$ $(= \boldsymbol{\Phi}_i(\Delta_0))$ converges to the coordinate on the curve whose origin is at $\boldsymbol{c}(L_i)$ by **Theorem 12**. Let $\boldsymbol{\Phi}(L_i)$ be the limit coordinate, i.e.,

$$\boldsymbol{\Phi}(L_i) := \lim_{k\to\infty} \boldsymbol{\Phi}_i. \tag{8.16}$$

The following theorem gives the conditions for axes $\boldsymbol{a}_{s,i}$, $\boldsymbol{a}_{m,i}$ such that $\boldsymbol{\Phi}(L_i)$ satisfies Frenet-Serret formula.

Theorem 13 (Kinematic Structure)

Direct kinematics of an HDOF manipulator (2.20), (2.15), (2.25) converges to Frenet-Serret formula (2.4), (2.5) by increase in DOF if and only if

$$\forall i \in \{1, \cdots, n\} \quad \boldsymbol{a}_{s,i} = \boldsymbol{e}_x, \ \boldsymbol{a}_{m,i} = \boldsymbol{e}_z. \tag{8.17}$$

This means that the manipulator have 2DOF joints with twisting and bending axes uniformly. □

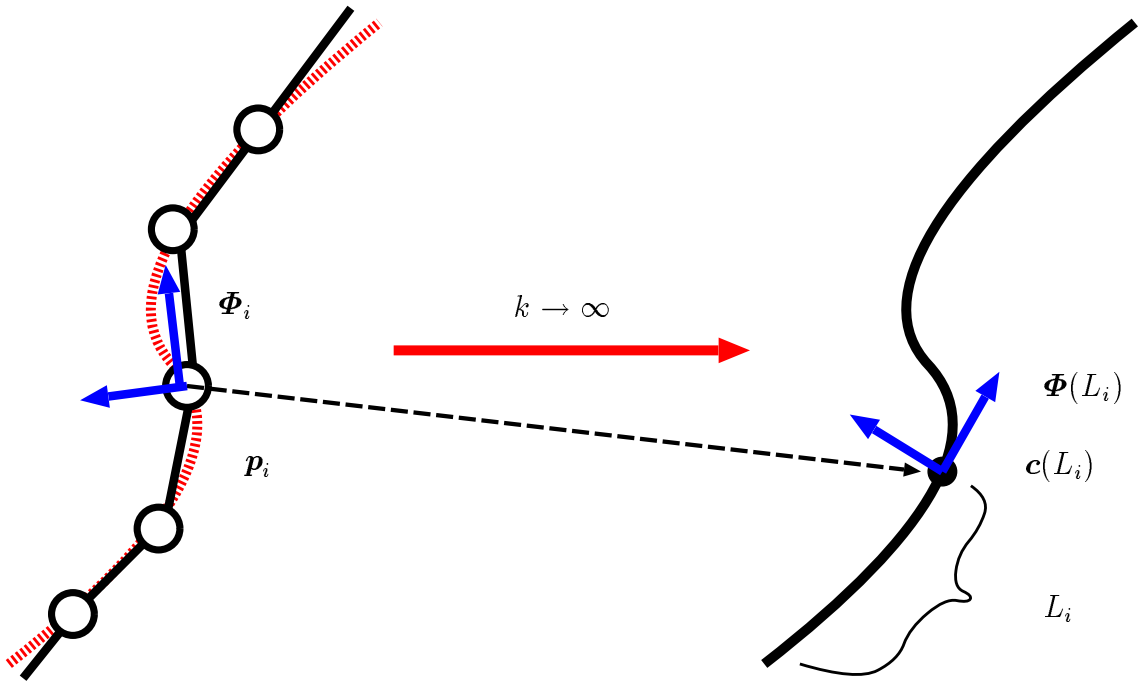

Figure 8.2: Frame convergence

Proof. First, we check that $\boldsymbol{\Phi}(L_i)$ satisfies equation (2.4). The derivative of $\boldsymbol{c}(L_i)$ is

$$\frac{d\boldsymbol{c}}{d\sigma}(L_i) \quad = \quad \lim_{\delta\sigma_i \to 0} \frac{\boldsymbol{c}(L_\iota(\Delta_k)) - \boldsymbol{c}(L_\iota(\Delta_k) - \delta\sigma_i)}{\delta\sigma_i}. \tag{8.18}$$

If we choose $\delta\sigma_i$, depending on Δ_k, as

$$\delta\sigma_i(\Delta_k) = l_\iota(\Delta_k), \tag{8.19}$$

then $k \to \infty$ implies $\delta\sigma_i \to 0$. Thus, we obtain

$$\frac{d\boldsymbol{c}}{d\sigma}(L_i) \quad = \quad \lim_{\delta\sigma_i \to 0} \frac{\lim_{k\to\infty} \boldsymbol{p}_\iota(\Delta_k) - \lim_{k\to\infty} \boldsymbol{p}_{\iota-1}(\Delta_k)}{\delta\sigma_i(\Delta_k)}$$

$$
\begin{aligned}
&= \lim_{k\to\infty} \frac{\boldsymbol{p}_\iota(\Delta_k) - \boldsymbol{p}_{\iota-1}(\Delta_k)}{l_\iota(\Delta_k)} \\
&= \lim_{k\to\infty} \boldsymbol{\Phi}_\iota(\Delta_k)\boldsymbol{e}_x \\
&= \boldsymbol{\Phi}(L_i)\boldsymbol{e}_x, \qquad (8.20)
\end{aligned}
$$

which shows that equation (2.4) in Frenet-Serret formula is satisfied.

The derivative of $\boldsymbol{\Phi}(L_i)$ becomes

$$
\begin{aligned}
\frac{d}{d\sigma}\boldsymbol{\Phi}(L_i) &= \lim_{\delta\sigma_i\to 0} \frac{\lim_{k\to\infty} \boldsymbol{\Phi}_\iota(\Delta_k) - \lim_{k\to\infty} \boldsymbol{\Phi}_{\iota-1}(\Delta_k)}{\delta\sigma_i(\Delta_k)} \\
&= \lim_{k\to\infty} \frac{\boldsymbol{\Phi}_\iota(\Delta_k) - \boldsymbol{\Phi}_{\iota-1}(\Delta_k)}{l_\iota(\Delta_k)} \\
&= \lim_{k\to\infty} \boldsymbol{\Phi}_\iota(\Delta_k) \lim_{k\to\infty} \frac{\boldsymbol{I}_3 - \boldsymbol{R}_{w,\iota}{}^T}{l_\iota(\Delta_k)} \\
&= \boldsymbol{\Phi}(L_i) \lim_{k\to\infty} \frac{\boldsymbol{I}_3 - \boldsymbol{R}_{w,\iota}{}^T}{l_\iota(\Delta_k)}. \qquad (8.21)
\end{aligned}
$$

Comparing the above expression and Frenet-Serret formula (2.5), we obtain the following condition:

$$
[\boldsymbol{\omega}(L_i)\times] = \lim_{k\to\infty} \frac{\boldsymbol{I}_3 - \boldsymbol{R}_{w,\iota}{}^T}{l_\iota(\Delta_k)}. \qquad (8.22)
$$

By Rodrigues' Formula [15], $\boldsymbol{R}_{w,i}$ is evaluated as

$$
\begin{aligned}
\boldsymbol{R}_{w,i} &= \boldsymbol{R}(\boldsymbol{a}_{s,i}, \theta_{s,i})\boldsymbol{R}(\boldsymbol{a}_{m,i}, \theta_{m,i}) \\
&= \exp\left([\boldsymbol{a}_{s,i}\times]\,\theta_{s,i}\right)\exp\left([\boldsymbol{a}_{m,i}\times]\,\theta_{m,i}\right) \\
&= \left\{\boldsymbol{I}_3 + \sin\theta_{s,i}\,[\boldsymbol{a}_{s,i}\times] + (1-\cos\theta_{s,i})\,[\boldsymbol{a}_{s,i}\times]^2\right\} \\
&\quad \left\{\boldsymbol{I}_3 + \sin\theta_{m,i}\,[\boldsymbol{a}_{m,i}\times] + (1-\cos\theta_{m,i})\,[\boldsymbol{a}_{m,i}\times]^2\right\} \\
&= \boldsymbol{I}_3 + \sin\theta_{s,i}\,[\boldsymbol{a}_{s,i}\times] + \sin\theta_{m,i}\,[\boldsymbol{a}_{m,i}\times] + \boldsymbol{Z}(\Delta_k),
\end{aligned}
$$

where $\boldsymbol{Z}(\Delta_k) \in \Re^{3\times 3}$ is a matrix which consists of more than second order terms of $\theta_{s,\iota}$ and $\theta_{m,\iota}$.

Consider the curve projected on the plane perpendicular to $\boldsymbol{a}_{s,i}$ and let $\kappa_{s,i} \in \Re$ be the curvature of the projected curve. If rotational axes are orthogonal [†], the following expression is derived geometrically (see Figure 8.3):

$$
\frac{\sin\theta_{s,i}}{l_i} = \frac{\sin(\theta_\alpha + \theta_\beta)}{l_i}
$$

[†]In case that rotational axes are not orthgonal, we need more complicated discussion. However, we can obtain the same result.

$$= \frac{l'_{i-1}\cos\theta_\beta}{2l_i r_{i-1}} + \frac{l'_i \cos\theta_\alpha}{2l_i r_i}$$

$$= \|\boldsymbol{e}_x \times \{\boldsymbol{R}(\boldsymbol{a}_{s,i}, \theta_{s,i})\boldsymbol{a}_{m,i}\}\| \frac{l_{i-1}\cos\theta_\beta}{2l_i r_{i-1}} + \|\boldsymbol{a}_{m,i} \times \boldsymbol{e}_x\| \frac{\cos\theta_\alpha}{2r_i} \qquad (8.23)$$

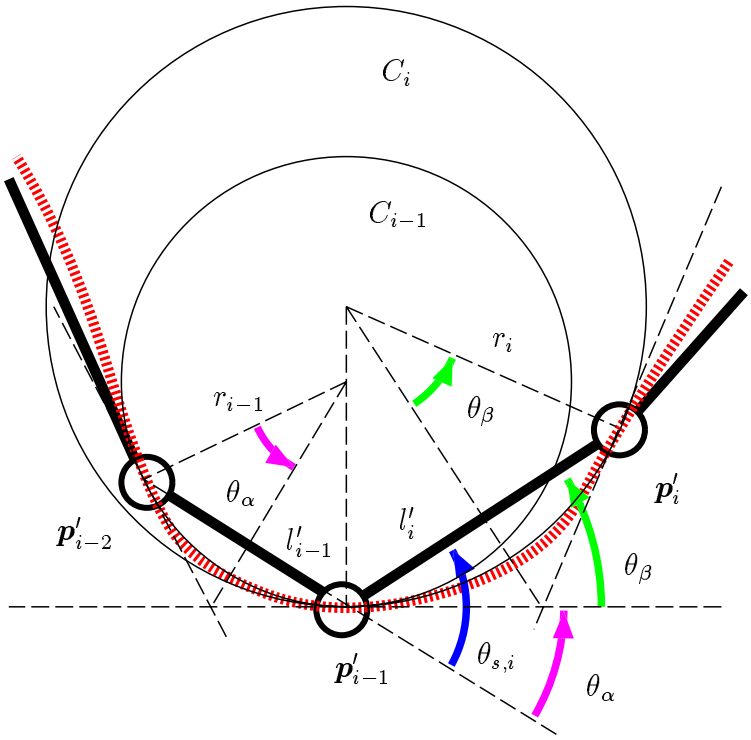

Figure 8.3: Projected curve

Since $\lim_{k\to\infty} \frac{1}{r_{i-1}} = \lim_{k\to\infty} \frac{1}{r_i} = \kappa_{s,i}$, we obtain

$$\lim_{k\to\infty} \frac{\sin\theta_{s,\iota}}{l_\iota} = \begin{cases} \tau(L_i) & (\boldsymbol{a}_{s,i} = \boldsymbol{e}_x) \\ \|\boldsymbol{a}_{s,i} \times \boldsymbol{e}_x\| \kappa_{s,i}(L_i) & (\text{otherwise}) \end{cases} . \qquad (8.24)$$

As the same manner,

$$\lim_{k\to\infty} \frac{\sin\theta_{m,\iota}}{l_\iota} = \begin{cases} \text{undefined} & (\boldsymbol{a}_{m,i} = \boldsymbol{e}_x) \\ \|\boldsymbol{a}_{m,i} \times \boldsymbol{e}_x\| \kappa_{m,i}(L_i) & (\text{otherwise}) \end{cases} . \qquad (8.25)$$

Thus, $\lim_{k\to\infty} \frac{\sin\theta_{s,\iota}}{l_\iota}$ and $\lim_{k\to\infty} \frac{\sin\theta_{m,\iota}}{l_\iota}$ are bounded, which leads to $\boldsymbol{Z}(\Delta_k)/l_\iota \to \boldsymbol{o}$ as $k \to \infty$. Since increase in DOF does not effect on a kinematic structure,

$$\lim_{k\to\infty} [\boldsymbol{a}_{s,\iota}\times] = [\boldsymbol{a}_{s,i}\times] , \quad \lim_{k\to\infty} [\boldsymbol{a}_{m,\iota}\times] = [\boldsymbol{a}_{m,i}\times] .$$

Thus, the right-hand side of (8.22) becomes

$$\lim_{k\to\infty} \frac{\boldsymbol{I}_3 - \boldsymbol{R}_{w,\iota}{}^T}{l_\iota(\Delta_k)} = \left[\left(\lim_{k\to\infty} \frac{\sin\theta_{s,\iota}}{l_\iota}\boldsymbol{a}_{s,i} + \lim_{k\to\infty} \frac{\sin\theta_{m,\iota}}{l_\iota}\boldsymbol{a}_{m,i}\right)\times\right].$$

Therefore, condition (8.22) can be rewritten into the following vector equation:

$$\tau(L_i)\boldsymbol{e}_x + \kappa(L_i)\boldsymbol{e}_z = \lim_{k\to\infty} \frac{\sin\theta_{s,\iota}}{l_\iota}\boldsymbol{a}_{s,i} + \lim_{k\to\infty} \frac{\sin\theta_{m,\iota}}{l_\iota}\boldsymbol{a}_{m,i}. \tag{8.26}$$

We have to choose $\boldsymbol{a}_{s,i} = \boldsymbol{e}_x$ since it is the only way to obtain torsion $\tau(L_i)$. Furthermore, curvature $\kappa_{m,i}(L_i)$ is given by

$$\kappa_{m,i}(L_i) = \mathrm{sgn}\left\{\det\left[\boldsymbol{e}_x\, \boldsymbol{e}_y\, \boldsymbol{a}_{m,i}\right]\right\} \frac{\|\boldsymbol{a}_{m,i}\times\boldsymbol{e}_y\|}{\|\boldsymbol{a}_{m,i}\times\boldsymbol{e}_x\|}\kappa(L_i). \tag{8.27}$$

This shows that we have to take $\boldsymbol{a}_{m,i} = \boldsymbol{e}_z$, which completes the proof. (Q.E.D.)

Vectors $\boldsymbol{a}_{s,i}$ and $\boldsymbol{a}_{m,i}$ are relative to link coordinates $\boldsymbol{\Phi}_{i-1}$ and $\boldsymbol{\Phi}_i$ respectively. Every link coordinate has been attached to the corresponding link such that its x-axis align with the link length direction. Therefore, $\boldsymbol{a}_{s,i} = \boldsymbol{e}_x$ means that a rotation about the Sub-axis contributes to a twist, while $\boldsymbol{a}_{m,i} = \boldsymbol{e}_z$ denotes that a rotation about the Main-axis brings a bend. This result is very natural because Frenet-Serret formula has such a structure. However, it is important to note that there is an order in the bend and the twist; twist first, and then bend. This order can not be observed directly from Frenet-Serret formula. In other words, this order of the bend and the twist disappears at the limit of increase in DOF.

By the definition of curvature, $\kappa \geq 0$. This indicates that it is enough to use one-directional DOF for bending. Actually, almost of bending mechanisms in animals including human beings are one-directional. This is very helpful information to consider to construct real hardwares of an HDOF manipulator.

Summary

The essentials of an HDOF manipulator were discussed from the viewpoint of shape control. The underlying philosophy is that there are the essentials at the limit of increase in DOF. Then, an operation of increase in DOF was defined by using a sequence of position vectors. After the proof of the intuitively clear fact that the "zig-zag" form of an HDOF manipulator on a curve converges to the curve, the conditions of a specific kinematic structure were derived from the geometrically natural requirement that its direct kinematics tends to Frenet-Serret formula by increase in DOF. The result said

that the manipulator had to have 2DOF joints with twisting and bending mechanisms uniformly.

Chapter 9

Conclusions

The main contributions of this thesis are summarized as follows:

New Concepts for Shape Control

We formulated some basic new concepts for shape control of an HDOF manipulator. These concepts include the shape correspondence between a spatial curve and a manipulator (Chapter **3**), the shape inverse problem in order to define the shape correspondence (Chapter **3**), the Shape Jacobian which expresses the relation between the joint angular velocity and the shape velocity error (Chapter **3**) and the increase in DOF to find essentials of an HDOF manipulator (Chapter **8**). These new concepts enabled rigorous discussions on shape control.

Dynamics-based Shape Control

We established the framework of shape control based on the dynamic model of an HDOF manipulator (Chapters **2** – **5**). The success of the establishment owes to the idea of estimating the desired curve parameters in the course of control. This estimation idea allowed us to apply Lyapunov stability theory to our control problems. The estimation law was derived in the similar manner to adaptive control. However, we do not estimate any real physical values, but do the curve parameters which are virtual. This feature of the estimation distinguishes our framework from the conventional one in robot control theory.

New Task in the Shape Control Framework

We showed that, in the shape control framework, we could accomplish a new task which was never done before (Chapter **7**). The task is the motion control along a

collision-free curve useful for an obstacle avoidance. There will appear a lot of creative uses of an HDOF manipulator in this control framework.

Novel Analysis to Obtain the Essentials of an HDOF Manipulator

We proposed the new kinematics for HDOF manipulators which was based on the geometric notation different from the conventional Denavit-Hartenberg notation (Chapter **2**). Based on the kinematics, we gave a novel analysis in order to look for essentials of an HDOF manipulator (Chapter **8**). The conditions of a specific kinematic structure were derived from the geometrically natural requirement that its direct kinematics tends to Frenet-Serret formula by increase in DOF. We have obtained a result that the manipulator has to have 2DOF joints with twisting and bending mechanisms uniformly. Substantial information on the manipulator will be discovered by this kind of limit analysis.

Bibliography

[1] H. Berghuis and H. Nijmeijer : "A Passivity Approach to Controller-Observer Design for Robots," *IEEE Trans. on Robotics and Automation*, Vol.9, No.6, 740/754, 1993.

[2] C. Canudas de Wit and N. Fixot : "Robot Control Via Robust Estimated State Feedback," *IEEE Trans. on Automatic Control*, Vol.36, No.12, 1497/1501, 1991.

[3] C. Canudas de Wit, N. Fixot and K.J. Astrom : "Trajectory Tracking in Robot Manipulators via Nonlinear Estimated State Feedback," *IEEE Trans. on Robotics and Automation*, Vol.8, No.1, 138/144, 1992.

[4] C. Canudas de Wit, B. Siciliano and G. Bastin Eds. : *Theory of Robot Control*, Springer, 1996.

[5] G.S. Chirikjian: *Theory and Applications of Hyper-Redundant Robotic Mechanisms*, Ph.D thesis, Dept.of Applied Mechanics, California Institute of Technology, June, 1992.

[6] G.S. Chirikjian and J.W. Burdick: "A Modal Approach to Hyper-Redundant Manipulator Kinematics," *IEEE Trans. on Robotics and Automation*, Vol.10, No.3, 343/354, 1994.

[7] G.S. Chirikjian and J.W. Burdick: "The Kinematics of Hyper-redundant Robot Locomotion," *IEEE Trans. on Robotics and Automation*, Vol.11, No.6, 781/793, 1995.

[8] G.S. Chirikjian and J.W. Burdick: "Kinematically Optimal Hyper-redundant Manipulator Configurations," *IEEE Trans. on Robotics and Automation*, Vol.11, No.6, 794/806, 1995.

[9] S. Hirose: *Biologically Inspired Robots: Snake-like Locomotors and Manipulators*, Oxford Science Publications, 1993.

[10] G. Immega and K. Antonelli: "The KSI Tentacle Manipulator," *Proc. 1995 IEEE Int. Conf. Robotics and Automation*, Vol.3, 3149/3154, 1995.

[11] M. Ivanescu and V. Stoian: "A Variable Structure Controller for a Tentacle Manipulator," *Proc. 1995 IEEE Int. Conf. Robotics and Automation*, Vol.3, 3155/3160, 1995.

[12] H. Khalil: *Nonlinear Systems, 2nd ed.*, Prentice Hall, 1996.

[13] H. Kobayashi and S. Otake: "Shape Control of Hyper Redundant Manipulator," *Proc. 1995 IEEE Int. Conf. Robotics and Automation*, Vol.3, 2803/2808, 1995.

[14] S. Ma and M. Konno: "An Obstacle Avoidance Scheme for Hyper-Redundant Manipulators –Global Motion Planning in Posture Space–," *Proc. 1997 IEEE Int. Conf. Robotics and Automation*, 161/166, 1995.

[15] R.M. Murray, Z. Li and S.S. Sastry : *A Mathematical Introduction to Robotic Manipulation*, CRC Press, 1994.

[16] F. Naccarato and P. Hughes: "Inverse Kinematics of Variable-Geometry Truss Manipulators," *J. of Robotic Systems*, Vol.8, No.2, 249/266, 1991.

[17] S. Nicosia and P. Tomei : "Robot Control by Using Only Joint Position Measurement, " *IEEE Trans. on Automatic Control*, Vol.35, No.9, 1058/1061, 1990.

[18] M. Nilsson : "Snake Robot Free Climbing," *Proc. 1997 IEEE Int. Conf. Robotics and Automation*, Vol.4, 3415/3420, 1997.

[19] J. Ostrowski, J.P. Desai and V. Kumar: "Optimal Gait Selection for Nonholonomic Locomotion Systems," *Proc. 1997 IEEE Int. Conf. Robotics and Automation*, 786/791, 1997.

[20] E. Paljug, T. Ohm and S. Hayati: "The JPL Serpentine Robot: a 12 DOF System for Inspection," *Proc. 1995 IEEE Int. Conf. Robotics and Automation*, Vol.3, 3143/3148, 1995.

[21] J.S. Pettinato and H.E. Stephanou: "Manipulability and Stability of a Tentacle Based Robot Manipulator," *Proc. 1989 IEEE Int. Conf. Robotics and Automation*, 458/463, 1989.

[22] R.J. Salerno, C.F. Reinholts and S.G. Dhande: "Kinematics of Long-Chain Variable Geometry Truss Manipulators: An Overview of Solution Techniques," *Proc. 2nd Int. Workshop on Advances in Robot Kinematics*, 179/187, 1990.

[23] K. Salisbury: "Whole Arm Manipulation," *Proc. the 4th Int. Sym. on Robotics Research*, 183/189, 1987.

[24] K. Salisbury, B. Eberman, M. Levin and W. Townsend: "The Design and Control of An Experimental Whole-Arm Manipulator," *Proc. the 5th Int. Sym. on Robotics Research*, 233/241, 1988.

[25] J.J.-E. Slotine and W. Li: "On the adaptive control of robot manipulators," *Int. J. Robotics Res.*, Vol.6, 49/59, 1987.

[26] N. Takanashi: "Complete Modular Link with the Active Universal Joint Mechanism for 3D Hyper Redundant Robot," *Proc. the 34th Society of Instrument and Control Engineers Annual Conference*, Vol.2, 843/844, 1995. (in Japanese)

[27] M. Takegaki and S. Arimoto: "A New Feedback Method for Dynamic Control of Manipulators," *Journal of Dynamic System, Measurement, and Control*, Vol.102, 119/125, 1981.

[28] K.E. Zanganeh and J. Angeles : "The Inverse Kinematics of Hyper-Redundant Manipulators Using Splines," *Proc. 1995 IEEE Int. Conf. Robotics and Automation*, Vol.3, 2797/2802, 1995.

[29] K.E. Zanganeh, R.S.K. Lee and P.C. Hughes : "A Discrete Model for the Configuration Control of Hyper-Redundant Manipulators," *Proc. 1997 IEEE Int. Conf. Robotics and Automation*, Vol.1, 167/172, 1997.

[30] S. Kobayashi : *Differential Geometry of Curves and Surfaces*, Shokabo, 1995. (in Japanese)

[31] T. Sunada : *Geometry of Surfaces*, Iwanami, 1996. (in Japanese)

Publications

[Journal Papers]

[1] H. Mochiyama, E. Shimemura and H. Kobayashi: "Control of Serial Rigid Link Manipulators with Hyper Degrees of Freedom (Shape Control by a Homogeneously Decentralized Scheme)," *Journal of the Robotics Society of Japan*, Vol. 15, No.1, 109/117, 1997. (in Japanese)

[2] H. Mochiyama, E. Shimemura and H. Kobayashi : "Control of Manipulators with Hyper Degrees of Freedom – Shape Control Based on Curve Parameter Estimation – ," *Trans. SICE*, Vol. 34, No.3, 1998. (to appear, in Japanese)

[3] H. Mochiyama, E. Shimemura and H. Kobayashi : "Control of Manipulators with Hyper Degrees of Freedom – Shape Tracking Based on Curve Parameter Estimation –," submitted to *Trans. SICE*. (in Japanese)

[4] H. Mochiyama, E. Shimemura and H. Kobayashi : "Control of Manipulators with Hyper Degrees of Freedom : Shape Tracking Using Only Joint Angle Information," *the International Journal of Systems Science*, 1998. (accepted)

[Reviewed Proceedings]

[5] H. Mochiyama, E. Shimemura and H. Kobayashi: "Control of Serial Rigid Link Manipulators with Hyper Degrees of Freedom: Shape Control by a Homogeneously Decentralized Scheme and its Experiment," *Proc. 1996 IEEE Int. Conf. Robotics and Automation*, Vol.3, 2877/2882, 1996.

[6] H. Mochiyama, E. Shimemura and H. Kobayashi: "Control of Manipulators with Hyper Degrees of Freedom: Shape Control Based on Curve Parameter Estimation," *Proc. the 11th Korea Automatic Control Conference*, 12/15, 1996.

[7] H. Mochiyama, E. Shimemura and H. Kobayashi : "Control of Manipulators with Hyper Degrees of Freedom: Shape Tracking Based on Curve Parameter Estimation," *Proc. 1997 IEEE Int. Conf. Robotics and Automation*, Vol.1, 173/178, 1997.

[8] H. Mochiyama, E. Shimemura and H. Kobayashi : "Control of Manipulators with Hyper Degrees of Freedom: Shape Tracking Using Only Position Measurement," *Proc. The 2nd Asian Control Conference*, Vol.2, 339/342, 1997.

[9] H. Mochiyama, E. Shimemura and H. Kobayashi : "Direct Kinematics of Manipulators with Hyper Degrees of Freedom and Frenet-Serret Formula," *1998 IEEE Int. Conf. Robotics and Automation*, 1998. (accepted)

[10] H. Mochiyama, E. Shimemura and H. Kobayashi : "Shape Correspondence between a Manipulator with Hyper Degrees of Freedom and a Spatial Curve," *the 3rd Robotics Symposia*, 1998. (accepted, in Japanese)

[11] H. Mochiyama, E. Shimemura and H. Kobayashi : "Shape Correspondence between a Spatial Curve and a Manipulator with Hyper Degrees of Freedom," submitted to *1998 IEEE/RSJ International Conference on Intelligent Robots and Systems*, 1998.

[Proceedings]

[12] H. Mochiyama, E. Shimemura and H. Kobayashi : "Control of the Manipulators with Hyper Degrees of Freedom (Shape Control by a Homogeneously Decentralized Scheme)," *Proc. of the 34th SICE Annual Conference*, Vol.I, 99/100, 1995. (in Japanese)

[13] H. Mochiyama, E. Shimemura and H. Kobayashi : "Control of Manipulators with Hyper Degrees of Freedom – Experimental Verification of Shape Control by a Homogeneously Decentralized Scheme –," *Proc. of the 13th Annual Conference of RSJ*, No.2, 503/504, 1995. (in Japanese)

[14] H. Mochiyama, E. Shimemura and H. Kobayashi : "Control of Manipulators with Hyper Degrees of Freedom – Shape Control Based on Curve Parameter Estimation – ," *Proc. of the 1st Robotics Symposia*, 63/68, 1996. (in Japanese)

[15] H. Mochiyama, E. Shimemura and H. Kobayashi : "Control of Manipulators with Hyper Degrees of Freedom: Shape Tracking Control Based on Curve Parameter

Estimation," *Proc. of the 25th SICE Symposium on Control Theory*, 63/68, 1996. (in Japanese)

[16] H. Mochiyama, E. Shimemura and H. Kobayashi : "Control of Manipulators with Hyper Degrees of Freedom: Shape Tracking Control Based on Curve Parameter Estimation," *Proc. of the 19th SICE Symposium on Dynamical System Theory*, 199/204, 1996. (in Japanese)

[17] H. Mochiyama, E. Shimemura and H. Kobayashi: "Control of Manipulators with Hyper Degrees of Freedom: Obstacle Avoidance Based on Shape Control," *Proc. of the 14th Annual Conference of RSJ*, No.2, 639/640, 1996. (in Japanese)

[18] H. Mochiyama, E. Shimemura and H. Kobayashi : "Direct Kinematics of Manipulators with Hyper Degrees of Freedom and the Frenet-Serret Formula," *Proc. of the 26th SICE Symposium on Control Theory*, 457/460, 1997. (in Japanese)

[19] H. Mochiyama, E. Shimemura and H. Kobayashi : "Shape Control of Manipulators with Hyper Degrees of Freedom: Singularities of the Shape Jacobian," *Proc. of the 36th SICE Annual Conference*, Vol.I, 459/460, 1997. (in Japanese)